Endoplasmic reticulum stress actively suppresses hepatic molecular identity in damaged liver

Vanessa Dubois, Celine Gheeraert, Wouter Vankrunkelsven, Julie Dubois-chevalier, Hélène Dehondt, Marie Bobowski-Gerard, Manjula Vinod, Francesco Paolo Zummo, Fabian Güiza, Maheul Ploton, et al.

▶ **To cite this version:**

Vanessa Dubois, Celine Gheeraert, Wouter Vankrunkelsven, Julie Dubois-chevalier, Hélène Dehondt, et al.. Endoplasmic reticulum stress actively suppresses hepatic molecular identity in damaged liver. Molecular Systems Biology, 2020, 16 (5), pp.e9156. 10.15252/msb.20199156 . inserm-02617039

HAL Id: inserm-02617039

https://inserm.hal.science/inserm-02617039

Submitted on 25 May 2020

HAL is a multi-disciplinary open access archive for the deposit and dissemination of scientific research documents, whether they are published or not. The documents may come from teaching and research institutions in France or abroad, or from public or private research centers.

L'archive ouverte pluridisciplinaire **HAL**, est destinée au dépôt et à la diffusion de documents scientifiques de niveau recherche, publiés ou non, émanant des établissements d'enseignement et de recherche français ou étrangers, des laboratoires publics ou privés.

Endoplasmic reticulum stress actively suppresses hepatic molecular identity in damaged liver

Vanessa Dubois [1,|], Céline Gheeraert [1,$], Wouter Vankrunkelsven [2,$], Julie Dubois-Chevalier [1,*], Hélène Dehondt [1,*], Marie Bobowski-Gerard [1], Manjula Vinod [1], Francesco Paolo Zummo [1], Fabian Güiza [2], Maheul Ploton [1], Emilie Dorchies [1], Laurent Pineau [1], Alexis Boulinguiez [1], Emmanuelle Vallez [1], Eloise Woitrain [1], Eric Baugé [1], Fanny Lalloyer [1], Christian Duhem [1], Nabil Rabhi [3], Ronald E. van Kesteren [4], Cheng-Ming Chiang [5], Steve Lancel [1], Hélène Duez [1], Jean-Sébastien Annicotte [3], Réjane Paumelle [1], Ilse Vanhorebeek [2], Greet Van den Berghe [2], Bart Staels [1], Philippe Lefebvre [1,§], Jérôme Eeckhoute [1, §, #]

[1] Univ. Lille, Inserm, CHU Lille, Institut Pasteur de Lille, U1011-EGID, F-59000 Lille, France.

[2] Clinical Division and Laboratory of Intensive Care Medicine, Department of Cellular and Molecular Medicine, KU Leuven, B-3000 Leuven, Belgium.

[3] Univ. Lille, UMR 8199 - EGID, CNRS, Institut Pasteur de Lille, F-59000 Lille, France.

[4] Center for Neurogenomics and Cognitive Research, Neuroscience Campus Amsterdam, VU University, Amsterdam, The Netherlands

[5] University of Texas Southwestern Medical Center, Simmons Comprehensive Cancer Center, Department of Biochemistry, and Department of Pharmacology, Dallas, TX 75390, USA.

[|] Present address: Clinical and Experimental Endocrinology, Department of Chronic Diseases, Metabolism and Ageing (CHROMETA), KU Leuven, B-3000 Leuven, Belgium.

[$,*] Contributed equally

[§] Joint senior authors

[#] Corresponding author

CORRESPONDING AUTHOR

Dr. Jérôme Eeckhoute

INSERM UMR 1011-Bâtiment J&K

Université de Lille, Faculté de Médecine de Lille-Pôle Recherche

Boulevard du Professeur Leclerc

59045 Lille cedex

France

Tel : 33(0)3 20 97 42 20 / Fax : 33(0)3 20 97 42 01

E-mail: jerome.eeckhoute@inserm.fr

Running title: ERS disrupts hepatic molecular identity

Character count: 95,984

ABSTRACT

Liver injury triggers adaptive remodeling of the hepatic transcriptome for repair/regeneration. We demonstrate that this involves particularly profound transcriptomic alterations where acute induction of genes involved in handling of endoplasmic reticulum stress (ERS) is accompanied by partial hepatic dedifferentiation. Importantly, widespread hepatic gene downregulation could not simply be ascribed to cofactor squelching secondary to ERS gene induction, but rather involves a combination of active repressive mechanisms. ERS acts through inhibition of the liver identity (LIVER-ID) transcription factor (TF) network, initiated by rapid LIVER-ID TF protein loss. In addition, induction of the transcriptional repressor NFIL3 further contributes to LIVER-ID gene repression. Alteration to the liver TF repertoire translates into compromised activity of regulatory regions characterized by the densest co-recruitment of LIVER-ID TFs and decommissioning of BRD4 super-enhancers driving hepatic identity. While transient repression of the hepatic molecular identity is an intrinsic part of liver repair, sustained disequilibrium between the ERS and LIVER-ID programs is linked to liver dysfunction as shown using mouse models of acute liver injury and livers from deceased human septic patients.

KEYWORDS

Liver injury / endoplasmic reticulum stress / cell identity / transcriptional ecosystem / super-enhancer / PAR-bZIP / NFIL3 / sepsis

INTRODUCTION

The liver exerts instrumental homeostatic and detoxifying functions. This organ is also characterized by a unique capacity to regenerate (Abu Rmilah et al., 2019). Studies in mice subjected to liver regeneration subsequent to partial hepatectomy (PHx), a model of liver resection which is a frequent clinical practice to remove liver tumors (Liu et al., 2015a), have identified a role for endoplasmic reticulum stress (ERS) in this process (Argemi et al., 2017, Liu et al., 2015b). ERS, which results from the accumulation of unfolded/misfolded proteins in the ER lumen, triggers the unfolded protein response (UPR), aimed at restoring ER homeostasis. The UPR is controlled by three major ERS sensors, namely the endoplasmic reticulum to nucleus signaling 1 (ERN1/IRE1), eukaryotic translation initiation factor 2 alpha kinase 3 (EIF2AK3/PERK) and activating transcription factor 6 (ATF6) (Almanza et al., 2019). Signalling triggered by these sensors leads to activation of the Xbox-binding protein 1 (XBP1S), ATF4 and ATF6 transcription factors (TFs) and subsequent collaborative induction of ERS handling genes such as ER chaperones (Almanza et al., 2019, Vihervaara et al., 2017). Additional, non-transcriptional effects of the UPR involved in alleviating ERS also comprise the regulation of protein synthesis (mRNA translation) and degradation (Almanza et al., 2019). However, it has become clear that ERS bears functions beyond proteostasis *per se* (Hetz, 2012). For instance, liver regeneration upon PHx requires transient ERS to induce genes involved not only in proteostasis but also in acute-phase and DNA damage responses (Argemi et al., 2017, Liu et al., 2015b). Moreover, ERS has been linked to the (patho)physiological control of lipid and glucose metabolism in the liver (Rutkowski, 2019). The molecular mechanisms involved in ERS-mediated control of liver metabolic functions are still poorly defined. TFs activated by the UPR (including XBP1S, ATF4, DDIT3/CHOP, ATF6) can directly bind to and modulate expression of specific metabolic genes. In addition, a handful of liver-enriched TFs display reduced expression or activity upon ERS through ill-defined mechanisms (Rutkowski, 2019). In general, while gene silencing substantially contributes to ERS-induced transcriptional regulation, the mechanisms accounting for these downregulations are seldom defined (Almanza et al., 2019, Vihervaara et al., 2018). Hence, ERS-induced transcriptional

remodelling, especially gene downregulation, remains to be fully understood and its relevance towards liver pathophysiology to be better defined.

We and others have reported that hepatic gene transcription relies on networks of highly interconnected TFs (Kyrmizi et al., 2006), which are co-recruited to *cis*-regulatory modules (CRMs) (Dubois-Chevalier et al., 2017), a conclusion corroborated by several studies in other systems reporting that extensive collaboration of TFs at CRMs is essential for their activities (e.g. (Levo et al., 2017)). These findings point to a requirement for a comprehensive assessment of changes in global TF expression/activity induced by (patho)physiological signals when aiming to define how transcriptional outputs are controlled. Here, we have used a functional genomics approach to characterize the molecular mechanisms responsible for hepatic gene transcriptional alterations triggered by ERS and to define how this relates to liver damage in mouse models of acute liver injury and livers from deceased human septic patients.

RESULTS

Acute ERS recapitulates the loss of hepatic molecular identity observed following liver PHx through extensive and preferential repression of liver identity genes

The hepatic response to ERS was defined using transcriptomic analysis of mouse primary hepatocytes (MPH) treated with thapsigargin for 4h (Appendix Fig.S1A). In addition to induction of the UPR (hereafter referred to as the ERS UP genes), we found a substantial fraction of regulated genes (~45%) downregulated upon ERS in MPH (ERS DOWN genes) (Appendix Fig.S1A). This regulatory pattern was conserved when analyzing the mouse liver transcriptome 8h after a single intraperitoneal injection of tunicamycin, another ERS-inducing drug (Appendix Fig.S1B-C) (Arensdorf et al., 2013). Moreover, transcriptomic data mining using Short Time-series Expression Miner (STEM) (Ernst et al., 2005, Rib et al., 2018), a tool defining the preferential dynamic patterns of gene expression, confirmed that transient ERS occurs upon PHx (Fig.1A and Appendix Fig.S2) (Liu et al., 2015b, Reimold et al., 2000). Strikingly, unlike ERS UP genes, which are mostly involved in

housekeeping functions, ERS DOWN genes are linked to liver-specific functions (e.g. coagulation, xenobiotic drug metabolism) (Fig.1B). Concomitant to transient ERS, mouse liver regeneration following PHx has been linked to transient decrease in metabolic gene expression (Argemi et al., 2017, White et al., 2005). We found this was related to ERS DOWN genes being transiently downregulated upon liver PHx (Fig.1A). As the transcriptome of cells has been proposed to be ruled by ecosystem-like equilibriums where resources required to induce novel programs are used at the expense of established ones (Silveira & Bilodeau, 2018), we monitored the extent of transcriptomic alterations triggered by PHx or chemically-induced ERS compared to physiological transcriptomic changes unrelated to liver injury, i.e. triggered by fasting to feeding transition in mice (Benegiamo et al., 2018, Kalvisa et al., 2018). Bagplots (bivariate boxplots showing fold-changes in expression relative to baseline mouse liver gene expression levels) revealed that downregulation of the hepatic program upon PHx and ERS was associated with more complex and widespread transcriptomic alterations including a greater induction of genes expressed at low/moderate levels in the healthy mouse liver (Fig.1C).

To further characterize the impact of PHx and ERS on the hepatic transcriptional program, we defined cell identity genes, i.e. master liver transcriptional regulators and effector genes. Identity genes establish/maintain tissue-specific functions and distinguish themselves by broad H3K4me3 domains encompassing the transcription start site, a feature functionally related to high transcriptional expression and consistency (Benayoun et al., 2014). We defined liver identity (LIVER-ID) genes as those displaying this epigenetic feature preferentially in liver (Appendix Fig.S3A and Table EV1). We verified that LIVER-ID genes displayed expression levels which are higher (Fig.1D), liver-specific (Fig.1E), and linked to hepatic functions when compared to non-LIVER-ID genes, i.e. ubiquitously labelled with broad H3K4me3 (UBQ genes) or lacking liver broad H3K4me3 (Other genes) (Appendix Fig.S3B). LIVER-ID genes were transiently downregulated upon liver PHx (Fig.1F) as well as upon ERS both *in-vitro* in MPH and *in-vivo* in mouse liver (Fig.1G-H and Appendix Fig.S3C-D). LIVER-ID gene repression was specific and not linked to their high expression levels which could make

them more prone to repression, since ERS-mediated repression did not correlate with basal hepatic gene expression (Appendix Fig.S3E). Note that while microarray-based transcriptomic analyses reliably define fold-changes, this technology under-estimates their magnitude (Dallas et al., 2005). This notion should be taken into account when interpreting microarray-based results throughout the study. In particular, LIVER-ID genes were enriched among genes which were the most repressed by ERS (Fig.1I-K). Reciprocal induction of ERS UP genes and downregulation of LIVER-ID genes was validated using RT-qPCR in MPH (Fig.1L and Appendix Fig.S3F-G) and mouse liver (Fig.1M and Appendix Fig.S3F). Interestingly, ERS DOWN genes correspond to genes induced during hepatic differentiation, based on whole liver (Fig.1N and Appendix Fig.S3H) (Li et al., 2009) or hepatobiliary single-cell (Fig.1O and Appendix Fig.S3I-J) (Yang et al., 2017) transcriptomic data obtained at different developmental stages.

Altogether, these data point to loss of hepatic molecular identity upon liver PHx, which can be recapitulated by acute ERS acting as a widespread repressor of the liver transcriptional program.

Acute ERS triggers a global loss of activity of the LIVER-ID TF network and its densely co-bound CRMs

To define how liver molecular identity loss is induced by ERS at the transcriptional regulatory level, we monitored changes in CRM activities in MPH using alterations to H3K27 acetylation (H3K27ac) levels as a surrogate. H3K27ac ChIP-seq assays identified regions with increased (62%) or decreased (38%) H3K27ac signal intensities (denoted H3K27ac UP or H3K27ac DOWN), respectively (Appendix Fig.S4A and Dataset EV1). Genes linked to H3K27ac UP regions were significantly enriched in ERS UP genes, while ERS DOWN genes were more strongly linked to H3K27ac DOWN regions (Fig.2A). In line, LIVER-ID genes were most significantly linked to H3K27ac DOWN regions (Fig.2B).

Locus overlap analysis (LOLA) (Sheffield & Bock, 2016) was next used to compare genomic localization of H3K27ac regions with the chromatin binding sites (cistromes) of mouse TFs (657 cistromes) from the Gene Transcription Regulation Database (GTRD) (Yevshin et al., 2017). We found that 81% of the mouse hepatic TF cistromes comprised in this database (61 out of 75 cistromes)

belonged to the cluster displaying the strongest overlap with H3K27ac DOWN regions (Appendix Fig.S4B and Table EV2), suggesting these regions might be characterized by dense hepatic TF co-recruitment. In line, monitoring the co-recruitment patterns of 47 transcriptional regulators in mouse liver (Dubois-Chevalier et al., 2017) revealed that H3K27ac DOWN regions were uniquely characterized by a node of highly co-recruited transcriptional regulators, which was not found for H3K27ac UP or unchanged regions (Fig.2C). Moreover, several of these regulators were defined as LIVER-ID TFs (Fig.2C, panel d), i.e. TFs comprised within the previously described LIVER-ID gene list (Appendix Fig.S5 and Table EV1; 43 TFs).

Additional analyses of hepatic enhancers indicated that the extent of LIVER-ID TF co-binding positively associated with their chance of being inactivated by ERS, as judged through their overlap with H3K27ac DOWN regions (Fig.2D). Importantly, this could not be attributed to any single LIVER-ID TF. Indeed, this pattern was observed for each individual LIVER-ID TF, when focusing on its specific set of bound CRMs. Additionally, lack of several individual LIVER-ID TFs was linked to reduced propensity for ERS-mediated repression. Thus, deficiency in activity of a single LIVER-ID TF could not explain ERS-induced loss of H3K27ac at mouse CRM but rather pointed to ERS-mediated inactivation being linked to a concomitant impaired activity of several LIVER-ID TFs (Fig.2D). This led us to investigate whether ERS is linked to a coordinated and global loss of master hepatic TF activities. In line with this hypothesis, we found that LIVER-ID TFs mostly belonged to ERS DOWN genes (Fig.2E and Appendix Fig.S6A-B). Similar conclusions were reached when defining LIVER-ID TFs based on high and specific expression in the human liver (D'Alessio et al., 2015) or on reconstructed gene regulatory networks (Zhou et al., 2017), which largely overlap with our epigenetically-defined LIVER-ID TF list (Appendix Fig.S6C-D), hence supporting the robustness of our findings. RT-qPCR assays confirmed ERS-mediated downregulation of LIVER-ID TFs in mouse AML12 hepatocytes, MPH and mouse liver (Fig.2F and Appendix Fig.S6E-G). LIVER-ID TF gene downregulation in MPH was blunted by pre-treating the cells with the chemical chaperone 4-phenylbutyrate (PBA), which, as expected, alleviated ERS response as judged through lower induction of ERS UP genes (Fig.2G). The diminished

LIVER-ID TF gene expression induced by ERS was accompanied by loss of LIVER-ID TF activity as evidenced by a drastic decrease in both nuclear and chromatin-bound levels of HNF4A, NR1H4/FXR and FOXA2/HNF3B (Fig.2H-I), which have well-established hepatic functions and were used as examples in these analyses.

These data indicate that ERS triggers a global impairment of LIVER-ID TF expression/activities. Among LIVER-ID TF with decreased expression, HLF (Fig.2F and Appendix Fig.S6E-F) belongs to the PAR-bZIP family together with TEF, DBP and NFIL3. While HLF, TEF and DBP behave as transcriptional activators, repressive functions have been ascribed to NFIL3 thereby establishing a balance in the transcriptional regulation of shared target genes (e.g. (Mitsui et al., 2001)). Recently, NFIL3 has been found to be induced upon ERS in mouse pancreatic islets (Ohta et al., 2017). Interestingly, acute hepatic ERS triggers a switch in the expression profile of the PAR-bZIP TF family members including strong induction of *Nfil3* levels (Fig.3A-B and Appendix Fig.S7A-D) and chromatin binding (Fig.3C). This switch in expression of the PAR-bZIP TF family members was also observed upon liver PHx (Appendix Fig.S7E). Transcriptomic analyses of the liver of *Nfil3*$^{-/-}$ (NFIL3 KO) mice subjected to ERS (Appendix Fig.S8) revealed that repression of LIVER-ID gene expression was blunted in NFIL3 KO mice, as illustrated by GSEA showing enrichment of LIVER-ID genes in NFIL3 KO compared to WT livers subjected to acute ERS (Fig.3D). Further investigation of the genes contributing the most to this enrichment, i.e. LIVER-ID genes less efficiently repressed by ERS in NFIL3 KO compared to WT mice (Table EV3), revealed "Drug metabolism and cytochrome P450" as the main pathway (Fig.3D). Several of these genes are involved in xenobiotic metabolism (*Gsta3*, *Adh1*, *Cyp3a11*, *Fmo5* and *Ugt2b1*), a liver function previously defined as being critically regulated by the PAR-bZIP TF family (Gachon et al., 2006). Additional cytochrome P450-related liver functions are also less repressed by ERS in NFIL3 KO mice (Table EV3). Blunted ERS-mediated repression in NFIL3 KO mouse livers of specific genes related to xenobiotic metabolism is shown in Fig.3E. In addition to the features defining the highest sensitivity to ERS-mediated repression (i.e. dense LIVER-ID TF co-recruitment and, as described hereafter, overlap with BRD4 SE), these genes are bound by NFIL3 at CRMs which

are specifically active in hepatocytes when compared to the non-parenchymal cells (NPC) (Fig.3F and Appendix Fig.S9).

Altogether, these data reveal that acute ERS profoundly remodels the liver TF repertoire where a global loss of LIVER-ID TF expression is reinforced, within the PAR-bZIP TF family, by induction of the transcriptional repressor NFIL3.

Acute ERS triggers decommissioning of BRD4 at super-enhancers (SE) and preferentially represses SE-associated genes

We next investigated how compromised LIVER-ID TF expression/activities translate into loss of the hepatic transcriptional program. TFs activate target gene expression through recruitment of transcriptional coactivators. Among those, BRD4 has been identified as crucial to establish and maintain transcriptomic cellular identity (Di Micco et al., 2014, Lee et al., 2017). BRD4 recruitment to CRMs requires EP300-mediated protein acetylation, including acetylation of H3 at K27 (Roe et al., 2015). Considering that LIVER-ID TFs target EP300 at liver CRMs to catalyze H3K27ac (Thakur et al., 2019), through their interaction with EP300 (Appendix Fig.S10A) (Eeckhoute et al., 2004, Kemper et al., 2009, von Meyenn et al., 2013), we hypothesized that the ERS-mediated decrease in LIVER-ID TFs and H3K27ac might culminate into compromised BRD4 recruitment at CRMs. Using ChIP-qPCR, we found that ERS decreased BRD4 binding at H3K27ac DOWN CRMs in MPH and mouse liver (Fig.4A and Appendix Fig.S10B). This decrease could not be ascribed to reduced BRD4 expression levels upon ERS (Fig.4B and Appendix Fig.S10C).

To verify the importance of BRD4 loss with regards to expression of LIVER-ID genes, MPH were treated with the BRD4 inhibitors JQ1, which impedes recognition of acetylated proteins by the BRD4 bromodomain, and MZ1, which targets BRD4 for degradation (Zengerle et al., 2015) (Fig.4B). Both treatments severely compromised basal expression of LIVER-ID genes, which could moreover not be further repressed by ERS (Fig.4C and Appendix Fig.S11). The decreased LIVER-ID gene expression observed upon BRD4 inhibition was not kinetically preceded by decreased protein expression of the LIVER-ID TFs HNF4A, NR1H4/FXR and FOXA2/HNF3B (Appendix Fig.S12), indicating

it was most likely a direct consequence of deficient BRD4-mediated gene transcription. Activation of canonical ERS UP genes was also blunted, although these genes appeared less sensitive to BRD4 inhibition (Fig.4C and Appendix Fig.S11). MPH treatment with C646, an inhibitor of the EP300 histone acetyltransferase, also reduced basal expression of LIVER-ID genes and blocked further repression by ERS (Appendix Fig.S13), while treatment with the histone deacetylase (HDAC) inhibitor trichostatin A impeded their repression by ERS (Appendix Fig.S14).

BRD4 control of cell identity is linked to its recruitment at CRMs densely co-bound by master TFs, organized in clusters defining so called super-enhancers (SE) (Whyte et al., 2013). BRD4 SE (defined using mouse liver BRD4 ChIP-seq data (Kim et al., 2018)) largely overlapped LIVER-ID domains (i.e. liver preferential broad H3K4me3 regions as defined above) (Appendix Fig.S15A). Interestingly, LIVER-ID domains overlapping BRD4 SE showed stronger binding of EP300 and LIVER-ID TFs (Appendix Fig.S15B) together with stronger H3K27ac basal levels in MPH, which displayed a more pronounced decrease upon acute ERS (Fig.4D). Accordingly, LIVER-ID domains overlapping BRD4 SE showed enrichment for H3K27ac DOWN regions (Appendix Fig.S15C) and their associated genes (Appendix Fig.S15D). In line, genes associated with both LIVER-ID domains and BRD4 SE showed the highest basal and most liver-specific expression (Appendix Fig.S15E). Importantly, these genes were more strongly downregulated by ERS (Fig.4E).

Altogether, these data point to BRD4 SE decommissioning as central to LIVER-ID gene expression loss upon acute ERS in hepatocytes. In this context, BRD4 SE defines a subset of LIVER-ID genes with greatest sensitivity to acute ERS-mediated repression.

Loss of liver identity is initiated by a rapid decrease in LIVER-ID TF protein levels upon acute ERS

Kinetic experiments in MPH indicated that the decrease of LIVER-ID TF expression triggered by ERS precedes that of non-TF LIVER-ID genes (Fig.5A), consistent with impairment of the hepatic TF network driving subsequent loss of liver CRM activities and target gene expression. LIVER-ID TFs are organized as an interdependent transcriptional network involving auto- and cross-regulatory loops (Kyrmizi et al., 2006) at BRD4 SE (Appendix Fig.S16). Therefore, we reasoned that any alteration to

LIVER-ID TF protein levels could serve as an initial trigger which would secondarily be amplified by decreased expression of their encoding genes. Interestingly, further analyses of the kinetics of LIVER-ID TF loss of expression upon acute ERS revealed that the decrease in protein levels of HNF4A, NR1H4/FXR and FOXA2/HNF3B was already effective 1h after induction of ERS, at a time when mRNA levels are still unchanged (Fig.5B-C and Appendix Fig.S17). While promoting translation of specific ERS-induced genes such as *Atf4*, ERS is also known to trigger global translation inhibition through the EIF2AK3/PERK pathway (Almanza et al., 2019). We therefore hypothesized that ERS may modulate LIVER-ID TF activities by inhibiting their translation. In line with this hypothesis, treatment of MPH with the EIF2AK3/PERK signaling inhibitor ISRIB dampened loss of NR1H4 after 1h of ERS (Fig.5D-E). Since translational inhibition could not alone account for acute ERS-induced LIVER-ID TF loss, and since ERS may modulate TF activities by inducing their degradation as shown for FOXO1 (Zhou et al., 2011) and CREB3L3 (Wei et al., 2018), we investigated a role for proteasomal degradation in LIVER-ID TF loss. We observed that treatment with the proteasome inhibitor MG132 blunted repression of LIVER-ID TFs, especially that of HNF4A, in MPH subjected to 1h of ERS (Fig.5F-G and Appendix Fig.S18A). Since proteasomal degradation of HNF4A can be induced by the SRC kinase (Chellappa et al., 2012) following liver PHx (Huck et al., 2019) and since ERS has been reported to activate SRC through its interaction with ERN1/IRE1a in HeLa cells (Tsai et al., 2018), we monitored SRC activation in MPH subjected to ERS using phosphorylation levels of SRC at Y416 (p-Y416-SRC) as a marker. We found that ERS leads to SRC activation in MPH, which could be prevented by treatment with its inhibitor PP2 (Fig.5H). Importantly, this was associated with a dampening of ERS-mediated degradation of HNF4A (1h after ERS induction) (Fig.5F and I and Appendix Fig.S18B) and of subsequent (4h after ERS induction) LIVER-ID TF gene repression (Fig.5J).

These data indicate that ERS triggers loss of hepatic identity through a global impairment of LIVER-ID TF expression/activities, involving EIF2AK3/PERK and SRC-dependent rapid decrease in their protein levels.

Sustained loss of LIVER-ID genes and concomitant induction of ERS gene expression in

dysfunctional mouse and human livers

To assess whether similar responses occur upon acute liver injury, we performed experiments on injured/dysfunctional livers of mice subjected to bacterial injection (sepsis^{BIM} model) (Paumelle et al., 2019). Our results show that sepsis triggers profound alterations in the liver transcriptome (Appendix Fig.S19A) compatible with loss of hepatic molecular identity (Fig.6A compared to 1C). Indeed, sepsis also decreased expression of LIVER-ID genes (Fig.6B and Appendix Fig.S19B-F), concomitant with an enrichment for ERS UP genes among the most strongly upregulated genes in septic mouse livers (Fig.6C). Similar observations were made when mining the transcriptomic response occurring in other mouse models of liver damage including drug-induced liver injury (Appendix Fig.S20). Overall, impaired LIVER-ID gene expression in injured livers was linked to partial hepatic dedifferentiation as judged using principal component analysis (Fig.6D). Indeed, the transcriptome of injured livers resembles more that of newborn livers than that of mature adult livers, in line with postnatal liver maturation being linked to significant transcriptomic changes (Fig.1N) (Bhate et al., 2015, Peng et al., 2017).

Further mining the transcriptional changes induces by sepsis, we observed that genes significantly modulated by ERS in MPH (from Fig.1) showed a similar regulation pattern in liver (Fig.6E, Appendix Fig.S21A-B) or purified hepatocytes (Appendix Fig.S21C-E) from septic mice. Importantly, LIVER-ID TF expression was globally compromised (Fig.6F-G and Appendix Fig.S21F-G), accompanied by a switch in expression of the PAR-bZIP TF family members (Appendix Fig.S22A) and reduced expression of genes involved in xenobiotic metabolism (Appendix Fig.S22B). Pre-treatment of septic mice with the ERS inhibitor tauroursodeoxycholic acid (TUDCA) blunted ERS and displayed hepatoprotective effects, as indicated by reduced XBP1S (Fig.6H-I and Appendix Fig.S22D) and decreased levels of circulating liver serum aminotransferases (Fig.6J), respectively. Interestingly, TUDCA concomitantly allowed to protect from a general loss of LIVER-ID TF expression (Fig.6H-I and Appendix Fig.S22D-E), pointing to the functional link between ERS and loss of LIVER-ID gene expression in injured liver.

To monitor ERS and LIVER-ID gene expression upon liver recovery, we made use of a second sepsis mouse model (denoted sepsis^{CLP}), which combines caecal ligation and puncture to induce sepsis with intravenous fluid resuscitation in order to mimic the clinical setting encountered in intensive care units (ICUs) (Derde et al., 2017). Indeed, this model allows an assessment of transcriptional changes in both the acute and post-acute resolutive phase (3 days after CLP) of liver injury (Thiessen et al., 2017). ERS gene upregulation and LIVER-ID TF repression, together with a switch in PAR-bZIP TF expression, was observed in the acute phase of sepsis (10h after CLP) (Fig.7A and Appendix Fig.S22F). At later time points, transcriptional changes were blunted with most genes returning to near baseline levels 3 days after CLP (Fig.7A). Hence, reminiscent of liver regeneration following PHx, loss of molecular identity together with ERS gene induction transiently co-occur in the mouse liver upon sepsis. This indicated that ERS resolution was phased with recovery of the LIVER-ID program. To further assess the functional relationship between recovery from ERS and loss of liver identity, we mined mouse liver transcriptomic data obtained from tunicamycin-injected WT or *Atf6*$^{-/-}$ (Atf6 KO) mice, the latter being characterized by an inability to resolve ERS (Arensdorf et al., 2013). Indeed, while ERS UP genes have returned to baseline levels 34h after ERS in WT mice, their decreased expression is only partial in *Atf6*$^{-/-}$ mice leading to sustained ERS UP gene levels (Fig.7B). This was accompanied by a failure of ERS DOWN and LIVER-ID genes to fully return to baseline levels in *Atf6*$^{-/-}$ compared to WT mice (Fig.7C). This indicated that sustained ERS impedes re-establishment of the LIVER-ID program. To define if sustained loss of LIVER-ID gene expression is linked to liver dysfunction, we mined transcriptomic data from hepatocyte-specific HNF4A KO mice subjected to PHx, since these mice fail to recover ultimately leading to their death (Fig.7D) (Huck et al., 2019). Importantly, we found that this was linked to sustained downregulation of LIVER-ID genes and TFs 5 days after PHx (Fig.7D) at a time when the hepatic program is normally re-established (Fig.1A). These data therefore indicate that LIVER-ID TF re-expression is critically required to preclude detrimental consequences of liver injury.

Despite intense ICU care, septic patients frequently present with liver failure leading to their

death (Nesseler et al., 2012). Interestingly, livers from deceased septic humans displayed downregulation of LIVER-ID TF encoding genes and concomitant upregulation of ERS UP genes when compared to control donors (undergoing elective restorative rectal surgery) (Appendix Fig.S23A-B). Moreover, correlative analyses revealed that LIVER-ID TFs behave as a group of genes with strong positive correlation, which are overall inversely correlated with ERS UP genes (including *NFIL3*), in livers of septic humans (Fig.7E). To further assess whether loss of hepatic molecular identity might contribute to human liver dysfunction, we compared LIVER-ID TF gene expression levels between livers from deceased septic patients with serum bilirubin levels below (Bil<2) or above (Bil>2) 2mg/dL (i.e. the most commonly used cut-off in clinics to define liver dysfunction in septic patients (Vincent et al., 1996)). We observed a stronger overall decrease in LIVER-ID TF gene expression in the Bil>2 group (Fig.7F), differences being the most pronounced for *NR1I2/PXR* and *HLF* (Fig.7G). This was associated with a more pronounced switch in the expression of the PAR bZIP TF family in the Bil>2 group compared to the Bil<2 group (Appendix Fig.S23C). While ERS gene induction was present in the two groups, *DDIT3/CHOP* was only upregulated in the Bil>2 group, suggestive of a more severe ERS and/or of activation of additional detrimental signaling pathways which would add up to ERS in patients with liver dysfunction (Fig.7H).

Altogether, these data indicate that sustained loss of LIVER-ID TF expression linked to persistent ERS gene induction is detrimental to liver function recovery, which may relate to liver dysfunction in septic patients.

DISCUSSION

ERS had previously been shown to repress a handful of genes involved in liver metabolic functions (Chikka et al., 2013). Here, we have redefined the paradigm related to acute ERS-induced changes in the liver by pointing to a more global loss of molecular identity and partial hepatic dedifferentiation, which we found to be characteristic of acute liver injury. As discussed hereafter and detailed in Fig.8A, loss of LIVER-ID gene expression results from several ERS-induced

signaling pathways, consistent with signalling from the different sensors of ERS being activated in liver injury (Wang et al., 2020) and functionally intermingled (Fig.5 and Appendix Fig.S24) (Brewer, 2014). Importantly, the relevance of our findings is indicated by several lines of evidence defining chemically-induced ERS as appropriate for the study of pathophysiological ERS-induced transcriptional regulations. First, repression of LIVER-ID genes was observed both with tunicamycin and thapsigargin, ruling out any drug-specific artifact (e.g. Appendix Fig.S3G). Second, this repression was readily linked to ERS and not any other potential drug-related effect as it was blunted by *i)* cycloheximide (Appendix Fig.S25A), which, by inhibiting protein synthesis, alleviates ERS and decreases UPR gene expression (Harding et al., 2000) ; *ii)* the chemical chaperone PBA (Fig.2G) ; and *iii)* inhibitors of the different ERS sensors (Fig.5D-E and Appendix Fig.S24). Third, chemically-induced ERS recapitulated both induction of the different arms of the UPR (Fig.1L-M and 6F) and the overall preferential downregulation of LIVER-ID genes observed in injured liver (Fig.1,6 and Appendix Fig.S19C-F). Fourth, this repression of LIVER-ID genes was not artificially linked to strong chemically-induced ERS. Indeed, dose-response experiments showed that ERS-mediated repression was proportional to the ERS intensity, i.e. not requiring maximal ERS response (Appendix Fig.S25B). Moreover, induction of *Klf9*, recently described as a marker of strong ERS (Fink et al., 2018), was not stronger in the chemically-induced ERS models (Appendix Fig.S25C). Fifth, inhibition of SRC kinase prevents HNF4A degradation both following acute ERS (Fig.5F,I and S18) and liver PHx (Huck et al., 2019).

In addition to translation inhibition induced by EIF2AK3/PERK, our study points to Initial loss in LIVER-ID TF expression involving ERS-mediated proteasomal degradation events. In particular, we report a role for SRC kinase mediated proteasomal degradation of HNF4A. These findings, which are in contrast with a previous study suggesting that HNF4A protein levels were not modulated by ERS (Arensdorf et al., 2013), are of importance when taking into account HNF4A's requirement for maintaining/establishing the LIVER-ID TF network and hepatocyte identity (Fig.7D) (Huck et al., 2019, Lau et al., 2018, Thakur et al., 2019). Additional mechanisms directing LIVER-ID TFs towards

degradation most probably co-occurs such as those triggered by interaction with XBP1S (Zhou et al., 2011). More generally, our findings are however in line with a recent study indicating that targets of endoplasmic reticulum-associated protein degradation also include TFs and epigenetic regulators (Wei et al., 2018). Loss of LIVER-ID TF expression is further amplified by their transcriptional downregulation being linked to their organization as an interdependent transcriptional network where LIVER-ID TF encoding genes form auto- and cross-regulatory loops (Appendix Fig.S16) (Fig.8A). The hepatic TF network increases in complexity and stability during development making LIVER-ID TF gene expression more robust to alterations in single TF expression/activity in the adult liver (Kyrmizi et al., 2006). Our finding that deletion of HNF4A dramatically impacts re-expression of the other LIVER-ID TFs involved in termination of liver regeneration following PHx (Fig.7D) indicates that liver stress/injury decreases the hepatic core TF network robustness. This is most probably linked to the global loss of LIVER-ID TF expression jeopardizing cross-regulatory loops therefore rendering hepatocytes more sensitive to loss of activities of individual TFs (Felix & Barkoulas, 2015, Gjuvsland et al., 2007). ERS-induced transcriptional downregulation of LIVER-ID TFs/genes involves decommissioning of BRD4 at LIVER-ID TF densely co-bound CRMs organized into SE. Importantly, this implies that not all LIVER-ID genes are equally sensitive to ERS-mediated repression defining partial hepatic dedifferentiation as being linked to preferential repression of highly expressed SE-associated LIVER-ID genes. TF recruitment complexity and SE have both been positively associated with particularly strong activity of regulatory regions important for cell identity (Santiago-Algarra et al., 2017, Whyte et al., 2013). In this context, we show that a widespread decrease in LIVER-ID TFs accounts for the breadth of detrimental transcriptional effects of ERS/liver injury on hepatic molecular identity.

Contrary to a recent study suggesting that BRD4 is required for establishment but not maintenance of cell identity (Lee et al., 2017), and in line with other previous reports (Di Micco et al., 2014), our work indicates a role for BRD4 in maintenance of mature hepatocyte molecular identity. ERS-induced loss of hepatic molecular identity is accompanied by BRD4 redistribution towards ERS

gene regulatory regions. Competition for transcriptional resources has been proposed to rule transient transcriptional adaptations to environmental disturbances in a model referred to as transcriptional ecosystem (Silveira & Bilodeau, 2018). In line, we have found that stressed/injured liver requires to enhance expression of an exceptionally large spectrum of genes, which may trigger hepatocytes to temporarily decommission highly active regulatory regions to supply the required transcriptional resources (Fig.8A-B). Squelching (competition between TFs for limited cofactor amounts) has been proposed, but never firmly proven, to be a driving force in cofactor redistribution responsible for trans-repression (Schmidt et al., 2016). This was for instance suggested as an explanation for transcriptional repression induced by tumor necrosis factor (Schmidt et al., 2015). In the context of acute ERS, our study points to a cascade of molecular events described here above involving early loss of LIVER-ID TF expression/activities, indicating repression of LIVER-ID gene expression does not rely *per se* on squelching i.e. ERS TFs competing off BRD4 binding from fully active LIVER-ID TFs. Together with the role of NFIL3, our data rather indicate that ERS-mediated repression is an active process and not an indirect consequence of ERS gene induction. While squelching on its own cannot explain loss of LIVER-ID gene expression, our data do not entirely rule out that competition for BRD4 might further contribute to LIVER-ID gene downregulation.

Our data using several models of liver injury and genetically deficient mice have established that the hepatic and ERS transcriptional programs are in competitive equilibrium with direct relevance towards the liver's ability to recover from injury. Indeed, while transient loss of hepatic molecular identity is linked to stress/injury handling, detrimental effects occur if the hepatic transcriptional program cannot be re-established. In line with loss of LIVER-ID TF expression being instrumental in triggering liver injury, forced hepatic expression of HNF4A or FOXA2 has been shown to be protective (Huck et al., 2019, Wang et al., 2017). Predictive models of transcriptomic regulation where alternative programs are in competitive equilibrium postulate that cessation of environmental disturbances would allow cells to restore their normal transcriptional program as the default one (Silveira & Bilodeau, 2018) (Fig.8B). The kinetic and feedback mechanisms allowing re-establishment

of the hepatic identity upon recovery from liver injury remain to be fully defined but critically require LIVER-ID TFs (re-expression (Fig.7A-D). Interestingly, ERS-induced loss of molecular identity is not restricted to the liver (Appendix Fig.S26 and Table EV4), but whether this mechanism is globally involved in organ repair and/or dysfunction beyond liver remains to be defined. The mechanisms leading to organ dysfunction in sepsis are still incompletely understood. Cell death has been ruled out as a potential main contributor (Takasu et al., 2013). In this context, our results obtained from the livers of deceased septic patients point to sustained loss of LIVER-ID TFs as a likely contributor to human liver dysfunction (Fig.8B). Switch in expression of the PAR-bZIP family members may relate to compromised xenobiotic metabolism associated with poor outcome in treated critically-ill septic patients (Gachon et al., 2006, Woznica et al., 2018) while loss of PPARA may impede liver's ability to adapt its metabolic activities during sepsis (Paumelle et al., 2019). While our data indicate that acute ERS directly represses LIVER-ID gene expression (events occurring in MPH in the absence of detectable activation of regulatory regions involved in the hepatic inflammatory response (Appendix Fig.S27)), additional signals including inflammatory cytokines (Brown et al., 2014) most probably combine with ERS during sepsis to trigger the exceptionally large alterations to the hepatic transcriptional equilibrium we observed in this condition.

MATERIALS AND METHODS

Cell culture

The immortalized mouse hepatocyte cell-line AML12 was obtained from ATCC (CRL-2254) and cultured as previously described (Ploton et al., 2018). Mouse primary hepatocytes (MPH) were prepared from livers of 10 weeks-old male C57BL/6J mice (Charles River) as described in (Bantubungi et al., 2014) and grown on collagen-coated plates in serum-free William's medium (Ploton et al., 2018). Non-parenchymal cells (NPC) from the same livers were obtained by differential centrifugation. Briefly, liver homogenates obtained after perfusion were pressed through a 70 µm cell strainer and centrifugated for 5 min at 27g. Pellets from this first centrifugation were washed and

centrifuged twice again for 5 min at 27g to obtain the MPH fraction. Supernatants from the first centrifugation were collected and centrifuged for 5 min at 400g to obtain the NPC fraction. Separation of MPH and NPC was confirmed by monitoring expression of selected marker genes (Appendix Fig.S2D). Acute endoplasmic reticulum stress (ERS) treatment in MPH is defined as 4h treatment with 1µM thapsigargin. Vehicle (0.04% DMSO) was used as control. In all figures from this study, ERS in MPH is defined as 4h treatment with 1µM thapsigargin unless indicated otherwise (shorter or longer treatment times with different concentrations were also used in some experiments as specifically indicated in the figures and their legends). Experiments involving MZ1 or JQ1 were performed by pre-treating MPH for 3h with 0.01, 0.1 or 1µM MZ1 or 1h with 500nM JQ1 before addition of 1µM thapsigargin for 4h. Experiments involving C646 were performed by co-treating MPH with 5, 10 or 20µM C646 and 1µM thapsigargin for 4h. Experiments involving trichostatin A were performed by co-treating MPH with 1µM trichostatin A and 1µM thapsigargin for 4h. Experiments involving cycloheximide were performed by co-treating MPH with 0, 1 or 10µg/mL cycloheximide and 1µM thapsigargin for 4h. Experiments involving PBA, ISRIB, MG132 or PP2 were performed by pre-treating MPH for 30 min with 5mM PBA, 1µM ISRIB, 10µM MG132 or 10µM PP2 before addition of 1µM thapsigargin for 1h or 4h. Experiments involving inhibitors of the three arms of the UPR were performed by pre-exposing AML12 cells to 30µM STF083010, 200µM ISRIB or 100µM AEBSF for 2h and subsequently treating them for 4h with 1µM thapsigargin or 2µg/mL tunicamycin.

Fluorescence activated cell sorting (FACS)-isolated hepatocytes were obtained by directly running the MPH fraction into an Influx sorter (Becton Dickinson) equipped with a 200 µm nozzle and tuned at a pressure of 3.6 psi and a frequency of 6.3 kHz. Sample fluid pressure was adjusted to reach an event rate of 2000 events/second. Hepatocytes were identified as FSChi SSChi events and sorted on a “pure” mode with 80% sorting efficiency.

HEK293 cells were grown as in (Ploton et al., 2018) and transfected using jetPEI (Polyplus Transfection) according to the manufacturer’s instructions.

Chemicals

All chemicals used in this study are provided in the Reagents and Tools table.

Animal experiments

Male C57BL/6J wildtype (WT) mice were purchased from Charles River at 8 weeks of age and housed in standard cages in a temperature-controlled room (22-24°C) with a 12h dark-light cycle. They had *ad libitum* access to tap water and standard chow and were allowed to acclimate for 2 weeks prior to initiation of the experimental protocol. ERS was induced by intraperitoneal injection of tunicamycin using 1 µg/g mouse *body* weight (Sigma-Aldrich, #T7765) or vehicle (150 mM dextrose) and liver was collected 8h later (5 mice per group). The *Nfil3*$^{-/-}$ (NFIL3 KO) mice used in this study (C57BL/6J background) were previously described (van der Kallen et al., 2015). WT littermates were used as controls. Mice of 10 weeks of age were treated with tunicamycin or vehicle as described above and liver was collected 8h after injection (8 mice per group). To induce ERS in muscle, 30 µg tunicamycin was injected intramuscularly into the gastrocnemius muscle. The contralateral leg was injected with a saline solution and used as control. Muscles were collected 24h after injection (9 mice per group).

Two different models of sepsis were used. For the bacterial injection model (BIM) of sepsis (sepsis^{BIM}), mice were injected intraperitoneally with 8×10^8 CFU of live *E. coli* (DH5α) bacteria or PBS (controls) and liver was collected 16h later (6 mice per group). In a separate experiment, mice were pre-treated for 4 consecutive days with tauroursodeoxycholic acid (TUDCA) (intraperitoneal injection of 500 mpk/day) or vehicle (PBS) followed by bacterial injection 2h after the last TUDCA administration on the fourth day (10 mice per group), and sacrificed 6h after bacterial injection which is sufficient to induce LIVER-ID TF loss (Appendix Fig.S22C). For the caecal ligation and puncture (CLP) model of sepsis (sepsis^{CLP}), male C57BL/6J wildtype mice of 24 weeks of age were randomly allocated to sepsis^{CLP} or healthy pair-fed control and sacrificed after 10h, 30h or 3 days (15 mice per group per timepoint). Mice in the sepsis^{CLP} groups were subjected to single-puncture CLP followed by intravenous fluid resuscitation as previously described (Derde et al., 2017). Briefly, mice were anesthetized, a catheter was inserted in the central jugular vein and the surgical CLP procedure

was performed (50% ligation of the caecum at half the distance between the distal pole and the base of the caecum and a single puncture through-and-through) followed by intravenous fluid resuscitation. They received pain medication and antibiotics 6 hours after CLP and from then on every 12 hours for the remainder of the experiment and mice of the "day 3" group (prolonged phase) received parenteral nutrition from the morning after surgery to mimic the human clinical situation. The data reported for the sepsis^{CLP} design correspond to the 10h time point (acute phase) unless indicated otherwise. Healthy pair-fed mice were used as control.

All animal studies were performed in compliance with EU specifications regarding the use of laboratory animals and approved by the Nord-Pas de Calais Ethical Committee (for ERS treatments and the sepsis^{BIM} design) or the KU Leuven Ethical Committee (P093/2014) (for the sepsis^{CLP} design).

Biochemical analyses

Plasma aspartate aminotransferase (AST) and alanine aminotransferase (ALT) activities were determined by colorimetic assays (Thermo Fischer Scientific) using serum obtained following retro-orbital blood collection.

Real-time quantitative PCR analyses of gene expression

RNA extraction, reverse transcription and real-time quantitative PCR (RT-qPCR) were performed as previously described (Dubois-Chevalier et al., 2017). The primer sequences are listed in Table EV5. All primers were designed to hybridize to different exons, and generation of single correct amplicons was checked by melting curve dissociation. Murine gene expression levels were normalized using hypoxanthine guanine phosphoribosyl transferase (*Hprt*) (sepsis^{CLP} experiments) or cyclophilin A (*PPia*) (all other experiments) housekeeping gene expression levels as internal control. Human gene expression levels were normalized using 18S ribosomal RNA (*RNA18S5*). For gene expression analyses, *in-vitro* experiments (AML12 and MPH) were repeated at least three times (independent experiments), each experiment being performed in technical triplicates. For *in-vivo* mouse studies, we used at least 5 animals per experimental condition (genotype or treatment). The number of biological replicates is indicated in the figure legends.

Gene expression microarrays

RNA was extracted from MPH treated for 4h with 1 µM thapsigargin (3 independent experiments), livers of NFIL3 KO and WT littermates treated for 8h with 1 µg/g tunicamycin (5 mice per genotype per treatment) or gastrocnemius muscles of WT mice treated for 24h with 30 µg tunicamycin (treated and contralateral control muscles from 9 mice) and was checked for quantity and quality using the Agilent 2100 Bioanalyzer (Agilent Biotechnologies) before being processed for analysis using MoGene-2_0-st Affymetrix arrays according to the manufacturer's instructions. Data were analyzed as described hereafter and have been submitted to GEO under accession number GSE122508.

Transcriptomic data analyses

Liver-specificity index

The liver-specificity index was calculated as the difference of normalized expression in liver and mean of normalized expression in control tissues using data from BioGPS (Table EV6).

Normalization of microarrays and identification of differentially expressed genes

Raw transcriptomic data from Affymetrix microarrays were normalized with Partek Genomics Suite 6.6 using background correction by Robust Multi-array Average (RMA), quantile normalization and summarization via median-polish. Principal component analyses (PCA) were used for quality control of the data. RMA values were also used to display expression changes for selected gene sets in different figures. Differential expression analyses were performed at probeset level with Partek Genomics Suite. Dysregulated genes were defined taking into account any potential factor interaction in the original experimental design and using a Benjamini–Hochberg corrected p-value cut-off (FDR) set at 0.05.

Single-cell RNA-seq data analyses

Raw counts from single-cell transcriptomic data (447 cells from E10.5 to E17.5) (Yang et al., 2017) were normalized by estimation of library size factor with DESeq 1.26.0 (Anders & Huber, 2010) according to (Brennecke et al., 2013). PCA was performed on normalized data using FactoMineR 1.41

(Lê et al., 2008). Then the average expression of ERS DOWN or ERS UP genes was projected for each cell on 2D PCA plot.

Identification of preferential patterns of gene expression following partial hepatectomy

Genes with different temporal expression profiles were identified using the Short Time-series Expression Miner (STEM v1.3.11) (Ernst et al., 2005), which fits dynamic patterns of gene expression to model profiles. Normalized gene expressions (rpkm) were obtained from (Rib et al., 2018) and average expression from replicates was used. Parameters were set at “Log normalize data”, 4 for “max unit change in model profiles between time points”, -0.05 for “minimum absolute expression change” and FDR for “Correction method”.

Comparison of the breadth of transcriptomic changes occurring in the mouse liver

To make fold-changes comparable with those obtained using RNA-seq, microarray data were normalized using the Affymetrix Power Tool (Thermo Fisher Scientific) run through the GIANT tools suite (Vandel et al., 2018) on a local instance of Galaxy (Afgan et al., 2018). Normalization was set to “scale intensity + rma” and normalization level to “probeset”. Normalized expression values retrieved for the studies which used RNA-seq (Table EV6) were Log_2-transformed. For each dataset, a single expression value per gene was defined using gene symbols as identifiers and by averaging values obtained from replicates. Fold-changes (Log_2) were next computed on scaled data, which were obtained using the scale function of the « graphics » R package (R_Core_Team, 2015) on each dataset separately. This was performed using global mean (mean of all expression values under all conditions of interest in a given study) for “center” parameter and global standard deviation for the “scale” parameter. Only genes common to all analysed datasets were considered for subsequent analyses and, for each dataset, the bottom 20% genes with lowest expression in the liver were discarded. Bagplots were drawn using the "bagplot" function of the “aplpack” (v1.3.2) R package using default parameters (R_Core_Team, 2015). Bagplots are bivariate boxplots showing the spread of the data using a “bag” containing 50% of the data points with the largest depth (around the median) and its extension by a “loop” whose limit exclude outliers (Rousseeuw et al., 1999).

Comparison of the transcriptome of injured livers with that of the developing mouse liver

Transcriptomic data of liver injuries were pooled and batch effects were corrected with the "ComBat" function of the "sva" R pakage (Leek et al., 2019) using the mouse liver differentiation study as the batch of reference (see Table EV6 for details regarding used datasets). Parameters were set to "mean.only=T" and "par.prior=T". Each study was defined as a different batch where the control condition (i.e. non-injured livers) was matched to the adult liver stage of the reference dataset. Next, a PCA was computed only on the mouse liver differentiation study with the "PCA" function of FactomineR (Lê et al., 2008) (using "scale.unit=F"). Liver injury studies were considered as supplemental individuals. Finally, the first principal component (representing 63.55% of the variability of the mouse liver differentiation study) was plotted and used to project the liver injury studies. Data corresponding to prenatal mouse livers were used in the analyses but were discarded for data visualization.

Functional enrichment analyses

Functional enrichment analyses were performed using the ToppGene Suite (Chen et al., 2009). KEGG Pathways with Bonferroni-corrected p-value $<10^{-3}$ and Gene Ontology (GO) Biological Processes with Bonferroni-corrected p-value $<10^{-6}$ were considered and similar terms were merged.

Gene set enrichment analyses

Gene set enrichment analyses (GSEA) were performed using the GSEA software (v3.0) developed at the Broad Institute (Subramanian et al., 2005). We used 1000 gene-set permutations and the following settings: "weighted" as the enrichment statistic and "difference of classes" as the metric for ranking genes. Ranking was performed by the GSEA software using the average expression value per gene when multiple probesets were present in the microarray. In addition to enrichment plots, figures also provide NES and FDR, which are the normalized enrichment score and the false discovery rate provided by the GSEA software, respectively. In experiments with multiple conditions, the BubbleGUM tool (GSEA Unlimited Map v1.3.19) (Spinelli et al., 2015) was used to integrate and compare numerous GSEA results with multiple testing correction. Non-oriented GO term enrichment

analyses were performed using the ‘‘MousePath_GO_gmt.gmt’’ set of genes from the Gene Set Knowledgebase (GSKB) (Lai et al., 2016).

Chromatin Immunoprecipitation

MPH (3 x 10^6 cells) were fixed for 30 min at room temperature with disuccinimidyl glutarate followed by a 10 min incubation with 1% formaldehyde and a 5 min incubation with 125 mM glycine. After two washes with ice-cold PBS, cells were scraped in PBS, pelleted by centrifugation at 400g for 5 min, resuspended in Lysis Buffer (50 mM Tris-HCl pH 8.0, 10 mM EDTA, 1% SDS and 1x PIC from Roche) and sonicated for 4 min (4 cycles 30 sec ON / 30 sec OFF using Bioruptor Pico from Diagenode). Mouse liver (200 mg of tissue) was cut in small pieces in ice-cold PBS, pressed through a 70 µm cell strainer followed by a few passages through a 18G needle. Fixation, lysis and sonication were performed as described for MPH. Chromatin (50 µg for H3K27ac ChIP and 200 µg for BRD4 ChIP) was diluted 10-fold in Dilution Buffer (20 mM Tris-HCl pH 8.0, 1% Triton X-100, 2 mM EDTA, 150 mM NaCl) and incubated overnight with 2 µg of H3K27ac antibody (Active Motif, #39685) or 3 µg of BRD4 antibody (Bethyl Labs, #A301-985A100) at 4°C. The next day, A/G sepharose bead mix (GE Healthcare) was added during 4 hours at 4°C in presence of 70 µg/mL yeast tRNA (Sigma-Aldrich). Beads were washed three times with RIPA buffer (50 mM HEPES pH 7.5, 1 mM EDTA, 0.7% Na Deoxycholate, 1% NP40 and 500 mM LiCl) containing 10 µg/mL yeast tRNA and once with TE buffer (10 mM Tris-HCl pH 8.0, 1 mM EDTA). DNA was then eluted in 100 mM $NaHCO_3$ containing 1% SDS and incubated overnight at 65°C for reverse-crosslinking. DNA purification was performed using the MinElute PCR purification kit (Qiagen, #2800) and samples were subjected to qPCR analyses. The primer sequences are listed in Table EV5.

H3K27ac ChIP and input samples from MPH treated for 4h with 1 µM thapsigargin or vehicle (0.04% DMSO) from 3 independent experiments were additionally sent for sequencing on an Illumina Hi-seq 4000 as single-end 50-base reads according to the manufacturer’s instructions. Data were analyzed as described hereafter and have been submitted to GEO under accession number GSE122508.

ChIP-seq data analyses

ChIP-seq data quality control and uniform reprocessing including mapping to the mm10 version of the mouse genome and signal normalization have been described in (Dubois-Chevalier et al., 2017) except Bowtie 2 (sensitive mode) (Langmead et al., 2009) was used for the BRD4 ChIP-seq analyses. ChIP-seq data were visualized using the Integrated Genome Browser (IGB 9.0.1) (Freese et al., 2016).

Broad H3K4me3 domain identification and identity gene definition

H3K4me3 ENCODE ChIP-seq data from several mouse tissues (Shen et al., 2012) (Table EV6) were used to call broad H3K4me3 enriched regions using MACS2 as described in (Chen et al., 2015). Broad H3K4me3 domains were defined as those spanning more than 3 times the median size of all H3K4me3 enriched regions in a given tissue. Broad H3K4me3 domains from mouse liver were separated into liver-identity (LIVER-ID) domains, which were defined as broad H3K4me3 domains specific to liver (i.e. detected in less than 25% of other analysed tissues), and in ubiquitous (UBQ) domains. LIVER-ID and UBQ domains were then assigned to genes according to overlapping TSS from the GENCODE (M9) database (Frankish et al., 2019), resulting in 621 LIVER-ID genes and 657 UBQ genes which are listed in Table EV1. TFs within these gene lists were subsequently obtained using comparison with mouse TFs listed in the Animal TFDB 2.0 (Zhang et al., 2015). Muscle-identity (MUSCLE-ID) and UBQ genes, listed in Table EV4, were defined in a similar way using H3K4me3 ChIP-seq data from the ROADMAP consortium processed by (Chen et al., 2015). Human to mouse gene name conversion was performed using the dbOrtho tool from bioDBnet (Mudunuri et al., 2009).

Super-enhancer identification

To define BRD4 super-enhancers (SE), we first used MACS2 to identify enriched peaks (Effective genome size = 2150570000, Band Width = 300, mfold = 5 to 50, FDR (q-value) = 0.05, Max duplicate tags at the same location = 1) using mapped reads previously filtered to remove duplicates and reads mapping to false-positives regions we had identified in (Dubois-Chevalier et al., 2017). SE were identified by applying Rank Ordering of Super-Enhancers (ROSE) (Loven et al., 2013, Whyte et

al., 2013) on the BRD4 peak-calling results using mouse liver ChIP-seq inputs (GSE26345) as control (setting: -s 12500, -t 0).

Identification of changes in H3K27ac induced by acute ERS

Regions with significant changes in H3K27ac ChIP-seq signals induced by ERS were identified using csaw 1.6.1 (Lun & Smyth, 2014, Lun & Smyth, 2016). Mapped reads were previously filtered to remove duplicates and reads mapping to ENCODE blacklisted regions (Encode_Project_Consortium, 2012) or mouse ChIP-seq false-positives regions we had identified in (Dubois-Chevalier et al., 2017). The command lines and full list of used parameters are provided in Computer Code EV1. Briefly, the genome was binned and reads counted, bins with background level signal as defined using input samples were discarded before normalization using a loess regression. Finally, after dispersion estimation with the function estimateDisp, a paired-differential analysis was performed on this filtered and normalized data using glmQLFit. Bins overlapping H3K27ac peaks (broad regions called with MACS2 using a pool of all H3K27ac ChIP-seq datasets and inputs as control - parameters: q-val narrow = 0.001 and q-val broad = 0.01) were identified using findOverlaps from GenomicRanges 1.24.3 (Lawrence et al., 2013) (parameters : minoverlap=75, maxgap=0). Bins overlapping a single H3K27ac peak were combined using combineOverlaps and only merged bins with FDR ≤ 0.05 were considered (merged bins with FDR > 0.05 were defined as unchanged H3K27ac regions). The ratio of UP to DOWN bins in the merged regions was next calculated and H3K27ac UP or DOWN regions were defined as those having a ratio ≥ 2 or ≤ 0.5, respectively. Coordinates for H3K27ac UP, DOWN and unchanged regions are provided in Dataset EV1. The bigwig signals were computed using the loess normalized signal on each dataset and/or averaging the loess normalized signal between replicates. Genes were assigned to H3K27ac regions as follows. First, genes whose TSS from the GENCODE (M9) database (Frankish et al., 2019) directly overlaps H3K27ac regions were retrieved. In addition, distal H3K27ac were linked to potentially regulated genes using CisMapper (O'Connor et al., 2017) as previously described in (Dubois-Chevalier et al., 2017).

Analyses of transcriptional regulators recruited to regions with changes in H3K27ac induced by acute

ERS

In order to identify TFs whose binding is enriched in H3K27ac UP and H3K27ac DOWN regions, we used Locus Overlap Analysis (LOLA 1.4.0) (Sheffield & Bock, 2016) to compare TF binding within UP, DOWN and ALL (i.e. also including H3K27ac unchanged) regions. Mouse TF binding sites were retrieved from the Gene Transcription Regulation Database (GTRD) (http://gtrd.biouml.org/downloads/16.07/mouse_meta_clusters.interval.2017_03_10) (Yevshin et al., 2017). Inputs were discarded and ChIP-seq datasets were ascribed to TFs using nomenclature information provided by the authors. A heatmap of log odds ratio was generated using the heatmap.2 function of the R package "gplots" (v3.0.1) (Warnes et al., 2016) and hierarchical clustering using the hclust function of the R package "Stats" (using Euclidean distance and ward.D2 agglomeration method) (R_Core_Team, 2015). A list of the TFs of each cluster is shown in Table EV2.

H3K27ac UP, DOWN or unchanged regions were overlapped with *cis*-regulatory modules (CRMs) defined in (Dubois-Chevalier et al., 2017) based on co-binding of 47 transcriptional regulators in mouse liver. Combinatorial co-binding of transcriptional regulators at H3K27ac UP, DOWN or unchanged was analyzed using multidimensional scaling (MDS) analyses as described in (Dubois-Chevalier et al., 2017). Plots were performed with the smoothScatter function of the « graphics » R package (R_Core_Team, 2015) using a conserved color scale.

Public transcriptomic and functional genomic data recovery

Public data used in this study were downloaded from Gene Expression Omnibus (GEO) (http://www.ncbi.nlm.nih.gov/geo/) (Edgar et al., 2002), ENCODE (Yue et al., 2014), UCSC Genome Browser (Dreszer et al., 2012) or BioGPS (Mouse MOE430 Gene Atlas) (Wu et al., 2016) and are listed in Table EV6.

Human samples

Postmortem liver biopsies from patients admitted to the intensive care unit (ICU) of Leuven University Hospital with sepsis (n=64), who died after a median ICU stay of 10 days (IQR 6-20 days), were compared with matched patients undergoing elective restorative rectal surgery (n=18). Written

informed consent was obtained from the patients or their closest family member and from the volunteers. The study protocols and consent forms were approved by the KU Leuven Institutional Review Board (ML1094, ML1820, and ML2707). Bilirubin was quantified with use of a standard routine automated assay in the University Hospital Clinical Laboratory.

Protein extraction

Total extracts

MPH and AML12 cells were scraped in ice-cold PBS, pelleted by centrifugation at 400g for 5 min, lysed in Laemmli buffer 6x (175 mM Tris-HCl pH 6.8, 15% glycerol, 5% SDS, 300 mM DTT and 0.01% Bromophenol Blue) and sonicated for 10 minutes. Mouse liver was cut in small pieces in ice-cold PBS and pressed through a 70 µm cell strainer. The pellet obtained after centrifugation at 400g for 5 min was lysed and sonicated as described for MPH. Western blottings shown in this study were obtained using total cellular extracts unless indicated otherwise.

Nuclear extracts

MPH were scraped in ice-cold PBS, mouse liver was cut in small pieces in ice-cold PBS and pressed through a 70 µm cell strainer. Pellets were obtained by centrifugation at 400g for 5 min, lysed in Hypotonic Buffer (20 mM Tris-HCl pH 8.0, 10 mM NaCl, 3 mM MgCl2, 0.2% NP40 and 1x PIC from Roche) and incubated for 5 min at 4°C. Samples were centrifuged at 600g for 5 min at 4°C and supernatants constituted the cytoplasmic fraction. Nuclear pellets were lysed in Nucleus Lysis Buffer (25 mM Tris-HCl pH 8.0, 500 mM NaCl, 1 mM EDTA, 0.5% NP40 and 1x PIC from Roche). Hypotonic Buffer and Nucleus Lysis Buffer were supplemented with Phosphatase Inhibitor Cocktail (#P044 from Sigma-Aldrich) as well as with 5 mM Sodium Butyrate and 5 µM Trichostatin A for deacetylase inhibition. After incubation for 30 min at 4°C, samples were sonicated for 10 min and centrifuged at 16000g for 5 min at 4°C. Laemmli 6x was added to the supernatants which were used for Western immunoblotting.

Chromatin fraction

MPH were scraped in ice-cold PBS, pelleted by centrifugation at 400g for 5 min, lysed in

Buffer A (50 mM HEPES pH 7.5, 10 mM KCl, 1.5 mM MgCl2, 340 mM sucrose, 10% glycerol, 1 mM DTT and 1x PIC from Roche) and incubated for 10 min at 4°C. Samples were centrifuged at 1300g for 5 min at 4°C and supernatants were discarded. Nuclear pellets were washed with Buffer A and subsequently lysed in solution B (3 mM EDTA, 0.2 mM EGTA, 1 mM DTT and 1x PIC from Roche). After incubation for 30 min at 4°C, samples were centrifuged at 1700g for 5 min at 4°C and supernatants were discarded. Chromatin pellets were washed with solution B, resuspended in Buffer C (50 mM Tris-HCl pH 8.0, 1 mM MgCl2 and 83 U/µL benzonase) and incubated for 20 min at 4°C. Laemmli buffer 6x was added before loading for Western immunoblotting.

Plasmids and *in-vitro* transcription and translation

The pcDNA3.1-mNFIL3 (Addgene 34572) and pSGG5-hHNF4A constructs were used for *in-vitro* transcription and translation (*in-vitro* TNT) using the TnT® Quick Coupled Transcription/Translation System (Promega).

Western immunoblotting

Western blot assays (WB)

One hundred µg of proteins were separated by 10% SDS-PAGE and immunodetected by Western immunoblotting using the primary antibodies listed in the Reagents and Tools table. Primary antibodies were detected using HRP-conjugated secondary antibodies (Sigma-Aldrich). Images were acquired using a G-box (Syngene, Cambridge UK) or using the iBright™ CL1500 Imaging System (Thermo Fisher Scientific). Quantifications were performed using Image Studio Lite v5.2 (LI-COR Biosciences, Lincoln, USA) and band intensities were defined using the signal value (sum of the pixel intensity in a shape minus the background value).

Simple Western immunoassays (WES)

Simple Western size-based assays were run on a WES system as recommended by the manufacturer (ProteinSimple, San Jose, USA). Protein concentrations ranged from 0.25 to 0.8 µg/µL depending on the target protein. Primary antibodies are listed in the Reagents and Tools table. Secondary antibodies were provided by the manufacturer (PS-MK14 and PS-MK15, ProteinSimple).

Data were analyzed using the Compass software (ProteinSimple). Quantifications were obtained using the area under the peak of the protein of interest.

Co-immunoprecipation assays

MPH cells were resuspended into hypotonic buffer (20 mM Tris-HCl, pH 7.5, 10 mM NaCl, 3 mM MgCl2, 0.2% NP40 and protease inhibitors) and the pellet was lysed for 30 min. After 10 min sonication (30 s on/off cycles with a Bioruptor (Diagenode) and centrifugation, 500 µg nuclear proteins from the soluble fraction were diluted with two volumes of a buffer containing 25 mM Tris-HCl pH7.5, 1 mM EDTA, 1.5 mM MgCl2 and incubated overnight with 2 µg of p300 antibody (Active motif, #61401) or control mouse IgG (sc-2025, Santa Cruz). Samples were then incubated for 4h with magnetic beads (Life technologies) previously blocked with 5 mg/ml of serum albumin bovine and washed 4 times using ice-cold washing buffer containing 25 mM Tris-HCl pH7.5, 150 mM NaCl, 1 mM EDTA, 0.2% NP40 and protease inhibitors. Beads were finally eluted in Laemmli buffer 6x.

Statistical analyses

Statistical analyses were performed using the Prism software (GraphPad, San Diego, CA) and R (R_Core_Team, 2015). The specific tests and corrections for multiple testing which were used as well as the number of samples per condition are indicated in the figure legends. In all instances, statistical significance was considered to be reached when p-values were below 0.05, which was indicated by * or $^{\#}$. All bar graphs show means ± SD (standard deviations). Box plots are composed of a box from the 25th to the 75th percentile with the median as a line and min to max as whiskers.

DATA AVAILABILITY

The datasets produced in this study are available in the following databases:

- Chip-Seq data: Gene Expression Omnibus GSE122613 (https://www.ncbi.nlm.nih.gov/geo/query/acc.cgi?acc=GSE122613)
- Transcriptomic data: Gene Expression Omnibus GSE122508 (https://www.ncbi.nlm.nih.gov/geo/query/acc.cgi?acc=GSE122508).

ACKNOWLEDGEMENTS

The authors acknowledge O. Molendi-Coste, A. Grenon, F. Firmin, C. Mazuy, X. Maréchal, A. Berthier, D. Sanchez-Lopez, O. Briand, B. Derudas, J. Vandel, L. L'homme (INSERM U1011, Lille, France), Lieselotte Thoolen (Amsterdam Animal Research Center, VU University Amsterdam, The Netherlands) and Shwu-Yuan Wu (University of Texas Southwestern Medical Center, Dallas, USA) for technical assistance and J. Dubois for administrative support. The authors also thank Lei Yin (University of Michigan Medical School, USA), L. Dubuquoy (INSERM U995, Lille, France) and Lies Langouche (KU Leuven, Belgium) for helpful discussions. This work was supported by grants from the Fondation pour la Recherche Médicale (Equipe labellisée, DEQ20150331724), "European Genomic Institute for Diabetes" (E.G.I.D., ANR-10-LABX-46) and European Commission. B.S. is supported by the European Research Council (ERC Grant Immunobile, contract 694717). C-M.C. is supported by US National Institutes of Health (NIH RO1CA103867), Cancer Prevention & Research Institute of Texas (CPRIT RP180349 and RP190077), and Welch Foundation (I-1805).

AUTHOR CONTRIBUTIONS: Conceptualization: V.D, P.L, B.S, J.E; Methodology: V.D, P.L, B.S, J.E, R.P, G.V, I.V, H.Du, J.S-A, E.W, E.B, F.L, M.B-G; Software: J.D-C, F.G; Validation: V.D, W.V, C.G, J.D-C, H.De, M.V, M.B-G; Formal Analysis: V.D, J.D-C, J.E, F.G; Investigation: V.D, W.V, C.G, J.D-C, H.De, M.V, F.P.Z, M.P, L.P, M.B-G; Resources: N.R, J.S-A, A.B, C.D, S.L, H.Du, R.E.v, C-M.C, I.V, G.V, R.P, E.D, E.V; Data Curation: V.D, J.D-C, J.E; Writing - Review & Editing: V.D, J.E with inputs from co-authors; Visualization: V.D, J.D-C; Project Administration: J.E; Funding Acquisition: J.E, P.L, B.S.

CONFLICT OF INTERESTS

BS is consultant for Genfit SA. The remaining authors declare no competing financial interest.

REFERENCES

Abu Rmilah A, Zhou W, Nelson E, Lin L, Amiot B, Nyberg SL (2019) Understanding the marvels behind liver regeneration. *Wiley Interdiscip Rev Dev Biol* 8: e340

Afgan E, Baker D, Batut B, van den Beek M, Bouvier D, Cech M, Chilton J, Clements D, Coraor N, Gruning BA, Guerler A, Hillman-Jackson J, Hiltemann S, Jalili V, Rasche H, Soranzo N, Goecks J, Taylor J, Nekrutenko A, Blankenberg D (2018) The Galaxy platform for accessible, reproducible and collaborative biomedical analyses: 2018 update. *Nucleic Acids Res* 46: W537-W544

Almanza A, Carlesso A, Chintha C, Creedican S, Doultsinos D, Leuzzi B, Luis A, McCarthy N, Montibeller L, More S, Papaioannou A, Puschel F, Sassano ML, Skoko J, Agostinis P, de Belleroche J, Eriksson LA, Fulda S, Gorman AM, Healy S et al. (2019) Endoplasmic reticulum stress signalling - from basic mechanisms to clinical applications. *FEBS J* 286: 241-278

Anders S, Huber W (2010) Differential expression analysis for sequence count data. *Genome Biol* 11: R106

Arensdorf AM, Dezwaan McCabe D, Kaufman RJ, Rutkowski DT (2013) Temporal clustering of gene expression links the metabolic transcription factor HNF4alpha to the ER stress-dependent gene regulatory network. *Front Genet* 4: 188

Argemi J, Kress TR, Chang HC, Ferrero R, Bertolo C, Moreno H, Gonzalez-Aparicio M, Uriarte I, Guembe L, Segura V, Hernandez-Alcoceba R, Avila MA, Amati B, Prieto J, Aragon T (2017) X-box Binding Protein 1 Regulates Unfolded Protein, Acute-Phase, and DNA Damage Responses During Regeneration of Mouse Liver. *Gastroenterology* 152: 1203-1216 e15

Bantubungi K, Hannou S-A, Caron-Houde S, Vallez E, Baron M, Lucas A, Bouchaert E, Paumelle R, Tailleux A, Staels B (2014) Cdkn2a/p16Ink4a Regulates Fasting-Induced Hepatic Gluconeogenesis Through the PKA-CREB-PGC1α Pathway. *Diabetes* 63: 3199-3209

Benayoun BA, Pollina EA, Ucar D, Mahmoudi S, Karra K, Wong ED, Devarajan K, Daugherty AC, Kundaje AB, Mancini E, Hitz BC, Gupta R, Rando TA, Baker JC, Snyder MP, Cherry JM, Brunet A (2014) H3K4me3 breadth is linked to cell identity and transcriptional consistency. *Cell* 158: 673-88

Benegiamo G, Mure LS, Erikson G, Le HD, Moriggi E, Brown SA, Panda S (2018) The RNA-

Binding Protein NONO Coordinates Hepatic Adaptation to Feeding. *Cell Metab* 27: 404-418 e7

Bhate A, Parker DJ, Bebee TW, Ahn J, Arif W, Rashan EH, Chorghade S, Chau A, Lee JH, Anakk S, Carstens RP, Xiao X, Kalsotra A (2015) ESRP2 controls an adult splicing programme in hepatocytes to support postnatal liver maturation. *Nat Commun* 6: 8768

Brennecke P, Anders S, Kim JK, Kolodziejczyk AA, Zhang X, Proserpio V, Baying B, Benes V, Teichmann SA, Marioni JC, Heisler MG (2013) Accounting for technical noise in single-cell RNA-seq experiments. *Nat Methods* 10: 1093-5

Brewer JW (2014) Regulatory crosstalk within the mammalian unfolded protein response. *Cell Mol Life Sci* 71: 1067-79

Brown JD, Lin CY, Duan Q, Griffin G, Federation A, Paranal RM, Bair S, Newton G, Lichtman A, Kung A, Yang T, Wang H, Luscinskas FW, Croce K, Bradner JE, Plutzky J (2014) NF-kappaB directs dynamic super enhancer formation in inflammation and atherogenesis. *Mol Cell* 56: 219-231

Chellappa K, Jankova L, Schnabl JM, Pan S, Brelivet Y, Fung CL, Chan C, Dent OF, Clarke SJ, Robertson GR, Sladek FM (2012) Src tyrosine kinase phosphorylation of nuclear receptor HNF4alpha correlates with isoform-specific loss of HNF4alpha in human colon cancer. *Proc Natl Acad Sci U S A* 109: 2302-7

Chen J, Bardes EE, Aronow BJ, Jegga AG (2009) ToppGene Suite for gene list enrichment analysis and candidate gene prioritization. *Nucleic Acids Res* 37: W305-11

Chen K, Chen Z, Wu D, Zhang L, Lin X, Su J, Rodriguez B, Xi Y, Xia Z, Chen X, Shi X, Wang Q, Li W (2015) Broad H3K4me3 is associated with increased transcription elongation and enhancer activity at tumor-suppressor genes. *Nat Genet* 47: 1149-57

Chikka MR, McCabe DD, Tyra HM, Rutkowski DT (2013) C/EBP homologous protein (CHOP) contributes to suppression of metabolic genes during endoplasmic reticulum stress in the liver. *J Biol Chem* 288: 4405-15

D'Alessio Ana C, Fan Zi P, Wert Katherine J, Baranov P, Cohen Malkiel A, Saini Janmeet S, Cohick E, Charniga C, Dadon D, Hannett Nancy M, Young Michael J, Temple S, Jaenisch R, Lee Tong I,

Young Richard A (2015) A Systematic Approach to Identify Candidate Transcription Factors that Control Cell Identity. *Stem Cell Reports* 5: 763-775

Dallas PB, Gottardo NG, Firth MJ, Beesley AH, Hoffmann K, Terry PA, Freitas JR, Boag JM, Cummings AJ, Kees UR (2005) Gene expression levels assessed by oligonucleotide microarray analysis and quantitative real-time RT-PCR -- how well do they correlate? *BMC Genomics* 6: 59

Derde S, Thiessen S, Goossens C, Dufour T, Van den Berghe G, Langouche L (2017) Use of a Central Venous Line for Fluids, Drugs and Nutrient Administration in a Mouse Model of Critical Illness. *J Vis Exp*

Di Micco R, Fontanals-Cirera B, Low V, Ntziachristos P, Yuen SK, Lovell CD, Dolgalev I, Yonekubo Y, Zhang G, Rusinova E, Gerona-Navarro G, Canamero M, Ohlmeyer M, Aifantis I, Zhou MM, Tsirigos A, Hernando E (2014) Control of embryonic stem cell identity by BRD4-dependent transcriptional elongation of super-enhancer-associated pluripotency genes. *Cell Rep* 9: 234-247

Dreszer TR, Karolchik D, Zweig AS, Hinrichs AS, Raney BJ, Kuhn RM, Meyer LR, Wong M, Sloan CA, Rosenbloom KR, Roe G, Rhead B, Pohl A, Malladi VS, Li CH, Learned K, Kirkup V, Hsu F, Harte RA, Guruvadoo L et al. (2012) The UCSC Genome Browser database: extensions and updates 2011. *Nucleic Acids Res* 40: D918-23

Dubois-Chevalier J, Dubois V, Dehondt H, Mazrooei P, Mazuy C, Sérandour AA, Gheeraert C, Guillaume P, Baugé E, Derudas B, Hennuyer N, Paumelle R, Marot G, Carroll JS, Lupien M, Staels B, Lefebvre P, Eeckhoute J (2017) The logic of transcriptional regulator recruitment architecture at cis-regulatory modules controlling liver functions. *Genome Res* 27: 985-996

Edgar R, Domrachev M, Lash AE (2002) Gene Expression Omnibus: NCBI gene expression and hybridization array data repository. *Nucleic Acids Res* 30: 207-210

Eeckhoute J, Formstecher P, Laine B (2004) Hepatocyte nuclear factor 4alpha enhances the hepatocyte nuclear factor 1alpha-mediated activation of transcription. *Nucleic Acids Res* 32: 2586-93

Encode_Project_Consortium (2012) An integrated encyclopedia of DNA elements in the human genome. *Nature* 489: 57-74

Ernst J, Nau GJ, Bar-Joseph Z (2005) Clustering short time series gene expression data. *Bioinformatics* 21 Suppl 1: i159-68

Felix MA, Barkoulas M (2015) Pervasive robustness in biological systems. *Nat Rev Genet* 16: 483-96

Fink EE, Moparthy S, Bagati A, Bianchi-Smiraglia A, Lipchick BC, Wolff DW, Roll MV, Wang J, Liu S, Bakin AV, Kandel ES, Lee AH, Nikiforov MA (2018) XBP1-KLF9 Axis Acts as a Molecular Rheostat to Control the Transition from Adaptive to Cytotoxic Unfolded Protein Response. *Cell Rep* 25: 212-223 e4

Frankish A, Diekhans M, Ferreira AM, Johnson R, Jungreis I, Loveland J, Mudge JM, Sisu C, Wright J, Armstrong J, Barnes I, Berry A, Bignell A, Carbonell Sala S, Chrast J, Cunningham F, Di Domenico T, Donaldson S, Fiddes IT, Garcia Giron C et al. (2019) GENCODE reference annotation for the human and mouse genomes. *Nucleic Acids Res* 47: D766-D773

Freese NH, Norris DC, Loraine AE (2016) Integrated genome browser: visual analytics platform for genomics. *Bioinformatics* 32: 2089-95

Gachon F, Olela FF, Schaad O, Descombes P, Schibler U (2006) The circadian PAR-domain basic leucine zipper transcription factors DBP, TEF, and HLF modulate basal and inducible xenobiotic detoxification. *Cell Metab* 4: 25-36

Gjuvsland AB, Plahte E, Omholt SW (2007) Threshold-dominated regulation hides genetic variation in gene expression networks. *BMC Syst Biol* 1: 57

Harding HP, Zhang Y, Bertolotti A, Zeng H, Ron D (2000) Perk is essential for translational regulation and cell survival during the unfolded protein response. *Mol Cell* 5: 897-904

Hetz C (2012) The unfolded protein response: controlling cell fate decisions under ER stress and beyond. *Nat Rev Mol Cell Biol* 13: 89-102

Huck I, Gunewardena S, Espanol-Suner R, Willenbring H, Apte U (2019) Hepatocyte Nuclear Factor 4 Alpha Activation Is Essential for Termination of Liver Regeneration in Mice. *Hepatology* 70: 666-681

Kalvisa A, Siersbaek MS, Praestholm SM, Christensen LJL, Nielsen R, Stohr O, Vettorazzi S, Tuckermann J, White M, Mandrup S, Grontved L (2018) Insulin signaling and reduced glucocorticoid receptor activity attenuate postprandial gene expression in liver. *PLoS Biol* 16: e2006249

Kemper JK, Xiao Z, Ponugoti B, Miao J, Fang S, Kanamaluru D, Tsang S, Wu SY, Chiang CM, Veenstra TD (2009) FXR acetylation is normally dynamically regulated by p300 and SIRT1 but constitutively elevated in metabolic disease states. *Cell Metab* 10: 392-404

Kim YH, Marhon SA, Zhang Y, Steger DJ, Won K-J, Lazar MA (2018) Rev-erbα dynamically modulates chromatin looping to control circadian gene transcription. *Science* 359: 1274-1277

Kyrmizi I, Hatzis P, Katrakili N, Tronche F, Gonzalez FJ, Talianidis I (2006) Plasticity and expanding complexity of the hepatic transcription factor network during liver development. *Genes Dev* 20: 2293-305

Lai L, Hennessey J, Bares V, Son EW, Ban Y, Wang W, Qi J, Jiang G, Liberzon A, Xijin Ge S (2016) GSKB: A gene set database for pathway analysis in mouse. *bioRxiv* 082511

Langmead B, Trapnell C, Pop M, Salzberg SL (2009) Ultrafast and memory-efficient alignment of short DNA sequences to the human genome. *Genome Biol* 10: R25

Lau HH, Ng NHJ, Loo LSW, Jasmen JB, Teo AKK (2018) The molecular functions of hepatocyte nuclear factors - In and beyond the liver. *J Hepatol* 68: 1033-1048

Lawrence M, Huber W, Pages H, Aboyoun P, Carlson M, Gentleman R, Morgan MT, Carey VJ (2013) Software for computing and annotating genomic ranges. *PLoS Comput Biol* 9: e1003118

Lê S, Josse J, Husson F (2008) FactoMineR: An R Package for Multivariate Analysis. *Journal of Statistical Software* 25: 1-18

Lee JE, Park YK, Park S, Jang Y, Waring N, Dey A, Ozato K, Lai B, Peng W, Ge K (2017) Brd4 binds to active enhancers to control cell identity gene induction in adipogenesis and myogenesis. *Nat Commun* 8: 2217

Leek JT, Johnson WE, H.S. P, Fertig EJ, Jaffe AE, Storey JD, Zhang Y, Torres LC (2019) sva: Surrogate Variable Analysis. R package version 3.34.0.

Levo M, Avnit-Sagi T, Lotan-Pompan M, Kalma Y, Weinberger A, Yakhini Z, Segal E (2017) Systematic Investigation of Transcription Factor Activity in the Context of Chromatin Using Massively Parallel Binding and Expression Assays. *Mol Cell* 65: 604-617 e6

Li T, Huang J, Jiang Y, Zeng Y, He F, Zhang MQ, Han Z, Zhang X (2009) Multi-stage analysis of gene expression and transcription regulation in C57/B6 mouse liver development. *Genomics* 93: 235-42

Liu CY, Chen KF, Chen PJ (2015a) Treatment of Liver Cancer. *Cold Spring Harb Perspect Med* 5: a021535

Liu Y, Shao M, Wu Y, Yan C, Jiang S, Liu J, Dai J, Yang L, Li J, Jia W, Rui L, Liu Y (2015b) Role for the endoplasmic reticulum stress sensor IRE1alpha in liver regenerative responses. *J Hepatol* 62: 590-8

Loven J, Hoke HA, Lin CY, Lau A, Orlando DA, Vakoc CR, Bradner JE, Lee TI, Young RA (2013) Selective inhibition of tumor oncogenes by disruption of super-enhancers. *Cell* 153: 320-34

Lun AT, Smyth GK (2014) De novo detection of differentially bound regions for ChIP-seq data using peaks and windows: controlling error rates correctly. *Nucleic Acids Res* 42: e95

Lun AT, Smyth GK (2016) csaw: a Bioconductor package for differential binding analysis of ChIP-seq data using sliding windows. *Nucleic Acids Res* 44: e45

Mitsui S, Yamaguchi S, Matsuo T, Ishida Y, Okamura H (2001) Antagonistic role of E4BP4 and PAR proteins in the circadian oscillatory mechanism. *Genes Dev* 15: 995-1006

Mudunuri U, Che A, Yi M, Stephens RM (2009) bioDBnet: the biological database network. *Bioinformatics* 25: 555-6

Nesseler N, Launey Y, Aninat C, Morel F, Mallédant Y, Seguin P (2012) Clinical review: The liver in sepsis. *Crit Care* 16: 235

O'Connor T, Boden M, Bailey TL (2017) CisMapper: predicting regulatory interactions from transcription factor ChIP-seq data. *Nucleic Acids Res* 45: e19

Ohta Y, Taguchi A, Matsumura T, Nakabayashi H, Akiyama M, Yamamoto K, Fujimoto R,

Suetomi R, Yanai A, Shinoda K, Tanizawa Y (2017) Clock Gene Dysregulation Induced by Chronic ER Stress Disrupts beta-cell Function. *EBioMedicine* 18: 146-156

Paumelle R, Haas J, Hennuyer N, Bauge E, Deleye Y, Mesotten D, L. L, Vanhoutte J, Cudejko C, Wouters K, Hannou SA, Legry V, Lancel S, Lalloyer F, Polizzi A, Smati S, Gourdy P, Vallez E, Bouchaert E, Derudas B et al. (2019) Hepatic PPARa is critical in the metabolic adaptation to sepsis. *J Hepatol* 70: 963-973

Peng L, Piekos SC, Guo GL, Zhong X-b (2017) Role of Farnesoid X Receptor in the Determination of Liver Transcriptome during Postnatal Maturation in Mice. *Nuclear Receptor Research* 4

Ploton M, Mazuy C, Gheeraert C, Dubois V, Berthier A, Dubois-Chevalier J, Marechal X, Bantubungi K, Diemer H, Cianferani S, Strub JM, Helleboid-Chapman A, Eeckhoute J, Staels B, Lefebvre P (2018) The nuclear bile acid receptor FXR is a PKA- and FOXA2-sensitive activator of fasting hepatic gluconeogenesis. *J Hepatol* 69: 1099-1109

R_Core_Team (2015) R: A language and environment for statistical computing. *R Foundation for Statistical Computing*

Reimold AM, Etkin A, Clauss I, Perkins A, Friend DS, Zhang J, Horton HF, Scott A, Orkin SH, Byrne MC, Grusby MJ, Glimcher LH (2000) An essential role in liver development for transcription factor XBP-1. *Genes Dev* 14: 152-7

Rib L, Villeneuve D, Minocha S, Praz V, Hernandez N, Guex N, Herr W, Cycli XC (2018) Cycles of gene expression and genome response during mammalian tissue regeneration. *Epigenetics Chromatin* 11: 52

Roe JS, Mercan F, Rivera K, Pappin DJ, Vakoc CR (2015) BET Bromodomain Inhibition Suppresses the Function of Hematopoietic Transcription Factors in Acute Myeloid Leukemia. *Mol Cell* 58: 1028-39

Rousseeuw PJ, Ruts I, Tukey JW (1999) The Bagplot: A Bivariate Boxplot. *The American Statistician* 53: 382-387

Rutkowski DT (2019) Liver function and dysfunction - a unique window into the physiological reach of ER stress and the unfolded protein response. *FEBS J* 286: 356-378

Santiago-Algarra D, Dao LTM, Pradel L, Espana A, Spicuglia S (2017) Recent advances in high-throughput approaches to dissect enhancer function. *F1000Res* 6: 939

Schmidt SF, Larsen BD, Loft A, Mandrup S (2016) Cofactor squelching: Artifact or fact? *Bioessays* 38: 618-26

Schmidt SF, Larsen BD, Loft A, Nielsen R, Madsen JG, Mandrup S (2015) Acute TNF-induced repression of cell identity genes is mediated by NFkappaB-directed redistribution of cofactors from super-enhancers. *Genome Res* 25: 1281-94

Sheffield NC, Bock C (2016) LOLA: enrichment analysis for genomic region sets and regulatory elements in R and Bioconductor. *Bioinformatics* 32: 587-9

Shen Y, Yue F, McCleary DF, Ye Z, Edsall L, Kuan S, Wagner U, Dixon J, Lee L, Lobanenkov VV, Ren B (2012) A map of the cis-regulatory sequences in the mouse genome. *Nature* 488: 116-20

Silveira MAD, Bilodeau S (2018) Defining the Transcriptional Ecosystem. *Mol Cell* 72: 920-924

Spinelli L, Carpentier S, Montanana Sanchis F, Dalod M, Vu Manh TP (2015) BubbleGUM: automatic extraction of phenotype molecular signatures and comprehensive visualization of multiple Gene Set Enrichment Analyses. *BMC Genomics* 16: 814

Subramanian A, Tamayo P, Mootha VK, Mukherjee S, Ebert BL, Gillette MA, Paulovich A, Pomeroy SL, Golub TR, Lander ES, Mesirov JP (2005) Gene set enrichment analysis: A knowledge-based approach for interpreting genome-wide expression profiles. *Proc Natl Acad Sci U S A* 102: 15545-50

Takasu O, Gaut JP, Watanabe E, To K, Fagley RE, Sato B, Jarman S, Efimov IR, Janks DL, Srivastava A, Bhayani SB, Drewry A, Swanson PE, Hotchkiss RS (2013) Mechanisms of cardiac and renal dysfunction in patients dying of sepsis. *Am J Respir Crit Care Med* 187: 509-17

Thakur A, Wong JCH, Wang EY, Lotto J, Kim D, Cheng JC, Mingay M, Cullum R, Moudgil V, Ahmed N, Tsai SH, Wei W, Walsh CP, Stephan T, Bilenky M, Fuglerud BM, Karimi MM, Gonzalez FJ,

Hirst M, Hoodless PA (2019) Hepatocyte Nuclear Factor 4-Alpha Is Essential for the Active Epigenetic State at Enhancers in Mouse Liver. *Hepatology* 70: 1360-1376

Thiessen SE, Derde S, Derese I, Dufour T, Vega CA, Langouche L, Goossens C, Peersman N, Vermeersch P, Vander Perre S, Holst JJ, Wouters PJ, Vanhorebeek I, Van den Berghe G (2017) Role of Glucagon in Catabolism and Muscle Wasting of Critical Illness and Modulation by Nutrition. *Am J Respir Crit Care Med* 196: 1131-1143

Tsai YL, Ha DP, Zhao H, Carlos AJ, Wei S, Pun TK, Wu K, Zandi E, Kelly K, Lee AS (2018) Endoplasmic reticulum stress activates SRC, relocating chaperones to the cell surface where GRP78/CD109 blocks TGF-beta signaling. *Proc Natl Acad Sci U S A* 115: E4245-E4254

van der Kallen LR, Eggers R, Ehlert EM, Verhaagen J, Smit AB, van Kesteren RE (2015) Genetic Deletion of the Transcriptional Repressor NFIL3 Enhances Axon Growth In Vitro but Not Axonal Repair In Vivo. *PLoS One* 10: e0127163

Vandel J, Gheeraert C, Eeckhoute J, Staels B, Lefebvre P, Dubois-Chevalier J (2018) GIANT: Galaxy-based Interactive tools for ANalaysis of Transcriptomic data.

Vihervaara A, Duarte FM, Lis JT (2018) Molecular mechanisms driving transcriptional stress responses. *Nat Rev Genet* 19: 385-397

Vihervaara A, Mahat DB, Guertin MJ, Chu T, Danko CG, Lis JT, Sistonen L (2017) Transcriptional response to stress is pre-wired by promoter and enhancer architecture. *Nat Commun* 8: 255

Vincent JL, Moreno R, Takala J, Willatts S, De Mendonça A, Bruining H, Reinhart CK, Suter PM, Thijs LG (1996) The SOFA (Sepsis-related Organ Failure Assessment) score to describe organ dysfunction/failure. On behalf of the Working Group on Sepsis-Related Problems of the European Society of Intensive Care Medicine. *Intensive Care Med* 22: 707-10

von Meyenn F, Porstmann T, Gasser E, Selevsek N, Schmidt A, Aebersold R, Stoffel M (2013) Glucagon-induced acetylation of Foxa2 regulates hepatic lipid metabolism. *Cell Metab* 17: 436-47

Wang J, Hu B, Zhao Z, Zhang H, Zhang H, Zhao Z, Ma X, Shen B, Sun B, Huang X, Hou J, Xia Q

(2020) Intracellular XBP1-IL-24 axis dismantles cytotoxic unfolded protein response in the liver. *Cell Death Dis* 11: 17

Wang W, Yao LJ, Shen W, Ding K, Shi PM, Chen F, He J, Ding J, Zhang X, Xie WF (2017) FOXA2 alleviates CCl4-induced liver fibrosis by protecting hepatocytes in mice. *Sci Rep* 7: 15532

Warnes GR, Bolker B, Bonebakker L, Gentleman R, Liaw WHA, Lumley T, Maechler M, Magnusson A, Moeller S, Schwartz M, Venables B (2016) gplots: Various R Programming Tools for Plotting Data. R package version 3.0.1.

Wei J, Chen L, Li F, Yuan Y, Wang Y, Xia W, Zhang Y, Xu Y, Yang Z, Gao B, Jin C, Melo-Cardenas J, Green RM, Pan H, Wang J, He F, Zhang K, Fang D (2018) HRD1-ERAD controls production of the hepatokine FGF21 through CREBH polyubiquitination. *EMBO J* 37

White P, Brestelli JE, Kaestner KH, Greenbaum LE (2005) Identification of transcriptional networks during liver regeneration. *J Biol Chem* 280: 3715-22

Whyte WA, Orlando DA, Hnisz D, Abraham BJ, Lin CY, Kagey MH, Rahl PB, Lee TI, Young RA (2013) Master transcription factors and mediator establish super-enhancers at key cell identity genes. *Cell* 153: 307-19

Woznica EA, Inglot M, Woznica RK, Lysenko L (2018) Liver dysfunction in sepsis. *Adv Clin Exp Med* 27: 547-551

Wu C, Jin X, Tsueng G, Afrasiabi C, Su AI (2016) BioGPS: building your own mash-up of gene annotations and expression profiles. *Nucleic Acids Res* 44: D313-6

Yang L, Wang WH, Qiu WL, Guo Z, Bi E, Xu CR (2017) A single-cell transcriptomic analysis reveals precise pathways and regulatory mechanisms underlying hepatoblast differentiation. *Hepatology* 66: 1387-1401

Yevshin I, Sharipov R, Valeev T, Kel A, Kolpakov F (2017) GTRD: a database of transcription factor binding sites identified by ChIP-seq experiments. *Nucleic Acids Res* 45: D61-D67

Yue F, Cheng Y, Breschi A, Vierstra J, Wu W, Ryba T, Sandstrom R, Ma Z, Davis C, Pope BD, Shen Y, Pervouchine DD, Djebali S, Thurman RE, Kaul R, Rynes E, Kirilusha A, Marinov GK, Williams

BA, Trout D et al. (2014) A comparative encyclopedia of DNA elements in the mouse genome. *Nature* 515: 355-64

Zengerle M, Chan KH, Ciulli A (2015) Selective Small Molecule Induced Degradation of the BET Bromodomain Protein BRD4. *ACS Chem Biol* 10: 1770-7

Zhang HM, Liu T, Liu CJ, Song S, Zhang X, Liu W, Jia H, Xue Y, Guo AY (2015) AnimalTFDB 2.0: a resource for expression, prediction and functional study of animal transcription factors. *Nucleic Acids Res* 43: D76-81

Zhou Q, Liu M, Xia X, Gong T, Feng J, Liu W, Liu Y, Zhen B, Wang Y, Ding C, Qin J (2017) A mouse tissue transcription factor atlas. *Nat Commun* 8: 15089

Zhou Y, Lee J, Reno CM, Sun C, Park SW, Chung J, Lee J, Fisher SJ, White MF, Biddinger SB, Ozcan U (2011) Regulation of glucose homeostasis through a XBP-1-FoxO1 interaction. *Nat Med* 17: 356-65

FIGURE LEGENDS

Figure 1. Acute ERS triggers massive transcriptomic alterations characterized by repression of LIVER-ID genes and loss of hepatic molecular identity.

(A) Top 2 significantly overrepresented expression patterns for ERS UP and ERS DOWN genes following PHx. Data show changes in expression at 4, 10, 48h and 1 week after PHx (0h) for genes comprised within each model profile of dynamic expression identified by STEM. The complete set of identified model profiles is provided in Appendix Fig.S2.

(B) Functional enrichment analyses were performed using ERS UP (*upper panels*) or ERS DOWN (*lower panels*) genes and the ToppGene Suite. KEGG Pathways with Bonferroni-corrected p-value $<10^{-3}$ were considered and similar terms were merged.

(C) Bagplots showing the breadth of transcriptomic changes for the indicated datasets. Genes were positioned based on their basal expression levels in the control conditions and their FC (Log_2) in the indicated (patho)physiological context. The dark blue area is the “bag” (50% of the data points

around the median, which is indicated by a red cross) while the light blue area delimits the "loop" (see Materials and Methods for details). Red dots are outliers.

(D-E) Box plots showing normalized expression in liver (D) and liver-specificity index (E) of LIVER-ID genes, UBQ genes and other genes. Liver-specificity index was calculated as the difference of normalized expression in liver (2 replicates) and mean of normalized expression in control tissues (2 replicates per tissue) using data from BioGPS (Table EV6) and is reported as Log_2. Box plots are composed of a box from the 25th to the 75th percentile with the median as a line and min to max as whiskers. One-way ANOVA with Welch's correction and Dunnett's Modified Tukey-Kramer pairwise multiple comparison test was used to assess statistical significance, *P < 0.05.

(F) Similar analyses as in (A) using LIVER-ID genes.

(G-H) Box plots showing Log_2 FC ERS/Control in MPH (3 independent experiments) (G) or mouse liver (3 mice per group) (H) for LIVER-ID genes, UBQ genes and other genes. Box plots are composed of a box from the 25th to the 75th percentile with the median as a line and min to max as whiskers. One-way ANOVA with Welch's correction and Dunnett's Modified Tukey-Kramer pairwise multiple comparison test was used to assess statistical significance, *P < 0.05.

(I) Enrichment plots from gene set enrichment analyses (GSEA) performed using LIVER-ID genes as the gene set and transcriptomic changes induced by acute ERS in MPH (*upper panel*) or mouse liver (*lower panel*) as the ranked gene list. NES and FDR (as in all subsequent GSEA panels) are the normalized enrichment score and the false discovery rate provided by the GSEA software, respectively.

(J-K) Genes repressed by ERS in MPH (3 independent experiments) (J) or mouse liver (3 mice per group) (K) were ranked based on their Log_2 FC ERS/Control and divided into quartiles (increased repression from Q1 to Q4). The fraction of LIVER-ID genes in the 4 quartiles was defined and is displayed relative to that obtained for Q1 arbitrarily set to 1. The bar graphs show means ± SD (standard deviations). Chi-square test with BH correction for multiple testing was used to assess statistical significance, *P < 0.05.

(L-M) RT-qPCR analyses of selected ERS UP and LIVER-ID genes monitoring expression changes induced by acute ERS in MPH (3 to 9 independent experiments) (L) or mouse liver (5 to 7 mice per group) (M). The bar graphs show means ± SD (standard deviations). One-sample t-test with BH correction for multiple testing was used to determine if the mean Log_2 FC ERS/Control is statistically different from 0, *P < 0.05. Panel (L) is also displayed in Appendix Fig.S3G.

(N) Heatmaps showing normalized expression of ERS UP and ERS DOWN genes from MPH (*upper panel*) or mouse liver (*lower panel*) in mouse liver at the indicated stages of development.

(O) Average expression of ERS DOWN genes from MPH in single-cells from the hepatobiliary lineage. See Materials and Methods together with Appendix Fig.S3I for details regarding data processing. The hepatoblast-to-hepatocyte and hepatoblast-to-cholangiocyte differentiation paths are indicated with arrows.

Figure 2. Acute ERS compromises LIVER-TF expression and activities of their densely co-bound hepatic CRMs.

(A) Comparison of transcriptomics (data from 3 independent experiments) and H3K27ac ChIP-seq (data from 3 independent experiments) from MPH. Genes were assigned to H3K27ac regions as described in Material and Methods. The number of ERS DOWN genes is indicated relative to the number of ERS UP genes for the 3 categories of H3K27ac regions. The bar graph shows means ± SD (standard deviations). Fisher's exact test with BH correction for multiple testing was used to assess statistical significance, *P < 0.05, $^{\#}$P < 0.05.

(B) Similar analyses to (A). The number of LIVER-ID and UBQ genes is indicated relative to the number of other genes for the 3 categories of H3K27ac regions. The H3K27ac ChIP-seq data were obtained from 3 independent MPH experiments. The bar graph shows means ± SD (standard deviations). Chi-square test with BH correction for multiple testing was used to assess statistical significance, $^{\#}$P < 0.05.

(C) Multidimensional scaling (MDS) was performed as described in Materials and Methods and transcriptional regulator co-recruitment was depicted using density plots for regions with increased

(a), decreased (b) or unchanged (c) H3K27ac levels in MPH upon acute ERS. The boxed area (d) represents a subset of transcriptional regulators (TR) with a high degree of co-binding in H3K27ac DOWN regions. LIVER-ID TFs are depicted in red.

(D) Heatmaps showing the percentage of enhancers overlapping H3K27ac down regions. Enhancers were first split into those bound or not by a given LIVER-ID TF (right) and then based on co-binding of additional LIVER-ID TFs (defining 3 subgroups with 0-2, 3-5 or 6-8 co-bound additional LIVER-ID TFs).

(E) Enrichment plots from GSEA performed using LIVER-ID TFs as the gene set and transcriptomic changes induced by acute ERS in MPH (*upper panel*) or mouse liver (*lower panel*) as the ranked gene list.

(F) RT-qPCR analyses of selected LIVER-ID TFs monitoring expression changes induced by acute ERS in MPH (4 to 7 independent experiments). The bar graph shows means ± SD (standard deviations). One-sample t-test with BH correction for multiple testing was used to determine if the mean Log_2 FC ERS/Control is statistically different from 0, *P < 0.05. This graph is also displayed in Appendix Fig.S6E.

(G) RT-qPCR analyses of selected ERS UP and LIVER-ID TF genes monitoring expression changes induced by 4h ERS in MPH pre-treated or not for 30min with 5mM PBA (3 independent experiments). Mean Log2 FC ERS/Control are shown. The bar graph shows means ± SD (standard deviations). Two-way ANOVA with Bonferroni's post-hoc test was used to assess statistical significance, *P < 0.05.

(H-I) Nuclear extracts (H) and chromatin fractions (I) from MPH were subjected to Western blot with antibodies against HNF4A, NR1H4/FXR, FOXA2/HNF3B or DDIT3/CHOP. LMNA or histone H3 were used as loading controls. Results obtained from 3 independent biological replicates are shown. See Appendix Fig.S6H and Ploton et al. (Ploton et al., 2018) for antibody validation.

Figure 3. Induction of NFIL3 by acute ERS contributes to repression of genes involved in xenobiotic metabolism.

(A) RT-qPCR analyses of *Hlf*, *Tef*, *Dbp* and *Nfil3* expression monitoring changes induced by acute ERS in MPH (3 to 5 independent experiments) (*left panel*) or mouse liver (5 mice per group) (*right panel*).

The bar graphs show means ± SD (standard deviations). One-sample t-test with BH correction for multiple testing was used to determine if the mean Log_2 FC ERS/Control is statistically different from 0, *P < 0.05.

(B) Total protein extracts from MPH (*left panel*) or mouse liver (*right panel*) were subjected to Western blot with an antibody against NFIL3. ACTB was used as loading control. See Appendix Fig.S7B for antibody validation.

(C) Chromatin fractions from MPH (*upper panel*) or mouse liver (*lower panel*) were subjected to Western blot with an antibody against NFIL3. Histone H3 was used as loading control.

(D) Enrichment scores from GSEA performed using LIVER-ID genes repressed by acute ERS in MPH (MPH ERS DOWN) as the gene set and liver transcriptomic changes induced by acute ERS and/or deletion of *Nfil3* (NFIL3 KO) as the ranked gene lists were integrated and corrected for multiple testing using the BubbleGUM tool. For the NFIL3 KO ERS vs WT ERS comparison, the Core Enrichment genes (i.e. the subset of genes that contributes most to the enrichment result) were subjected to functional enrichment analyses using the ToppGene Suite. The top ranked KEGG Pathway with its Bonferroni-corrected p-value is shown.

(E) Box plots showing mRNA expression for 5 genes from the Core Enrichment from D involved in xenobiotic metabolism issued from the transcriptomic analyses. Shown are Log_2 FC relative to the mean normalized expression in the WT Control group (5 mice per group). Box plots are composed of a box from the 25th to the 75th percentile with the median as a line and min to max as whiskers. Two-way ANOVA with Bonferroni's post-hoc test was used to assess statistical significance, *P < 0.05.

(F) The Integrated Genome Browser (IGB) was used to visualize ChIP-seq profiles for NFIL3 (green) and several LIVER-ID TFs (red) in the mouse liver at the *Gsta3* gene locus. Levels of H3K27ac in MPH and cells from the non-parenchymal fraction (NPC) are shown in blue. The grey bar indicates the position of a BRD4 SE.

Figure 4. Acute ERS triggers hepatic SE decommissioning through impaired recruitment of the cell identity maintenance cofactor BRD4.

(A) BRD4 occupancy (*left panels*) and H3K27ac levels (*right panels*) at regulatory regions associated with ERS UP or LIVER-ID genes (8 regions at ERS gene loci and 10 regions at LIVER-ID gene loci, depicted in Appendix Fig.S10B and listed in Table EV5) were assessed by ChIP-qPCR in MPH (10 independent experiments) or mouse liver (10 mice per group) to define changes induced by acute ERS. Box plots are composed of a box from the 25th to the 75th percentile with the median as a line and min to max as whiskers. One-sample t-test with BH correction for multiple testing was used to determine if the mean Log_2 FC ERS/Control is statistically different from 0, *P < 0.05.

(B) *Left panel,* BRD4 mRNA (4 independent experiments) or protein expression levels (5 independent experiments; densitometric quantification of Fig.4B and Appendix Fig.S10C) in MPH subjected to acute ERS. The bar graphs show means ± SD (standard deviations). Student's t-test was used to assess statistical significance. *Right panel,* Total protein extracts from MPH pre-treated for 3h with 0.01µM MZ1 followed by addition of 1µM thapsigargin (ERS) for 4h were subjected to Western blot with an antibody against BRD4. LMNA was used as loading control.

(C) Heatmaps showing Log_2 FC (relative to the DMSO/Control condition) for 5 ERS UP and LIVER-ID genes issued from RT-qPCR analyses (Appendix Fig.S11) of MPH pre-treated with 500nM JQ1 (*left*) or 0.01µM MZ1 (*right*) followed by addition of 1µM thapsigargin (ERS) for 4h (3 to 6 independent experiments). Two-way ANOVA with Bonferroni's post-hoc test was used to assess statistical significance.

(D) Heatmaps showing average H3K27ac ChIP-seq signals in MPH at LIVER-ID domains overlapping (+) or not (-) with BRD4 SE. The arrow indicates the position of gene transcriptional start sites.

(E) Box plots showing Log_2 FC ERS/Control in MPH (3 independent experiments) (*left panel*) or mouse liver (3 mice per group) (*right panel*) for genes associated with LIVER-ID + BRD4 SE or LIVER-ID - BRD4 SE, which are listed in Table EV1. Box plots are composed of a box from the 25th to the 75th percentile with the median as a line and min to max as whiskers. Student's t-test was used to assess statistical significance, *P < 0.05.

Figure 5. Loss of LIVER-ID TF protein expression is a primary event upon acute ERS.

(A) RT-qPCR analyses of 21 LIVER-ID genes (12 TFs and 9 non-TFs, listed in Table EV5) in MPH which were treated with 1µM thapsigargin (ERS) for 4h, 8h, 16h or 24h (4 independent experiments). For each gene, the timepoint showing maximal repression by ERS was recorded. The heatmap depicts the percentage of genes maximally repressed by ERS at each timepoint.

(B) RT-qPCR analyses of *Hnf4a*, *Nr1h4* and *Foxa2* expression in MPH treated with vehicle (Control) or 1µM thapsigargin (ERS) for 1h or 4h (4 independent experiments). The bar graph shows means ± SD (standard deviations). One-sample t-test with BH correction for multiple testing was used to determine if the mean Log_2 FC ERS/Control is statistically different from 0, *P < 0.05.

(C) Densitometric quantification of the protein expression data shown in Fig.5D, Fig.5F and Fig.S18A-B for the 1h timepoint (average of 9 biological replicates) and Fig.2H for the 4h timepoint (average of 3 biological replicates). The bar graph shows means ± SD (standard deviations). One-sample t-test with BH correction for multiple testing was used to determine if the mean Log2 FC ERS/Control is statistically different from 0, *P < 0.05.

(D) Nuclear extracts from MPH pre-treated for 30min with 1µM ISRIB followed by addition of 1µM thapsigargin (ERS) for 1h were subjected to Western blot with antibodies against HNF4A, NR1H4, FOXA2 or DDIT3. LMNA was used as loading control. Results obtained from 3 independent biological replicates are shown.

(E) Densitometric quantification of the protein expression data shown in panel (D). Repression by ERS in the ISRIB condition (average of 3 biological replicates) is shown relative to repression by ERS in vehicle condition. The bar graph shows means ± SD (standard deviations). One-sample t-test with BH correction for multiple testing was used to determine if the mean relative repression is statistically different from 100%, *P < 0.05.

(F) Nuclear extracts from MPH pre-treated for 30min with 10µM MG132 or 10µM PP2 followed by addition of 1µM thapsigargin (ERS) for 1h were subjected to Western blot or Simple Western immunoassay with antibodies against HNF4A, NR1H4, FOXA2 or XBP1S. LMNA was used as loading control. Results obtained from 2 independent biological replicates are shown. Additional replicates

are shown in Appendix Fig.S18A-B.

(G) Densitometric quantification of the protein expression data shown in panel (F) and Appendix Fig.S18A. Repression by ERS in MG132 condition (average of 4 biological replicates) is shown relative to repression by ERS in vehicle condition. The bar graph shows means ± SD (standard deviations). One-sample t-test with BH correction for multiple testing was used to determine if the mean relative repression is statistically different from 100%, *P < 0.05.

(H) (*Left*) Cytoplasmic extracts issued from the MPH used in panel (F) (2 biological replicates) were subjected to Western blot with antibodies against p-Y416-SRC or total SRC. ACTB was used as loading control. (*Right*) Densitometric quantification of the protein expression data. The bar graphs show means ± SD (standard deviations). Two-way ANOVA with Bonferroni's post-hoc test was used to assess statistical significance.

(I) Densitometric quantification of the protein expression data shown in panel F and Appendix Fig.S18B. Repression by ERS in the PP2 condition (average of 4 biological replicates) is shown relative to repression by ERS in vehicle condition. The bar graph shows means ± SD (standard deviations). One-sample t-test with BH correction for multiple testing was used to determine if the mean relative repression is statistically different from 100%.

(J) RT-qPCR analyses of selected ERS UP and LIVER-ID TF genes monitoring expression changes induced by 4h ERS in MPH pre-treated or not for 30min with 10µM PP2 (3 independent experiments). Mean Log_2 FC ERS/Control are shown. The bar graph shows means ± SD (standard deviations). Two-way ANOVA with Bonferroni's post-hoc test was used to assess statistical significance, *P < 0.05.

Figure 6. ERS contributes to LIVER-ID gene downregulation and loss of hepatic identity in septic mice. (A) Similar analysis as in Fig.1C using transcriptomic data from the liver of $sepsis^{BIM}$ mice (16h after intraperitoneal injection of live *E. coli*).

(B-C) Enrichment plots from GSEA performed using LIVER-ID genes (B) or the response to ERS gene set (GO:0034976) (C) as the gene set and transcriptomic differences in $sepsis^{BIM}$ vs Control mouse

liver as the ranked gene list.

(D) Comparison of the transcriptome of the indicated liver injury models (details are provided in Appendix Fig.S20 and Table EV6) with that of the developing mouse liver performed as described in the Materials and Methods. PC1 is the first principal component which represents 63.55% of the variability within the mouse liver differentiation study. PC1 was used to project the liver injury studies. APAP, Acetaminophen overdose – Model of drug-induced acute liver injury. CCL4, Carbon tetrachloride hepatotoxicity – Model of drug-induced chronic liver injury. MCD-HF, Methionine-choline deficient diet with high fat - Model of NASH/fibrosis.

(E) Box plots showing Log_2 FC for ERS UP, DOWN or unchanged genes in $sepsis^{BIM}$ vs Control mouse liver (6 mice per group). Box plots are composed of a box from the 25th to the 75th percentile with the median as a line and min to max as whiskers. One-way ANOVA with Welch's correction and Dunnett's Modified Tukey-Kramer pairwise multiple comparison test was used to assess statistical significance, *P < 0.05.

(F) RT-qPCR analyses of selected ERS UP genes and LIVER-ID TFs monitoring expression changes in the liver of $sepsis^{BIM}$ vs Control mice (6 mice per group). The bar graph shows means ± SD (standard deviations). One-sample t-test with BH correction for multiple testing was used to determine if the mean Log_2 FC $sepsis^{BIM}$/Control is statistically different from 0, *P < 0.05.

(G) Nuclear extracts from livers of control or $sepsis^{BIM}$ mice were subjected to Western blot or Simple Western immunoassay with antibodies against HNF4A, NR1H4 or FOXA2. LMNA was used as loading control.

(H) Nuclear extracts from livers of $sepsis^{BIM}$ mice pre-treated for 4 consecutive days with vehicle or 500 mpk TUDCA were subjected to Western blot with antibodies against HNF4A, NR1H4, FOXA2 or XBP1S. TFIIB was used as loading control. Additional mice are shown in Appendix Fig.S22D.

(I) Densitometric quantification of the protein expression data from 6 mice precondition shown in panel (H) (3 mice per condition) and Appendix Fig.S22D (3 additional independent mice per condition). The bar graph shows means ± SD (standard deviations). One-sample t-test with BH

correction for multiple testing was used to determine if the mean Log2 FC TUDCA/Vehicle is statistically different from 0, *P < 0.05.

(J) Serum alanine aminotransferase (ALT) (*left*) and aspartate aminotransferase (AST) activities (*right*) from sepsis^{BIM} mice pre-treated for 4 consecutive days with vehicle or 500 mpk TUDCA (10 mice per group). The bar graphs show means ± SD (standard deviations). Student's t-test was used to assess statistical significance, *P < 0.05.

Figure 7. Competitive equilibrium between LIVER-ID and ERS gene expression in injured mouse and human livers.

(A) RT-qPCR analyses of selected ERS UP genes and LIVER-ID TFs in livers from sepsis^{CLP} mice collected 10h, 30h or 3 days after CLP (15 mice per group) vs livers from healthy pair-fed mice (Control) (15 mice per group). The bar graph shows means ± SD (standard deviations). Wilcoxon test with BH correction for multiple testing was used to assess statistical significance, *P < 0.05.

(B) Box plots showing Log_2 FC ERS/Control in mouse liver for ERS UP genes 8h and 34h after tunicamycin injection in WT or ATF6 KO mice (3 mice per experimental condition). Box plots are composed of a box from the 25th to the 75th percentile with the median as a line and min to max as whiskers. One-sample t-test with BH correction for multiple testing was used to determine if the mean Log_2 FC ERS/Control is statistically different from 0, *P < 0.05. NS, not significant.

(C) Similar analyses to panel (B) for ERS DOWN and LIVER-ID genes (3 mice per experimental condition). Box plots are composed of a box from the 25th to the 75th percentile with the median as a line and min to max as whiskers. One-sample t-test with BH correction for multiple testing was used to determine if the mean Log_2 FC ERS/Control is statistically different from 0, *P < 0.05.

(D) Main observations from (Huck et al., 2019) (*left*) and box plots showing Log_2 FC HNF4A KO/Control in mouse liver (3 mice per group) for LIVER-ID genes and TFs 5 days after PHx (*right*). Box plots are composed of a box from the 25th to the 75th percentile with the median as a line and min to max as whiskers. One-sample t-test with BH correction for multiple testing was used to determine if the mean Log_2 FC HNF4A KO/Control is statistically different from 0, *P < 0.05.

(E) Correlations of gene expressions within the critically-ill group were used to organize the analyzed genes as a network. Green bars indicate a positive correlation while red bars indicate a negative correlation. The color intensity is proportional to the correlation coefficient. The position of the genes is determined by both the directions and values of the correlation coefficients.

(F) Expression of LIVER-ID TF encoding genes from Appendix Fig.S23A was analyzed in the livers of deceased critically-ill patients with sepsis displaying agonal bilirubin levels below (Bil<2; n=34) or above (Bil>2; n=28) 2mg/dL. Median fold-change expression level of each group for the different genes has been used to generate the box plots. Expression levels in the critically-ill groups are expressed relative to those in the control group (n=18). Box plots are composed of a box from the 25th to the 75th percentile with the median as a line and min to max as whiskers. One-tailed t-test was used to assess whether expression of LIVER-ID TF encoding genes in the Bil>2 group is significantly greater than in the Bil<2 group, *P < 0.05.

(G) RT-qPCR analyses of indicated LIVER-ID TF encoding genes monitoring expression in the livers of Bil<2 (n=34) or Bil>2 (n=28) groups of deceased critically-ill patients with sepsis *vs* control donors (n=18). Data are shown as box plots, with mRNA levels of the critically-ill groups expressed relative to those of the control group. Box plots are composed of a box from the 25th to the 75th percentile with the median as a line and min to max as whiskers. Wilcoxon test was used to assess statistically significant differences with the Bil>2 group, *P < 0.05.

(H) RT-qPCR analyses of indicated ERS UP genes performed and analyzed as in panel (G). Box plots are composed of a box from the 25th to the 75th percentile with the median as a line and min to max as whiskers. Wilcoxon test was used to assess statistically significant differences with the Bil>2 group, *P < 0.05.

Figure 8. Summary of the molecular mechanisms involved in ERS-induced loss of hepatic molecular identity and implications for liver pathophysiology.

(A) Model for ERS-mediated loss of hepatic identity. Initial loss in LIVER-ID TF activities involves reduced protein levels linked to PERK and SRC signaling ❶, which is secondarily amplified by

decommissioning of BRD4 SE ❷ and impaired feedback loops within the LIVER-ID TF hepatic network ❸. This consequently leads to loss of hepatic molecular identity and partial dedifferentiation of hepatocytes ❸. Induction of NFIL3 operates as an additional mechanism further contributing to active repression of the LIVER-ID TF network target genes, especially those involved in xenobiotic metabolism.

(B) Implications of the competitive equilibrium between the hepatic and ERS transcriptional programs in liver pathophysiology. Please also refer to the discussion.

Figure 1

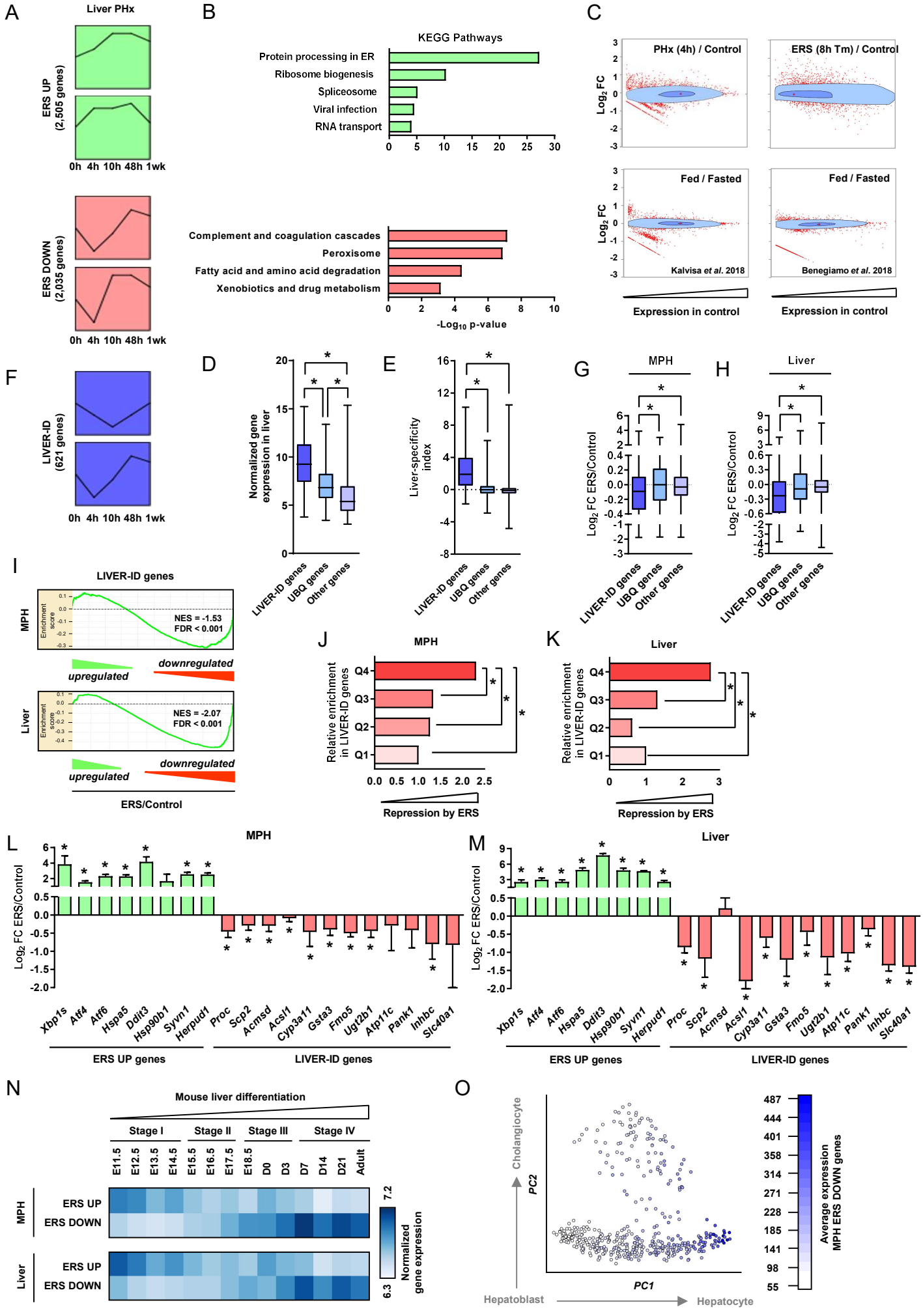
A
Liver PHx
ERS UP (2,505 genes)
ERS DOWN (2,035 genes)
0h 4h 10h 48h 1wk
B
KEGG Pathways
Protein processing in ER
Ribosome biogenesis
Spliceosome
Viral infection
RNA transport
Complement and coagulation cascades
Peroxisome
Fatty acid and amino acid degradation
Xenobiotics and drug metabolism
-Log10 p-value
C
PHx (4h) / Control
ERS (8h Tm) / Control
Fed / Fasted
Kalvisa et al. 2018
Benegiamo et al. 2018
Log2 FC
Expression in control
F
LIVER-ID (621 genes)
D
Normalized gene expression in liver
E
Liver-specificity index
G
MPH
H
Liver
Log2 FC ERS/Control
LIVER-ID genes
UBQ genes
Other genes
I
LIVER-ID genes
MPH
NES = -1.53
FDR < 0.001
upregulated
downregulated
Liver
NES = -2.07
FDR < 0.001
ERS/Control
J
MPH
K
Liver
Relative enrichment in LIVER-ID genes
Q4
Q3
Q2
Q1
Repression by ERS
L
MPH
M
Liver
Log2 FC ERS/Control
Xbp1s
Atf4
Atf6
Hspa5
Ddit3
Hsp90b1
Syvn1
Herpud1
Proc
Scp2
Acmsd
Acsl1
Cyp3a11
Gsta3
Fmo5
Ugt2b1
Atp11c
Pank1
Inhbc
Slc40a1
ERS UP genes
LIVER-ID genes
N
Mouse liver differentiation
Stage I
Stage II
Stage III
Stage IV
E11.5
E12.5
E13.5
E14.5
E15.5
E16.5
E17.5
E18.5
D0
D3
D7
D14
D21
Adult
MPH
Liver
ERS UP
ERS DOWN
7.2
6.3
Normalized gene expression
O
Cholangiocyte
PC2
PC1
Hepatoblast
Hepatocyte
Average expression MPH ERS DOWN genes
487
444
401
358
314
271
228
185
141
98
55

Figure 2

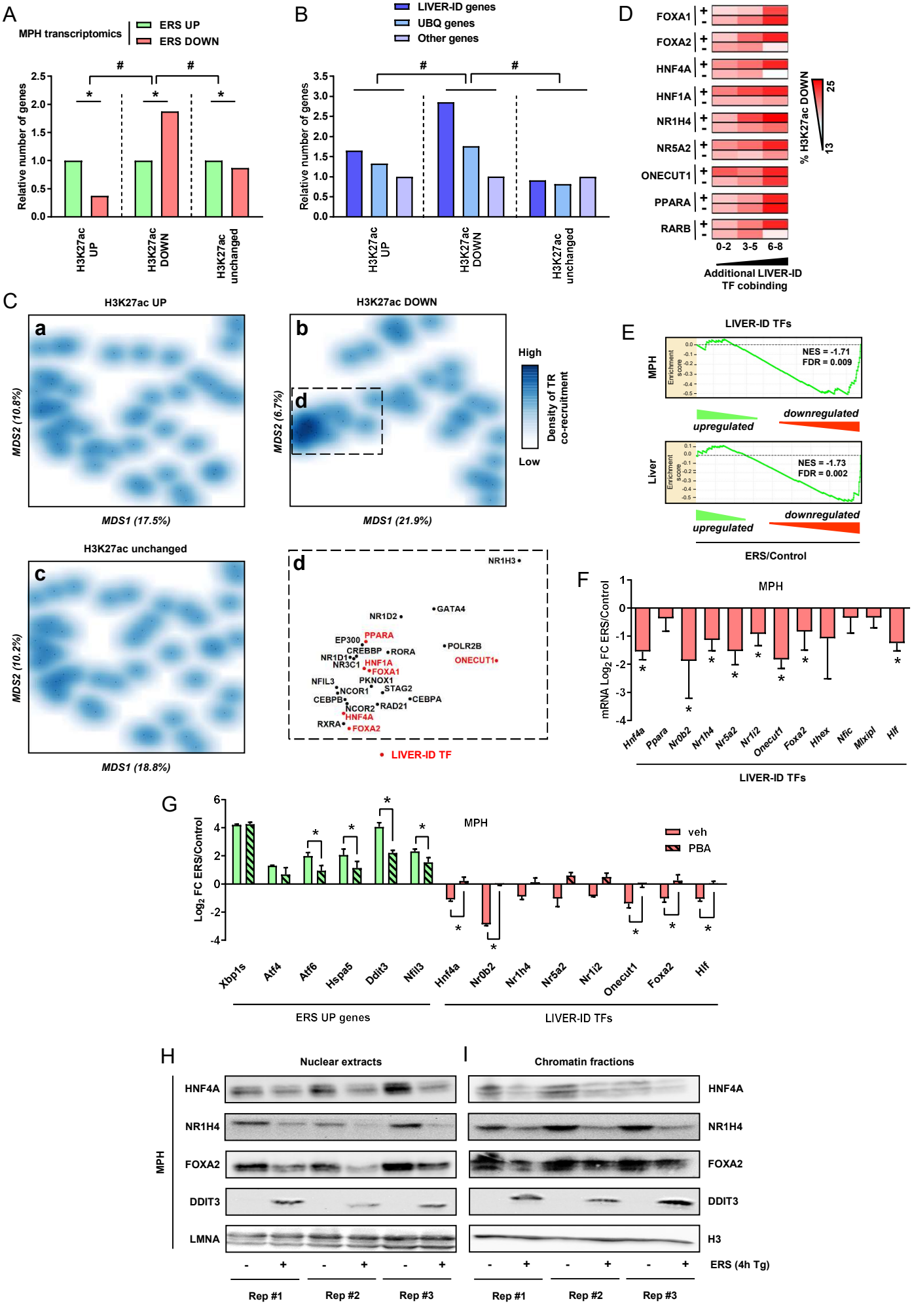
A
MPH transcriptomics
ERS UP
ERS DOWN
Relative number of genes
H3K27ac UP
H3K27ac DOWN
H3K27ac unchanged
B
LIVER-ID genes
UBQ genes
Other genes
Relative number of genes
H3K27ac UP
H3K27ac DOWN
H3K27ac unchanged
D
FOXA1
FOXA2
HNF4A
HNF1A
NR1H4
NR5A2
ONECUT1
PPARA
RARB
% H3K27ac DOWN
25
13
0-2
3-5
6-8
Additional LIVER-ID TF cobinding
C
H3K27ac UP
H3K27ac DOWN
H3K27ac unchanged
MDS2 (10.8%)
MDS1 (17.5%)
MDS2 (6.7%)
MDS1 (21.9%)
MDS2 (10.2%)
MDS1 (18.8%)
High
Density of TR co-recruitment
Low
NR1H3
GATA4
NR1D2
PPARA
EP300
CREBBP
RORA
POLR2B
ONECUT1
NR1D1
NR3C1
HNF1A
FOXA1
NFIL3
PKNOX1
NCOR1
STAG2
CEBPB
CEBPA
NCOR2
RAD21
HNF4A
RXRA
FOXA2
LIVER-ID TF
E
LIVER-ID TFs
MPH
NES = -1.71
FDR = 0.009
upregulated
downregulated
Liver
NES = -1.73
FDR = 0.002
upregulated
downregulated
ERS/Control
F
MPH
mRNA Log2 FC ERS/Control
Hnf4a
Ppara
Nr0b2
Nr1h4
Nr5a2
Nr1i2
Onecut1
Foxa2
Hhex
Nfic
Mlxipl
Hlf
LIVER-ID TFs
G
MPH
veh
PBA
Log2 FC ERS/Control
Xbp1s
Atf4
Atf6
Hspa5
Ddit3
Nfil3
Hnf4a
Nr0b2
Nr1h4
Nr5a2
Nr1i2
Onecut1
Foxa2
Hlf
ERS UP genes
LIVER-ID TFs
H
Nuclear extracts
MPH
HNF4A
NR1H4
FOXA2
DDIT3
LMNA
I
Chromatin fractions
HNF4A
NR1H4
FOXA2
DDIT3
H3
ERS (4h Tg)
Rep #1
Rep #2
Rep #3
Rep #1
Rep #2
Rep #3

Figure 3

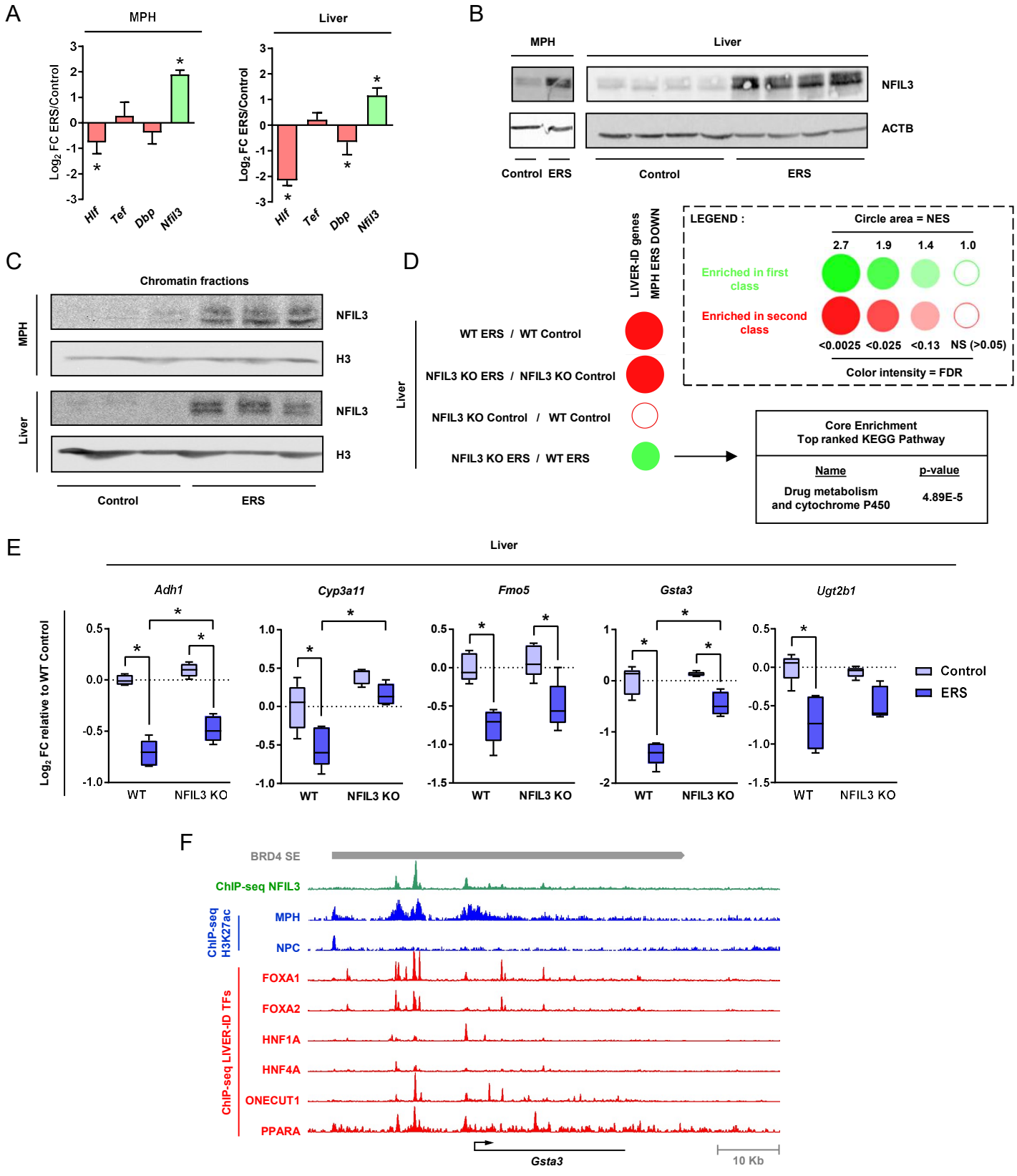
A
MPH
Liver
Log2 FC ERS/Control
Hlf
Tef
Dbp
Nfil3
B
MPH
Liver
NFIL3
ACTB
Control
ERS
C
Chromatin fractions
MPH
Liver
NFIL3
H3
Control
ERS
D
LIVER-ID genes
MPH ERS DOWN
WT ERS / WT Control
NFIL3 KO ERS / NFIL3 KO Control
NFIL3 KO Control / WT Control
NFIL3 KO ERS / WT ERS
LEGEND :
Circle area = NES
2.7
1.9
1.4
1.0
Enriched in first class
Enriched in second class
<0.0025
<0.025
<0.13
NS (>0.05)
Color intensity = FDR
Core Enrichment
Top ranked KEGG Pathway
Name
p-value
Drug metabolism and cytochrome P450
4.89E-5
E
Liver
Adh1
Cyp3a11
Fmo5
Gsta3
Ugt2b1
Log2 FC relative to WT Control
WT
NFIL3 KO
Control
ERS
F
BRD4 SE
ChIP-seq NFIL3
ChIP-seq H3K27ac
MPH
NPC
ChIP-seq LIVER-ID TFs
FOXA1
FOXA2
HNF1A
HNF4A
ONECUT1
PPARA
Gsta3
10 Kb

Figure 4

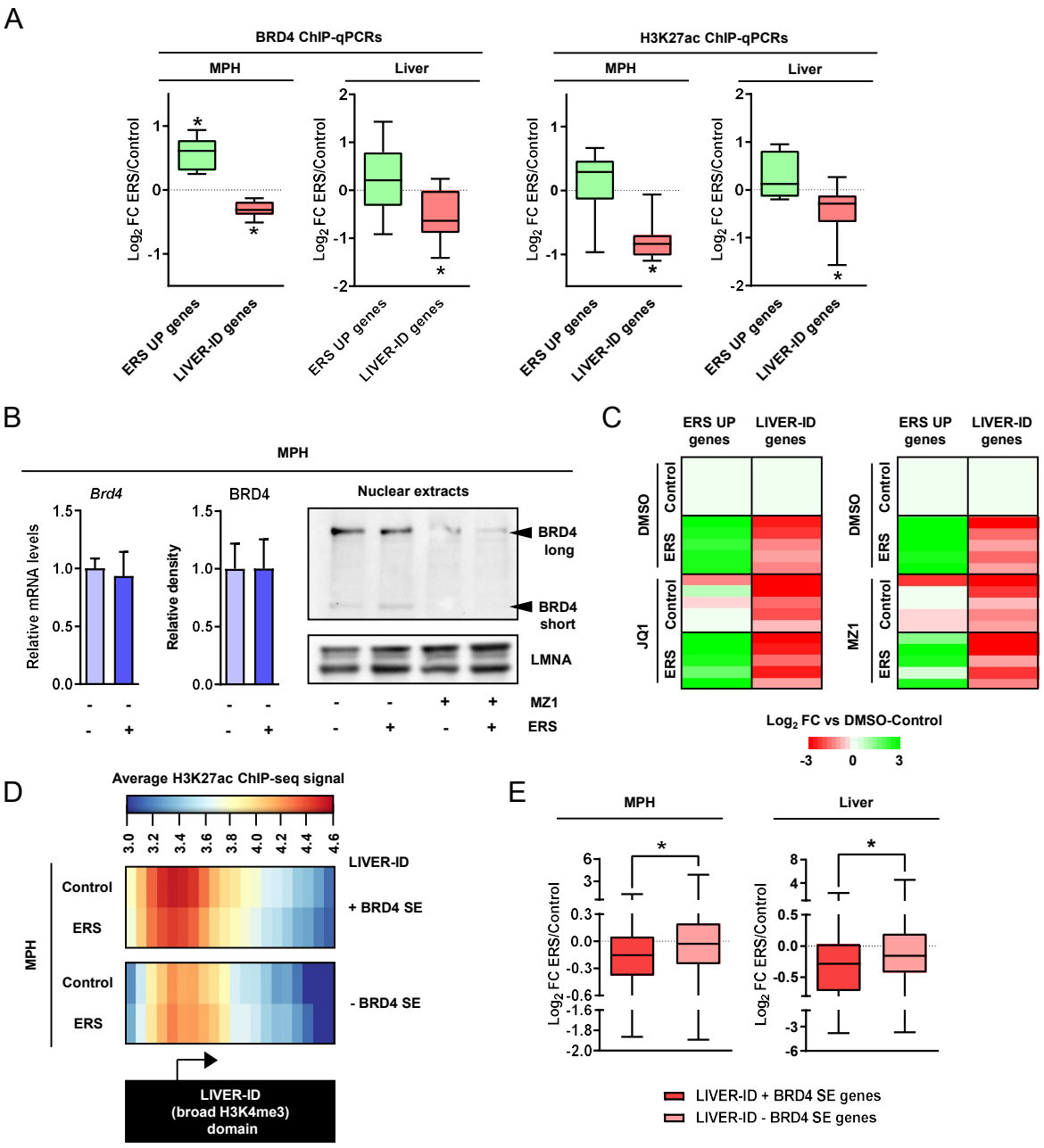
A
BRD4 ChIP-qPCRs
H3K27ac ChIP-qPCRs
MPH
Liver
Log2 FC ERS/Control
ERS UP genes
LIVER-ID genes
B
MPH
Brd4
BRD4
Nuclear extracts
Relative mRNA levels
Relative density
BRD4 long
BRD4 short
LMNA
MZ1
ERS
C
ERS UP genes
LIVER-ID genes
DMSO
JQ1
MZ1
Control
ERS
Log2 FC vs DMSO-Control
D
Average H3K27ac ChIP-seq signal
LIVER-ID
+ BRD4 SE
- BRD4 SE
LIVER-ID (broad H3K4me3) domain
E
LIVER-ID + BRD4 SE genes
LIVER-ID - BRD4 SE genes

Figure 5

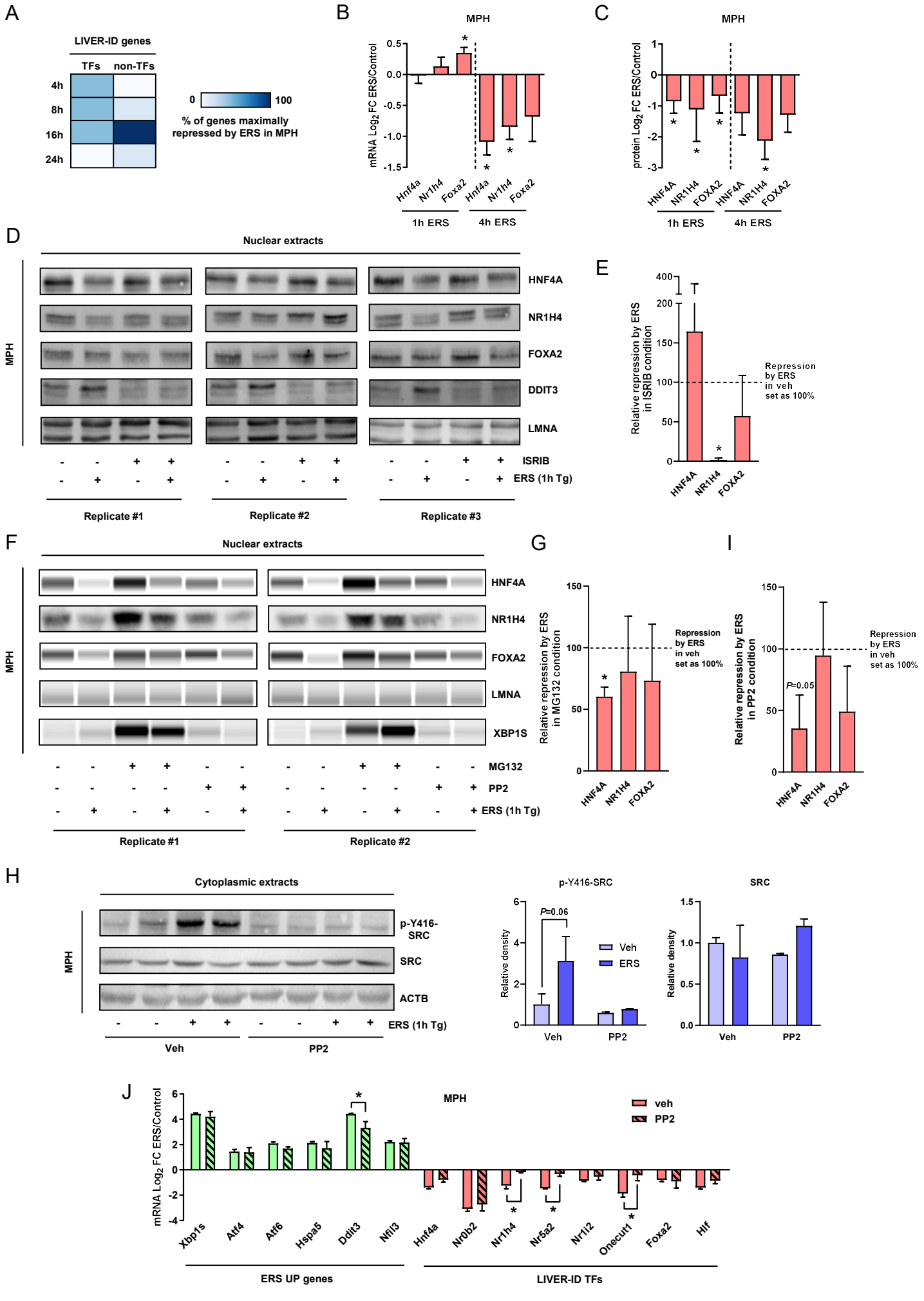
A
LIVER-ID genes
TFs
non-TFs
4h
8h
16h
24h
0
100
% of genes maximally repressed by ERS in MPH
B
MPH
mRNA Log2 FC ERS/Control
Hnf4a
Nr1h4
Foxa2
1h ERS
4h ERS
C
MPH
protein Log2 FC ERS/Control
HNF4A
NR1H4
FOXA2
1h ERS
4h ERS
D
Nuclear extracts
MPH
HNF4A
NR1H4
FOXA2
DDIT3
LMNA
ISRIB
ERS (1h Tg)
Replicate #1
Replicate #2
Replicate #3
E
Relative repression by ERS in ISRIB condition
Repression by ERS in veh set as 100%
HNF4A
NR1H4
FOXA2
F
Nuclear extracts
MPH
HNF4A
NR1H4
FOXA2
LMNA
XBP1S
MG132
PP2
ERS (1h Tg)
Replicate #1
Replicate #2
G
Relative repression by ERS in MG132 condition
Repression by ERS in veh set as 100%
HNF4A
NR1H4
FOXA2
I
Relative repression by ERS in PP2 condition
P=0.05
Repression by ERS in veh set as 100%
HNF4A
NR1H4
FOXA2
H
Cytoplasmic extracts
MPH
p-Y416-SRC
SRC
ACTB
ERS (1h Tg)
Veh
PP2
p-Y416-SRC
P=0.06
Relative density
Veh
ERS
Veh
PP2
SRC
Relative density
Veh
PP2
J
MPH
mRNA Log2 FC ERS/Control
veh
PP2
Xbp1s
Atf4
Atf6
Hspa5
Ddit3
Nfil3
Hnf4a
Nr0b2
Nr1h4
Nr5a2
Nr1i2
Onecut1
Foxa2
Hif
ERS UP genes
LIVER-ID TFs

Figure 6

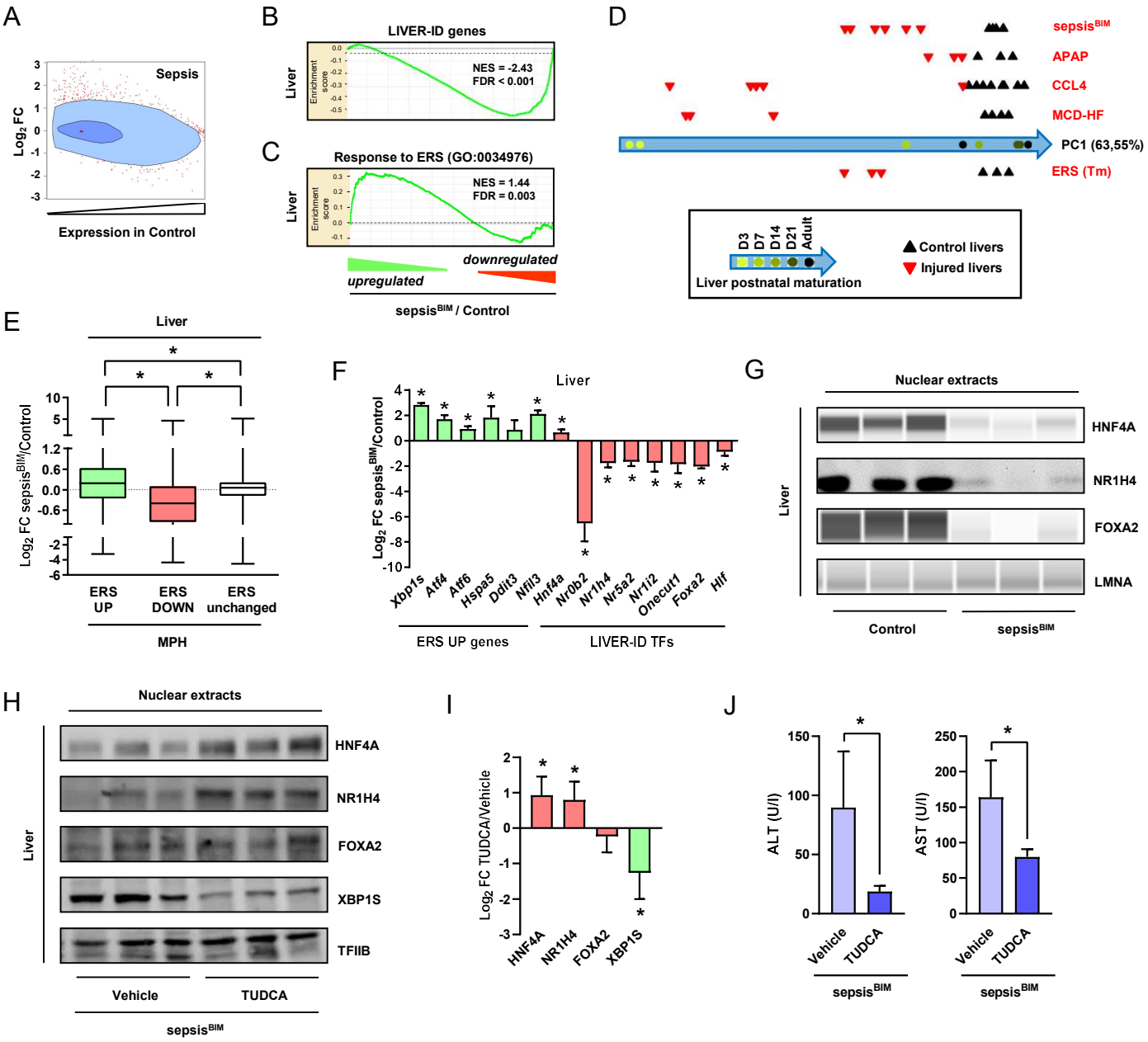
A
Sepsis
Log2 FC
Expression in Control
B
LIVER-ID genes
Liver
Enrichment score
NES = -2.43
FDR < 0.001
C
Response to ERS (GO:0034976)
Liver
Enrichment score
NES = 1.44
FDR = 0.003
upregulated
downregulated
sepsisBIM / Control
D
sepsisBIM
APAP
CCL4
MCD-HF
PC1 (63,55%)
ERS (Tm)
D3
D7
D14
D21
Adult
Liver postnatal maturation
Control livers
Injured livers
E
Liver
Log2 FC sepsisBIM/Control
ERS UP
ERS DOWN
ERS unchanged
MPH
F
Liver
Log2 FC sepsisBIM/Control
Xbp1s
Atf4
Atf6
Hspa5
Ddit3
Nfil3
Hnf4a
Nr0b2
Nr1h4
Nr5a2
Nr1i2
Onecut1
Foxa2
Hlf
ERS UP genes
LIVER-ID TFs
G
Nuclear extracts
Liver
HNF4A
NR1H4
FOXA2
LMNA
Control
sepsisBIM
H
Nuclear extracts
Liver
HNF4A
NR1H4
FOXA2
XBP1S
TFIIB
Vehicle
TUDCA
sepsisBIM
I
Log2 FC TUDCA/Vehicle
HNF4A
NR1H4
FOXA2
XBP1S
J
ALT (U/l)
AST (U/l)
Vehicle
TUDCA
sepsisBIM
sepsisBIM

Figure 7

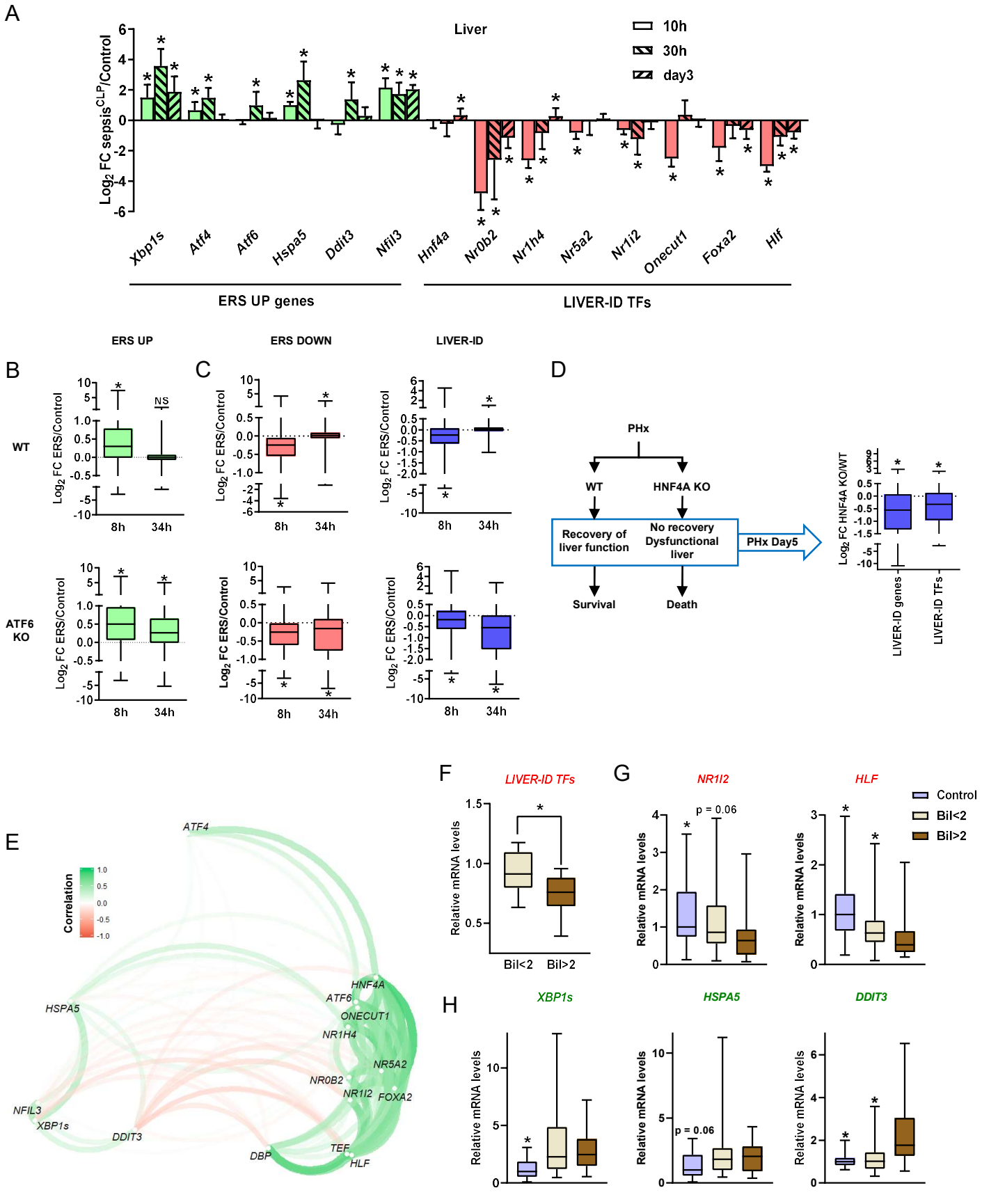
A
Liver
10h
30h
day3
Log2 FC sepsis CLP/Control
Xbp1s
Atf4
Atf6
Hspa5
Ddit3
Nfil3
Hnf4a
Nr0b2
Nr1h4
Nr5a2
Nr1i2
Onecut1
Foxa2
Hlf
ERS UP genes
LIVER-ID TFs
ERS UP
ERS DOWN
LIVER-ID
B
C
D
WT
ATF6 KO
Log2 FC ERS/Control
NS
8h
34h
PHx
WT
HNF4A KO
Recovery of liver function
No recovery Dysfunctional liver
PHx Day5
Survival
Death
Log2 FC HNF4A KO/WT
LIVER-ID genes
LIVER-ID TFs
E
Correlation
ATF4
HNF4A
ATF6
ONECUT1
NR1H4
NR5A2
NR0B2
NR1I2
FOXA2
HSPA5
NFIL3
XBP1s
DDIT3
DBP
TEF
HLF
F
LIVER-ID TFs
Relative mRNA levels
Bil<2
Bil>2
G
NR1I2
HLF
p = 0.06
Control
Bil<2
Bil>2
H
XBP1s
HSPA5
DDIT3
p = 0.06

Figure 8

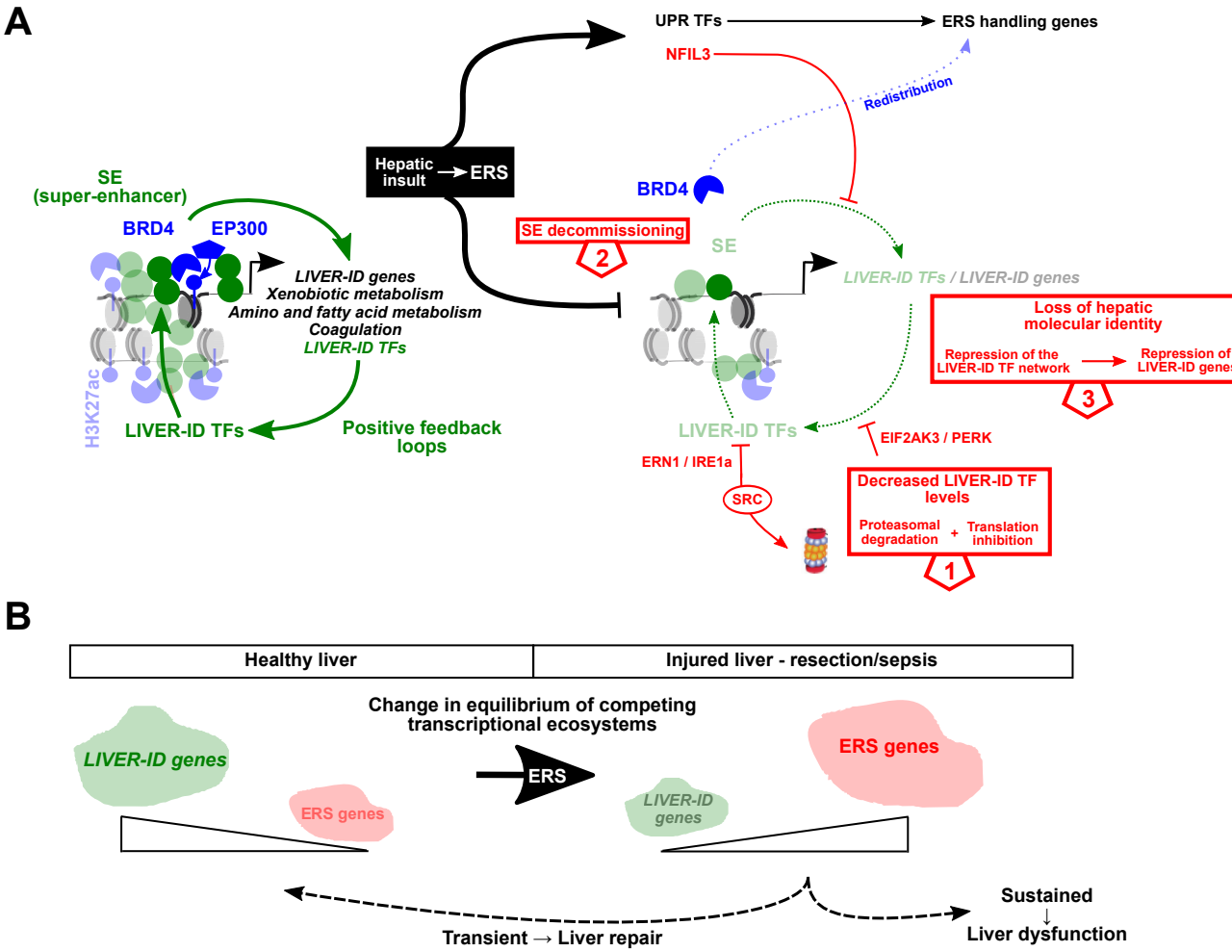
A
UPR TFs
ERS handling genes
NFIL3
Redistribution
Hepatic insult
ERS
BRD4
SE
(super-enhancer)
BRD4
EP300
SE decommissioning
2
SE
LIVER-ID TFs / LIVER-ID genes
Loss of hepatic molecular identity
Repression of the LIVER-ID TF network
Repression of LIVER-ID genes
3
LIVER-ID genes
Xenobiotic metabolism
Amino and fatty acid metabolism
Coagulation
LIVER-ID TFs
H3K27ac
LIVER-ID TFs
Positive feedback loops
LIVER-ID TFs
EIF2AK3 / PERK
ERN1 / IRE1a
SRC
Decreased LIVER-ID TF levels
Proteasomal degradation
+
Translation inhibition
1
B
Healthy liver
Injured liver - resection/sepsis
Change in equilibrium of competing transcriptional ecosystems
LIVER-ID genes
ERS genes
ERS
LIVER-ID genes
ERS genes
Transient → Liver repair
Sustained
↓
Liver dysfunction

Table EV1
This table provides the list of LIVER-ID and UBQ genes.
LIVER-ID genes identified as LIVER-ID TFs and linked to BRD4 SE are indicated.

BLUE CLUSTER

Kmt2b.EXP032360.immortalized_brown_preadipocytes..bed
Smad3.EXP000858.38B9_cells.TGF.bed
Gata3.EXP000796.CD8_Gata3_KO.NULL.bed
Ar.EXP032776.caput_epididymis.specificity_affecting_androgen_receptor_knock-in.bed
Rarb.EXP032486.Liver.RA-treatment.bed
Nr1d2.EXP031402.liver.time_5amZT22.bed
Ncor2.EXP032387.liver.ZT10.bed
Rxra.EXP032521.RMKO_314..bed
Ar.EXP032777.caput_epididymis.specificity_affecting_androgen_receptor_knock-in.bed
Rxra.EXP032518.RFKO_232..bed
Ncor2.EXP032388.liver.ZT22.bed
Nr1d1.EXP031403.liver.Rev-erb_alpha_KO.bed
Trp53.EXP030949.embryonic_stem_ES_cells.untreated.bed
Cebpb.EXP031832.C57BL6J.3_hours_after_partial_hepatectomy.bed
Rxra.EXP032520.RMKO_225..bed
Rxra.EXP032519.RFKO_233..bed
Rxra.EXP032524.RMWT_315..bed
Rxra.EXP032522.RFWT_234..bed
Hnf4a.EXP032824.colonic_epithelial_cells.3%_DSS.bed
Hnf4a.EXP031181.Mouse_villus..bed
Rxra.EXP032525.RMWT_227..bed
Ar.EXP032172.caput_epididymis.castratedplusvehicle.bed
Egr1.EXP031839.C57BL6J.36_hours_after_partial_hepatectomy.bed
Rxra.EXP032523.RFWT_235..bed
Stat5a.EXP032418.mammary.Ezh2_KO.bed
Ar.EXP032175.prostate.castratedplusvehicle.bed
Esr1.EXP030621.Liver..bed
Nfe2.EXP031818.primary_megakaryocytes..bed
Trp53.EXP030950.embryonic_stem_ES_cells.adriamycin.bed
PR.EXP031194.uterus.P4.bed
Cebpb.EXP031836.C57BL6J.36_hours_after_partial_hepatectomy.bed
Ar.EXP030586.Mouse_Prostate_R26-ERGERG..bed
Ar.EXP030588.Mouse_Prostate_Pten-ff_R26-ERGERG..bed
Ar.EXP030590.Mouse_Prostate_Pten-ff..bed
Nr5a2.EXP000283.pancreas.NULL.bed
Nr1d2.EXP031401.liver.time_5pmZT10.bed
Esrra.EXP031907.liver..bed
Kmt2b.EXP030685.mouse_brown_preadipocytes_WT_CEBPbeta_GFP_MLL4_ChIP..b
Rxra.EXP032487.Liver.RA-treatment.bed
Esr1.EXP032821.liver.10_nM_beta-estradiol_E2.bed
Esr1.EXP031407.uterus.vehicle.bed
Hnf4a.EXP031182.Mouse_villus_Cdx2_KO..bed
Cebpb.EXP032041.liver.dex.bed
Cebpb.EXP031992.mouse_whole_liver.Ad-lib_fed.bed
Cux2.EXP031264.CD-1_Charles_River_female..bed
Pparg.EXP032204.3T3-L1.adeno-LACZ.bed
Ppara.EXP031218.liver.Control.bed
Esr1.EXP032062.mouse_mammary_cells_express_GFP-GR_Cherry-ER_and_Afos_un
Elf5.EXP031810.Trophoblast_stem_cells..bed

Rxra.EXP032484.Liver..bed
Cebpa.EXP031829.C57BL6J.48_hours_after_partial_hepatectomy.bed
Rxra.EXP032105.liver..bed
Stat5b.EXP030769.Mammary_tissues.stat5a-null.bed
Rela.EXP032922.C57BL6.LPS.bed
Cebpa.EXP031830.C57BL6J.168_hours_after_partial_hepatectomy.bed
Pparg.EXP000533.thioglycollate-elicited_peritoneal_macrophages.NULL.bed
Cebpa.EXP031828.C57BL6J.36_hours_after_partial_hepatectomy.bed
Stat5a.EXP000123.CD-1_FL.NULL.bed
Cebpa.EXP031826.C57BL6J.16_hours_after_partial_hepatectomy.bed
Esr2.EXP032820.aorta.10_nM_beta-estradiol_E2.bed
Stat5a.EXP032237.mammary_gland.day_6_of_pregnancy.bed
Cebpa.EXP031824.C57BL6J.3_hours_after_partial_hepatectomy.bed
Cebpb.EXP032037.liver.dex_adDN-CEBP.bed
Nr1d1.EXP000373.liver.ZT10.bed
Cebpb.EXP031838.C57BL6J.168_hours_after_partial_hepatectomy.bed
Cebpb.EXP031834.C57BL6J.16_hours_after_partial_hepatectomy.bed
Hnf4a.EXP032179.kidney.castratedplusvehicle.bed
Smarcc2.EXP032586.Mouse_embryonic_day_11_5_e11_5_hindbrain..bed
Cebpb.EXP032036.liver.dex_adGFP.bed
Cebpb.EXP031837.C57BL6J.48_hours_after_partial_hepatectomy.bed
Ar.EXP032778.ventral_prostate..bed
Foxa1.EXP031141.CD1_outbred_mice..bed
Stat5a.EXP000121.CD-1_FH.NULL.bed
Cebpb.EXP031831.C57BL6J.0_hours_after_partial_hepatectomy.bed
Cebpa.EXP030885.liver_hepatocytes..bed
Cebpb.EXP031835.C57BL6J.24_hours_after_partial_hepatectomy.bed
Ar.EXP032774.caput_epididymis..bed
Stat5a.EXP000120.CD-1_MH.NULL.bed
Cebpa.EXP031827.C57BL6J.24_hours_after_partial_hepatectomy.bed
Cebpa.EXP031823.Total_hepatectomized_liver.0_hours_after_partial_hepatectomy.bed
Sox2_produced_in-house.EXP030985.ZHBTc4.Tet.bed
Cebpb.EXP031833.C57BL6J.8_hours_after_partial_hepatectomy.bed
TCF7L1_M-20.EXP000273.3T3-L1.24_hours_of_adipogenic_stimuli.bed
Foxa2.EXP030886.liver_hepatocytes..bed
Sox2_produced_in-house.EXP030987.ZHBTc4.Tet.bed
Gata4_C-20.EXP031209.heart..bed
Rxra.EXP031223.LXRdKO_liver.Bexarotene.bed
Ar.EXP030592.Mouse_Prostate..bed
Rxra.EXP031224.LXRdKO_liver.Control.bed
Hnf4a.EXP032169.kidney.castratedplustestosterone.bed
Rxra.EXP031225.LXRdKO_liver.T0901317.bed
Ppara.EXP031219.LXRdKO_liver.Control.bed
Cebpa.EXP031825.C57BL6J.8_hours_after_partial_hepatectomy.bed
Sox2_produced_in-house.EXP030988.ZHBTc4.Tet.bed
Rxra.EXP031222.liver.T0901317.bed
Ar.EXP032180.caput_epididymis.intact.bed
Rxra.EXP031221.liver.Control.bed
Yy1.EXP031227.ES-derived_cardiac_progenitor_cells_CPCs..bed
Rxra.EXP031220.liver.Bexarotene.bed

Stat5a.EXP000122.CD-1_ML.NULL.bed
Foxa2.EXP000383.liver.NULL.bed
Ar.EXP032178.kidney.castratedplustestosterone.bed
Foxa1.EXP030887.liver_hepatocytes..bed
anti-GATA4.EXP032274.C57BL6_x_Sv129..bed
Foxa2.EXP031805.Neuralized_embryoid_bodies.all_trans_retinoic_acid_RA_and_SAG_
Foxa2.EXP000905.Liver_tissue.NULL.bed
Ar.EXP032176.prostate.castratedplustestosterone.bed
GR_EXP031991.mouse_whole_liver.Ad-lib_fed.bed
Ar.EXP032775.caput_epididymis..bed
GR_Santa_Cruz_Biotechnologies_sc-1004_and_Affinity_BioReagents_PA1-511A.EXP0
Esr1.EXP032822.liver.10_nM_beta-estradiol_E2.bed
Esr1.EXP032819.aorta.10_nM_beta-estradiol_E2.bed
Nr1d1.EXP031165.liver..bed
Esr1.EXP032063.7438_cells.Dexamethasone_plus_Estradiol_for_30_minutes.bed
Foxp3.EXP031698.primary_CD4plus_Tconv_cells..bed
GR_sc-1004_from_SantaCruz.EXP031463.AtT-20.DexplusLIF.bed
GR.EXP032057.mouse_mammary_cells_express_GFP-GR_Cherry-ER_and_Afos_und
Nr1d2.EXP031166.liver..bed
GR.EXP032058.mouse_mammary_cells_express_GFP-GR_Cherry-ER_and_Afos_und
Cebpb.EXP032039.liver.veh.bed
GR.EXP032059.mouse_mammary_cells_express_GFP-GR_Cherry-ER_and_Afos_und
Stat5a.EXP030768.Mammary_tissues.stat5a-null.bed
Pax6.EXP031752.ES-derived_neural_progenitor_like_cells..bed
cocktail_of_PA-510A_and_PA-511A_from_Affinity_BioReagents_and_sc-1004_from_Sa
cocktail_of_PA-510A_and_PA-511A_from_Affinity_BioReagents_and_sc-1004_from_Sa
cocktail_of_PA-510A_and_PA-511A_from_Affinity_BioReagents_and_sc-1004_from_Sa
GR_sc-1004_from_SantaCruz.EXP031464.AtT-20.Dex.bed
cocktail_of_PA-510A_and_PA-511A_from_Affinity_BioReagents_and_sc-1004_from_Sa
PR.EXP031195.uterus_epithelium.P4.bed
Tead4.EXP031469.Blastocyst_derived_trophoblast_stem_cells..bed
Cux2.EXP031263.CD-1_Charles_River_male..bed
Trp53.EXP030951.embryonic_stem_ES_cells.untreated.bed
Tet1.EXP000665.mouse_embryonic_stem_MES_cells.tet1_mut1.bed
Tet1.EXP000666.mouse_embryonic_stem_MES_cells.tet1_mut2.bed

GREEN CLUSTER

Jarid2.EXP000313.embryonic_stem_cells.NULL.bed
Kmt2b.EXP032467.Embryonic_Stem_Cells_ESCs..bed
Zfx.EXP000482.Embryonic_stem_cells.NULL.bed
Zbtb17.EXP032614.T-lymphocytes.Doxycycline_1ugml_for_30_hours.bed
Fli1.EXP010950.Megakaryo.NULL.bed
Sp1.EXP031619.F1_CB_trophoblast_stem_cells..bed
Zbtb17.EXP032615.T-lymphocytes..bed
MAZ_ab85725.EXP011087.MEL.None.bed
Tet1.EXP000593.embryonic_stem_cells.NULL.bed
Spi1.EXP000211.Murine_erythroleukemia_MEL_cells_stably_transfected_with_Gata-1_
Rara.EXP031168.CMTi-1.shH2A_Z.bed
Srf.EXP000181.mouse_cardiomyocytes_HL1-cells.NULL.bed
Erg.EXP030846.spleen_cells..bed
Erg.EXP030847.spleen_cells_GATA1s..bed
Fli1.EXP031695.progenitors..bed
Rarb.EXP032483.Liver..bed
Anti-haemagglutinin_HA_Covance_.EXP031493.pre-B_cell_line_B3..bed
Rara.EXP031167.CMTi-1..bed
Sp1.EXP032825.E14__FLK1plus..bed
Ehf.EXP030581.C57Bl6_corneal_epithelium..bed
Sox9.EXP032507.intefollicular_epidermal_cells_IFE..bed
Runx1.EXP031139.primary_thymocyte..bed
Utf1.EXP030689.mouse_embryonic_stem_cells.Standard_Serum.bed
Sp1.EXP032826.Flkplus_cKitplus_progenitor..bed
Smad3.EXP000853.MC1R20tetMyod114_embryonic_stem_cells.plusMyod1_day_5.bec
Ctcf.EXP031035.Mouse_E14_5_limb..bed
Klf4.EXP032749.CGR8.KLF4_overexpression.bed
Rabbit_anti-C-terminal_Ikaros.EXP031492.pre-B_cell_line_B3..bed
Ctcf.EXP031041.Mouse_thymus..bed
Ctcf.EXP010565.Thymus.NULL.bed
Tet1.EXP000667.mouse_embryonic_stem_MES_cells..bed
Rest.EXP000927.V6_5_embryonic_stem_cells.NULL.bed
Ptf1a.EXP032950.ICR..bed
Pax5.EXP030465.mix_C57BL6_and_129..bed
Fli1.EXP032696.primary_mast_cells..bed
Smad3.EXP000851.MC1R20tetMyod114_embryonic_stem_cells.Activin_plusMyod1_da
homemade_Ikaros_Ikzf1.EXP031105.mouse_wt_DP_thymocytes..bed
Sox9.EXP032506.hair_follicle_stem_cells_HFSCs..bed
Tcf7l2.EXP031214.Hepatocytes_isolated_from_adult_liver..bed
Creb1.EXP031994.mouse_whole_liver.Fasted_24h_Re-fed_2h.bed
Klf5.EXP032750.CGR8.KLF5_overexpression.bed
Rabbit_anti-C-terminal_Ikaros_[from_Stephen_Smale_Lab].EXP031844.primary_pre-B_
Spi1.EXP031071.Fetal_liver_precursor_derived_DN1..bed
Ctcf.EXP031030.Mouse_spleen..bed
Pparg.EXP031795.C3H10T12_cells..bed
Pou5f1.EXP032977.epiblast_like_cells_EpiLC..bed
Foxa2.EXP030604.postnatal_day_12_female_mouse_uterus..bed
RD_Systems_RD_AF2018.EXP031248.ES-derived_neural_progenitor_cells_NPCs..bec
Ctcf.EXP032691.HPC7..bed

Pou5f1.EXP031880.ESC.jmjd2b_KD.bed
Srf.EXP030897.HL-1_cardiac_muscle_cell_line..bed
Runx2.EXP032846.mineralizing_osteoblast..bed
Kmt2b.EXP032320.immortalized_brown_preadipocytes.D7_of_adipogenesis_MLL4_KO
Pou5f1.EXP031883.ESC.jmjd2c_KD.bed
Creb1.EXP031993.mouse_whole_liver.Fasted_24h.bed
Erg.EXP030591.Mouse_Prostate_Pten-ff..bed
Kmt2b.EXP032319.immortalized_brown_preadipocytes.D2_of_adipogenesis_MLL4_KO
Gata2.EXP030541.Mast_cell..bed
Pou5f1.EXP031169.CMTi-1..bed
Gata2.EXP032697.primary_mast_cells..bed
Zfp143.EXP030478.MEF-like..bed
Spi1.EXP000855.38B9_cells.NULL.bed
Klf5.EXP032748.CGR8..bed
Runx2.EXP032844.preosteoblast..bed
Pou5f1.EXP031878.ESC..bed
Vdr.EXP032793.MC3T3-E1.ethanol_vehicle.bed
Rara.EXP032482.Liver..bed
Rara.EXP032106.liver..bed
Spi1.EXP031073.Fetal_liver_precursor_derived_DN2b..bed
Pou5f1.EXP031170.CMTi-1.shH2A_Z.bed
Gfi1b.EXP031099.MLL-ENL_immortalized_bone_marrow_progenitor_cells..bed
Tet1.EXP031131.P19_6..bed
Pou5f1.EXP032985.embryonic_stem_cells_ESC..bed
Smad3.EXP030726.neural_stem_cells.TGFb.bed
Ctcf.EXP010510.MEL.NULL.bed
Tet1.EXP031132.P19_6.all-trans_retinoic_acid_RA.bed
Runx2.EXP032845.matrix-depositing_osteoblast..bed
Tbx5.EXP030898.HL-1_cardiac_muscle_cell_line..bed
Prdm5.EXP032409.mouse_embryonic_fibroblast..bed
T.EXP032929.D3..bed
Myog.EXP010576.C2C12.EqS_2_0pct_24hr.bed
Foxo1.EXP000864.pro-B_cell.RAG1_KO.bed
Zfp143.EXP030477.mESC_J1..bed
Ctcf.EXP010117.G1E-ER4.diffProtD_24hr.bed
Tfap2a.EXP032171.kidney.castratedplustestosterone.bed
Pparg.EXP030874.3T3-L1_adipocytes.0_1%_DMSO_Vehicle_for_1_hour.bed
Tcf3.EXP032692.HPC7..bed
Tfap2a.EXP032181.caput_epididymis.castratedplusvehicle.bed
Spi1.EXP032476.Pro-B_cell..bed
Runx2.EXP032591.MC3T3-E1.ethanol_vehicle.bed
Ptf1a.EXP030597.Neural_Tube..bed
Spi1.EXP031072.Fetal_liver_precursor_derived_DN2a..bed
Pou5f1.EXP030812.Embryonic_stem_cells..bed
TCF3.EXP030868.Telogen_quiescent_hair_follicle_stem_cells_HFSCs..bed
Tet1.EXP000591.embryonic_stem_cells.NULL.bed
Nanog.EXP031877.ESC..bed
Smad3.EXP000850.MC1R20tetMyod114_embryonic_stem_cells.Activin_-Myod1_day_2
Nanog.EXP031882.ESC.jmjd2c_KD.bed
Spi1.EXP032699.primary_mast_cells..bed

Pou5f1.EXP032976.epiblast_like_cells_EpiLC.Activin_A.bed
Irf8.EXP032458.dendritic_cells..bed
Sox9.EXP032505.hair_follicle_stem_cells_HFSCs..bed
ikaros.EXP032480.Pre-pro-B_cell..bed
anti-Otx2.EXP032979.epiblast_like_cells_EpiLC..bed
Olig2.EXP001005.Ainv15_ATCC_SCRC-1029_with_inducible_V5-tagged_Olig2..bed
Clock.EXP032489.Liver..bed
Irf8.EXP032460.dendritic_cells..bed
Tfap2a.EXP032182.caput_epididymis.intact.bed
Myog.EXP031958.C2C12..bed
Nfib.EXP031855.Hair_follicle_stem_cells_HfSCs..bed
Ctcf.EXP011053.SmIntestine.NULL.bed
Utf1.EXP030688.mouse_embryonic_stem_cells.Standard_Serum.bed
Esr1.EXP032992.uterine_cells.saline_vehicle.bed
GFP_Abcam_Cambridge_UK.EXP032498.Neural_Retina..bed
Ascl2.EXP032453.CD4plus_T_cells.Ascl2_vector_transfected.bed
Spi1.EXP032329.FDCPmix..bed
Spi1.EXP032255.Macrophage.DMSO_7h_Kdo2_Lipid_A_KLA_6h.bed
Pou5f1.EXP000018.ESC.NULL.bed
Tbx3.EXP031208.heart..bed
Fli1.EXP031691.hemogenic_endothelium.dox.bed
Ctcf.EXP031037.Mouse_intestine..bed
Spi1.EXP031529.bone_marrow-derived_macrophages_7th_day_of_differentiation.IFNg
Pax5.EXP030466.mix_C57BL6_and_129..bed
Myog.EXP010707.C2C12.EqS_2_0pct_60hr.bed
anti-Otx2.EXP032983.embryonic_stem_cells_ESC.Dox.bed
Runx2.EXP032798.MC3T3-E1.100nM_125OH2D3.bed
Spi1.EXP032326.FDCPmix..bed
Jarid2.EXP000184.Embyonic_stem_cells.NULL.bed
Erg.EXP030593.Mouse_Prostate..bed
Spi1.EXP031526.bone_marrow-derived_macrophages_7th_day_of_differentiation..bed
Spi1.EXP032242.Macrophage.none.bed
Foxa2.EXP030601.Pancreas..bed
Spi1.EXP032096.resting_mature_peripheral_primary_B_cells.stimulated_for_3_days.be
Ctcf.EXP000677.Embryonic_stem_cells.Dnmt13a3b_KO.bed
Spi1.EXP031518.bone_marrow-derived_macrophages_7th_day_of_differentiation.stat1
Ctcf.EXP031621.F1_CB_trophoblast_stem_cells..bed
Pparg.EXP030875.3T3-L1_adipocytes.1_M_rosiglitazone__0_1%_DMSO_for_1_hour.b
Cebpa.EXP030872.3T3-L1_adipocytes.0_1%_DMSO_Vehicle_for_1_hour.bed
Vdr.EXP032794.MC3T3-E1.100nM_125OH2D3.bed
Prdm5.EXP032410.mouse_embryonic_fibroblast..bed
Kmt2b.EXP032358.immortalized_brown_preadipocytes..bed
Spi1.EXP032331.FDCPmix..bed
T.EXP032913.D3..bed
anti-Klf4.EXP032729.mESC_J1..bed
Tfap2c.EXP032396.ZHBTc4-TS_cells..bed
Myod1.EXP031190.P19_cells..bed
Utf1.EXP031631.Embryonic_Stem_Cell..bed
Nkx2-5_N-19.EXP031210.heart..bed
Rara.EXP032485.Liver.RA-treatment.bed

Tcf3.EXP000868.double-positive_T_cell.NULL.bed
anti-Otx2.EXP032978.epiblast_like_cells_EpiLC.Activin_A.bed
Spi1.EXP031538.BMDM_cells_7th_day_of_differentiation..bed
Fli1.EXP000332.Early_haematopoietic_cell_line_derived_from_ES_cells.NULL.bed
Spi1.EXP000841.bone_marrow-derived_macrophages.LXRD_KO.bed
Tcf3.EXP000866.pre-pro-B_cell.E2A_KO_1h.bed
Meis1.EXP031130.P19_6.all-trans_retinoic_acid_RA.bed
Spi1.EXP032095.resting_mature_peripheral_primary_B_cells.stimulated_for_1_day.bec
Ncoa2.EXP032905.Prostate..bed
sox2.EXP032894.D3_Embryonic_Stem_Cells..bed
Ctcf.EXP010450.CH12.None.bed
Erg.EXP030589.Mouse_Prostate_Pten-ff_R26-ERGERG..bed
Ctcf.EXP010468.Lung.NULL.bed
Ctcf.EXP031032.Bruce4_embryonic_stem_cells..bed
Pax5.EXP030464.C57BL6..bed
Ctcf.EXP031029.Mouse_lung..bed
Srebf1.EXP032718.C57BL6.ZT18.bed
Erg.EXP030587.Mouse_Prostate_R26-ERGERG..bed
Kmt2b.EXP032317.immortalized_brown_preadipocytes.D7_of_adipogenesis.bed
Tbx3.EXP031951.Mouse_embryonic_stem_cells..bed
anti-Klf4.EXP032727.mESC_J1..bed
Tfcp2l1.EXP000480.Embryonic_stem_cells.NULL.bed
Ctcf.EXP010091.Heart.NULL.bed
Ctcf.EXP010284.Kidney.NULL.bed
Nanog.EXP031954.Mouse_embryoid_bodies..bed
Ctcf.EXP031023.Mouse_cortex..bed
Ctcf.EXP010181.Liver.NULL.bed
Ctcf.EXP031026.Mouse_heart..bed
Ctcf.EXP031028.Mouse_liver..bed
Ctcf.EXP010301.Cortex.NULL.bed
Ascl1_Abcam_ab74065_lot_830280.EXP032187.Primary_adult_neural_progenitor_cell.
Clock.EXP032488.Liver..bed
Ctcf.EXP031027.Mouse_kidney..bed
Ctcf.EXP010612.MEF.NULL.bed
Spi1.EXP000535.thioglycollate-elicited_peritoneal_macrophages.NULL.bed
anti-Otx2.EXP032981.embryonic_stem_cells_ESC..bed
Gata2.EXP031715.Mouse_uterus.P4.bed
Cebpa.EXP030873.3T3-L1_adipocytes.1_M_rosiglitazone__0_1%_DMSO_for_1_hour.b
Ctcf.EXP031031.Mouse_embryonic_fibroblast..bed
Tbx3.EXP031952.Mouse_embryoid_bodies..bed
Rxra.EXP032802.MC3T3-E1_differentiated_for_15_days.100nM_125OH2D3.bed
Tcf3.EXP000867.pre-pro-B_cell.E2A_KO_6h.bed
Nanog.EXP031953.Mouse_embryonic_stem_cells..bed
ZNF384_HPA004051.EXP011017.ES-E14.None.bed
Rxra.EXP000681.F9_embryonal_carcinoma_cells.6hr_ATRA.bed
Ebf1.EXP031258.Bone_Marrow..bed
Spi1.EXP031560.Myeloid_progenitor_cells.MSCV-IRF8_transduced.bed
Tal1.EXP000085.Lin-_bone_marrow_hematopoietic_progenitor_cells.NULL.bed
Tfap2a.EXP032167.prostate.castratedplustestosterone.bed
Cebpb.EXP032347.immortalized_brown_preadipocytes..bed

Foxa2.EXP030605.day_of_pseudopregnancy_2_5_and_3_5_female_mouse_uterus..be
Gata1.EXP031251.G1ME..bed
Ebf1.EXP000188.A-MuLV_pre_B-cells.NULL.bed
Ebf1.EXP032475.Pro-B_cell..bed
Ascl1_ab74065.EXP030573.C57BL6_embryonic_fibroblasts.BAM_factors.bed
Anti-HA.EXP031689.differentiating_murine_hematopoietic_cells.dox.bed
Rbpjl.EXP030600.Pancreas..bed
Smad3.EXP000852.MC1R20tetMyod114_embryonic_stem_cells.-Myod1_day_5.bed
GFP_Abcam_Cambridge_UK.EXP032496.RPE..bed
Pparg.EXP030809.Brown_Adipose_Tissue..bed
Olig2.EXP001006.Ainv15_ATCC_SCRC-1029_with_inducible_V5-tagged_Olig2.plusDo
Nkx3-1.EXP031261.Recombinant_inbred_B6_x_129_Nkx3-1_plus-..bed
Esr2.EXP032993.uterine_cells.estradiol_250_ngmouse.bed
Rxra.EXP032801.MC3T3-E1_differentiated_for_15_days.ethanol_vehicle.bed
Ascl1_ab74065.EXP030566.C57BL6_neural_progenitor.Ascl1.bed
Tal1.EXP031693.differentiating_murine_hematopoietic_cells..bed
Atoh1.EXP000331.4_P5_cerebella_pooled.NULL.bed
Ar.EXP032779.ventral_prostate.specificity_affecting_androgen_receptor_knock-in.bed
Pparg.EXP030810.Epididymal_White_Adipose_Tissue..bed
Esr1.EXP031408.uterus.estradiol.bed
Foxo3-NFL_Brunet_Lab_Greer_et_al__2007_PMID_17900900.EXP032188.Primary_ad
Gata1.EXP011011.MEL.DMSO_2_0pct.bed
Sox2.EXP031239.embryonic_stem_cells_ESCs..bed
Cebpa.EXP030889.differentiated_3T3-L1_cells..bed
Arntl.EXP032491.Liver..bed
Rxra.EXP000679.F9_embryonal_carcinoma_cells.48hr_ethanol.bed
Myod1.EXP000856.C2C12_cells.NULL.bed
Rxra.EXP000682.F9_embryonal_carcinoma_cells.24hr_ATRA.bed
Rxra.EXP000683.F9_embryonal_carcinoma_cells.48hr_ATRA.bed
Atf2.EXP033004.3T3-L1..bed
FLAG_and_HA.EXP000359.mESCs.NULL.bed
Kmt2b.EXP032359.MyoD-induced_immortalized_brown_preadipocytes..bed
Pparg.EXP000491.3T3L1_cells.Day_0_of_differentiation.bed
Sox2_raised_by_ourselves.EXP032395.ZHBTc4-TS_cells..bed
Arntl.EXP032490.Liver..bed
Tbx20.EXP000266.adult_whole_heart.NULL.bed
Trp53.EXP030952.embryonic_stem_ES_cells.adriamycin.bed
custom_made_against_Esrrb.EXP000485.Embryonic_stem_cells.NULL.bed
PR.EXP031193.uterus.oil.bed
Srebf1.EXP032719.C57BL6.ZT22.bed
Nr5a2.EXP000179.embryonic_stem_cells.NULL.bed
Trp53.EXP032070.mouse_embryo_fibroblast_MEF.0_2ugml_doxorubicin_for_6h.bed
anti-Ascl1.EXP032949.ICR..bed
Hnf4a.EXP032823.colonic_epithelial_cells.water_only.bed
Esr1.EXP031898.mammary_gland..bed
Pparg.EXP000494.3T3L1_cells.Day_3_of_differentiation.bed

PURPLE CLUSTER

Cebpb.EXP032901.BV2..bed
Gata1.EXP031087.Megakaryocyte_Progenitor_Cell_Line_G1ME..bed
Nkx3-1.EXP031262.Recombinant_inbred_B6_x_129..bed
Nkx2-1.EXP031891.mixed_129B6..bed
Hsf1.EXP031482.striatal_cells_derived_from_wild_type_HdhQ7Q7_embryonic_mice.ce
Kmt2b.EXP032316.immortalized_brown_preadipocytes.D2_of_adipogenesis.bed
Cebpb.EXP010773.C2C12.EqS_2_0pct_60hr.bed
Nkx2-1.EXP031892.mixed_129B6..bed
Pparg.EXP000041.3T3-L1_adipocytes.NULL.bed
Cdx2.EXP032548.ESC_Ainv15_ATCC_SCRC-1029.plusDox_plusFGF.bed
Rela.EXP030425.primary_bone_marrow-derived_macrophages.Dexamethasone_treate
Myod1.EXP032355.MyoD-induced_immortalized_brown_preadipocytes..bed
Spi1.EXP032895.BV2..bed
Myog.EXP010753.C2C12.EqS_2_0pct_7d.bed
Pbx1.EXP033034.3T3-L1..bed
Neurod1.EXP000434.hand-picked_pancreatic_islets.NULL.bed
Klf5.EXP033033.3T3-L1..bed
Cebpa.EXP032345.immortalized_brown_preadipocytes..bed
Myod1.EXP010557.C2C12.None.bed
Pparg.EXP032349.immortalized_brown_preadipocytes..bed
Cebpb.EXP010962.C2C12.None.bed
Cebpa.EXP030545.Haematopoietic_progenitor_cells..bed
anti-KLF4.EXP033032.3T3-L1..bed
Cebpb.EXP030682.mouse_brown_preadipocytes_WT_CEBPbeta_GFP_CEBPbeta_Ch
Arntl.EXP000095.Liver_ZT02.NULL.bed
Anti-HA.EXP031688.differentiating_murine_hematopoietic_cells..bed
Myod1.EXP032275.C2C12_myoblasts_of_C3H_strain..bed
Esr1.EXP030622.Uterus..bed
Vdr.EXP032800.MC3T3-E1_differentiated_for_15_days.100nM_125OH2D3.bed
GRIP1.EXP030428.primary_bone_marrow-derived_macrophages.LPS-stimulated_macr
Cebpa.EXP032898.BV2..bed
Jund.EXP033005.3T3-L1..bed
GRIP1.EXP030429.primary_bone_marrow-derived_macrophages.Dexamethasone_trea
Spi1.EXP032897.BV2.mutant_human_Htt_overexpression.bed
Atf3.EXP032927.C57BL6.LPS.bed
Jun.EXP030427.primary_bone_marrow-derived_macrophages.Dexamethasone_treated
rabbit_anti-Runx1_EXP031986.BMiFLT315-3.bed
sc-7208.EXP031853.mammary_gland.17-estradiol_for_24_hours_and_then_17-estradio
runx1.EXP000340.Early_haematopoietic_cell_line_derived_from_ES_cells.NULL.bed
anti-NFATc1.EXP032431.Telogen_quiescent_hair_follicle_stem_cells..bed
Tcf12.EXP010142.C2C12.EqS_2_0pct_60hr.bed
Spi1.EXP032206.3T3-L1.adeno-PU1.bed
Myod1.EXP032276.C2C12_myoblasts_of_C3H_strain..bed
Tal1.EXP031694.differentiating_murine_hematopoietic_cells.dox.bed
Pparg.EXP000042.3T3-L1_adipocytes.NULL.bed
Cdx2.EXP032550.endoderm_cells..bed
Stat5a.EXP000715.mouse_embryonic_fibroblasts_MEFs.Stat5_KO_Growth_hormone.b
Rxra.EXP001011.F9.NULL.bed
Myog.EXP032277.C2C12_myoblasts_of_C3H_strain..bed

Nkx3-1.EXP031260.Recombinant_inbred_B6_x_129_Nkx3-1_--..bed
Kmt2b.EXP032315.immortalized_brown_preadipocytes.D0_of_adipogenesis.bed
Cebpb.EXP031692.differentiating_murine_hematopoietic_cells..bed
Vdr.EXP032799.MC3T3-E1_differentiated_for_15_days.ethanol_vehicle.bed
Cebpb.EXP030546.myeloid_progenitor_cells..bed
Ncor2.EXP030955.wild-type_primary_bone_marrow-derived_macrophages..bed
Pou5f1.EXP032982.embryonic_stem_cells_ESC.Dox.bed
Stat5a.EXP032238.mammary_gland.L1.bed
gata4.EXP030894.HL-1_cardiac_muscle_cell_line..bed
Cebpb.EXP031960.Primary_dermal_fibroblasts.Thapsigargin_treatment_for_3_hrs.bed
Spi1.EXP032896.BV2.wt_human_Htt_overexpression.bed
anti-NCoR.EXP030956.wild-type_primary_bone_marrow-derived_macrophages..bed
Cebpa.EXP030544.Hematopoietic_Stem_Cells..bed
Sox3_T__Edlund.EXP000015.ES-derived_neural_progenitor_cells.NULL.bed
Atf3.EXP032923.C57BL6.LPS.bed
Smad3.EXP000842.V6_5_embryonic_stem_cells.NULL.bed
AF2018.EXP000020.ESC.NULL.bed
Pparg.EXP030713.3T3-L1_cells_ATCC_CL-173..bed
Sox2_raised_by_ourselves.EXP032398.EGFP-TS3_5_TS_cells..bed
Mef2d.EXP031871.C2C12..bed
Ascl1_ab74065.EXP030565.C57BL6_embryonic_fibroblasts..bed
Vdr.EXP033036.3T3-L1..bed
Cdx2.EXP031623.Ainv15_ATCC_SCRC-1029_with_Dox-inducible_Cdx2-V5_construct.
Cebpa.EXP000638.3T3-L1_preadipocyte_cell_line.4_hours_of_differentiation.bed
Pparg.EXP000496.3T3L1_cells.Day_6_of_differentiation.bed
Lhx3.EXP031090.Ainv15_ATCC_SCRC-1029_with_Dox-inducible_Ngn2_Isl1_Lhx3-V5_
Rxra.EXP001010.F9.NULL.bed
Foxa1.EXP032165.prostate.castratedplusvehicle.bed
Thra.EXP031500.C17_2a_neural_progenitor_cells..bed
Cebpb.EXP000045.3T3-L1.NULL.bed
Cdx4.EXP001008.Ainv15_ATCC_SCRC-1029_with_inducible_Flag-tagged_Hoxc9.plus
Pou3f2.EXP031249.ES-derived_neural_progenitor_cells_NPCs..bed
Cebpb.EXP000635.3T3-L1_preadipocyte_cell_line.4_hours_of_differentiation.bed
Cebpa.EXP033002.3T3-L1.none.bed
Stat5a.EXP032419.mammary.none.bed
Stat5a.EXP030766.Mammary_tissues..bed
Nfkb1.EXP032915.C57BL6..bed
Stat5a.EXP032239.mammary_gland..bed
Cebpb.EXP033003.3T3-L1..bed
Cebpa.EXP030673.primary_B_cells.Estradiol_for_18h.bed
Pax7.EXP030937.primary_myoblasts..bed
Ebf1.EXP033046.3T3L1..bed
Ptf1a.EXP030973.266_6_Pancreatic_Cells..bed
Pparg.EXP000534.3T3-L1.NULL.bed
Myod1.EXP010522.C2C12.EqS_2_0pct_7d.bed
Stat5a.EXP000640.3T3-L1_preadipocyte_cell_line.4_hours_of_differentiation.bed
Rela.EXP032921.C57BL6.LPS.bed
Cdx2.EXP032547.ESC_Ainv15_ATCC_SCRC-1029.plusDox_plusFGF.bed
Cebpb.EXP000633.3T3-L1_preadipocyte_cell_line.day_0_of_differentiation.bed
Myod1.EXP030921.fibroblasts..bed

Msx1.EXP000382.C2C12.NULL.bed
Cebpb.EXP000634.3T3-L1_preadipocyte_cell_line.2_hours_of_differentiation.bed
Foxa2.EXP030514.ES-derived_definitive_endoderm_cells..bed
Pparg.EXP000643.3T3-L1_preadipocyte_cell_line.day_6_of_differentiation.bed
Pou3f2.EXP030571.C57BL6_neural_progenitor..bed
Pparg.EXP000495.3T3L1_cells.Day_4_of_differentiation.bed
Stat5b.EXP030767.Mammary_tissues..bed
Pparg.EXP000642.3T3-L1_preadipocyte_cell_line.day_2_of_differentiation.bed
Nanog.EXP000475.Embryonic_stem_cells.NULL.bed
anti-NCoR.EXP030958.Bcl6_knockout_primary_bone_marrow-derived_macrophages..b
Smad1.EXP000419.Erthyroid_Progenitor_G1E.NULL.bed
Pparg.EXP000493.3T3L1_cells.Day_2_of_differentiation.bed
Tead2.EXP032944.Py2T_breast_cancer_cells..bed
Cebpb.EXP000636.3T3-L1_preadipocyte_cell_line.day_2_of_differentiation.bed
Tal1.EXP010942.Megakaryo.NULL.bed
Foxa1.EXP032177.prostate.castratedplustestosterone.bed
Cebpb.EXP031959.Primary_dermal_fibroblasts.No_treatment.bed
Pparg.EXP031774.epididymal_white_adipose_tissue-derived_adipocytes.none.bed
sc-8635.EXP000022.ESC.NULL.bed
Ptf1a.EXP030598.Pancreas..bed
Cebpb.EXP000046.3T3-L1_6hr_of_differentiation.NULL.bed
Pou5f1.EXP032980.embryonic_stem_cells_ESC..bed
Mef2d.EXP031872.C2C12..bed
Pax3.EXP030938.primary_myoblasts..bed
Cdx4.EXP001007.Ainv15_ATCC_SCRC-1029_with_inducible_V5-tagged_Hoxc9.plusD
Esr1.EXP032050.mouse_mammary_cells_express_GFP-GR_and_Cherry-ER_under_a
Smad3.EXP000843.V6_5_embryonic_stem_cells.Activin.bed
Sox2_produced_in-house.EXP030984.ZHBTc4.control.bed
Glucocorticoid_Receptor.EXP030424.primary_bone_marrow-derived_macrophages.Dex
Pparg.EXP000902.Cultured_Adipocytes.NULL.bed
Bcl6.EXP000035.primary_bone_marrow-derived_macrophages..bed
Pparg.EXP031775.inguinal_white_adipous_tissue-derived_adipocytes.none.bed
Smad2.EXP000846.V6_5_embryonic_stem_cells.Activin.bed
RD_Systems_MAB2018.EXP030813.Embryonic_stem_cells..bed
Cdx2.EXP032397.ZHBTc4-TS_cells..bed
Pparg.EXP032205.3T3-L1.adeno-PU1.bed
Nr1i2.EXP033037.3T3-L1..bed
Esr1.EXP032051.mouse_mammary_cells_express_GFP-GR_and_Cherry-ER_under_a
Pparg.EXP031776.brown_adipous_tissue-derived_adipocytes.none.bed
Etv6.EXP031753.ES-derived_neural_progenitor_like_cells..bed
Nanog.EXP000021.ESC.NULL.bed
Ncor2.EXP030957.Bcl6_knockout_primary_bone_marrow-derived_macrophages..bed
Esr1.EXP032054.bed
Zfp57.EXP000268.embryonic_stem_ES_cells.NULL.bed
Glucocorticoid_Receptor.EXP030423.primary_bone_marrow-derived_macrophages.Dex
Esr1.EXP032052.mouse_mammary_cells_express_GFP-GR_and_Cherry-ER_under_a
Sox6.EXP000148.myotubes_induced_from_wild_type_mouse_fetal_E18_5_primary_my
Zfp57.EXP000269.embryonic_stem_ES_cells_expressing_HAZFP57.NULL.bed
GR.EXP032048.mouse_mammary_cells_express_GFP-GR_and_Cherry-ER_under_a_t
Esr1.EXP032055.bed

Myb.EXP000216.Conditional_Myb_transformed_myeloid_cell_line.inactivated_MYB.bed
Sox2_produced_in-house.EXP030986.ZHBTc4.Tet.bed
Rela.EXP030451.3T3-L1.differentiated_TNF.bed
GR.EXP000639.3T3-L1_preadipocyte_cell_line.4_hours_of_differentiation.bed
Esr1.EXP032053.mouse_mammary_cells_express_GFP-GR_and_Cherry-ER_under_a_
Myod1.EXP030918.myoblasts..bed
GR.EXP032047.mouse_mammary_cells_express_GFP-GR_and_Cherry-ER_under_a_t
GR.EXP032049.mouse_mammary_cells_express_GFP-GR_and_Cherry-ER_under_a_t

.bed

ɔed

ed

x.bed

lult_neural_progenitor_cell.LY.bed

RED CLUSTER

Gabpa.EXP011066.CH12.None.bed
Creb1.EXP030715.3T3-L1_cells_ATCC_CL-173.DMSO.bed
Creb1.EXP030716.3T3-L1_cells_ATCC_CL-173.lactacystin.bed
Jun.EXP032880.CD8plus_T_cells..bed
E2f4.EXP010412.C2C12.EqS_2_0pct_60hr.bed
Myc.EXP032616.Pancreatic_carcinoma_cells_derived_from_KrasG12Dplus_p53R172H
Mxi1.EXP010444.CH12.None.bed
Stat6.EXP000055.in_vitro_polarized_T_helper2_cells_for_7_days.STAT6_KO.bed
sc-592_Santa_Cruz_Biotechnology.EXP030516.primary_CD4plus_T_cells_from_spleer
Max.EXP010263.CH12.None.bed
Jun.EXP031656.Th17_Cells..bed
Batf.EXP031648.CD4plus_T_Cells.IRF4KO.bed
Irf4.EXP031651.CD4plus_T_Cells.BATFKO.bed
Batf.EXP031649.CD4plus_T_Cells.IL21_IRF4KO.bed
Max.EXP010133.C2C12.EqS_2_0pct_60hr.bed
Fos.EXP032703.primary_mast_cells..bed
Stat3.EXP031658.Th17_Cells..bed
Myc.EXP010764.CH12.None.bed
Ddit3.EXP031252.Mouse_embryonic_fibroblast.Tunicamycin.bed
Gabpa.EXP011012.MEL.None.bed
Irf4.EXP031654.Th17_Cells..bed
Myc.EXP032618.MEFs_derived_from_Miz1floxflox_CreER-mice..bed
Stat6.EXP000054.in_vitro_polarized_T_helper2_cells_for_7_days.NULL.bed
Jund.EXP031657.Th17_Cells..bed
Stat3.EXP000348.CD4plus_T_cells.IL-6_IL-23.bed
Max.EXP011026.C2C12.None.bed
Tbx21.EXP000710.in_vitro_polarized_T_helper1_cells_for_7_days.NULL.bed
Stat3.EXP000323.WT-Th17_polazied_T_cells_from_naive.NULL.bed
Stat6.EXP031762.Th9.Th9_conditions_72_hours.bed
Stat3.EXP000091.in_vitro_polarized_T_helper17_cells.NULL.bed
Batf.EXP031645.CD4plus_T_Cells..bed
Rela.EXP032925.C57BL6.LPS.bed
Jun.EXP031642.CD4plus_T_Cells.IL21.bed
Tbx21.EXP031709.Th1..bed
Stat5a.EXP000092.in_vitro_polarized_T_helper17_cells.NULL.bed
Bhlhe40.EXP010009.CH12.None.bed
Junb.EXP031655.Th17_Cells..bed
Mafk.EXP010977.MEL.DMSO_2_0pct.bed
Klf3.EXP031948.Klf3--_murine_embryonic_fibroblasts_rescued_with_Klf3-V5..bed
Cebpb.EXP030683.mouse_brown_preadipocytes_MLL4_KO_Vec_Cre_CEBPbeta_ChIl
STAT4SantaCruzsc486.EXP000052.in_vitro_polarized_T_helper1_cells_for_7_days.NU
Irf4.EXP030759.Th17_polarized_cells..bed
Batf.EXP031653.Th17_Cells..bed
Usf1.EXP010748.C2C12.EqS_2_0pct_60hr.bed
Usf1.EXP010947.C2C12.None.bed
Rela.EXP032252.Macrophage.Kdo2_Lipid_A_KLA_1h.bed
Jund.EXP032882.CD8plus_T_cells..bed
Stat5b.EXP000387.BalbC_Th1.2_rounds_priming.bed
Pknox1.EXP032892.Embryonic_fibroblast..bed

Ets1.EXP011112.CH12.None.bed
Stat5b.EXP031760.Th9.Th9_conditions_72_hours.bed
Batf.EXP030760.Th17_polarized_cells..bed
STAT4.EXP000385.BalbC_Th1.2_rounds_priming.bed
Bach2.EXP032019.in_vitro_polarized_inducible_regulatory_cells_for_3_days..bed
Atf4.EXP031254.Mouse_embryonic_fibroblast.Tunicamycin.bed
Rela.EXP032090.Peritoneal_macrophages_of_C57BL6J.100_ngml_Kdo2-LipidA_1_hr.b
anti-STAT1_santa_cruz_sc-417.EXP000461.Bone_marrow_macrophages.IFN_for_6_ho
Rela.EXP032248.Macrophage.Kdo2_Lipid_A_KLA_1h.bed
Irf4.EXP031638.CD4plus_T_Cells.IL21.bed
anti-STAT1_santa_cruz_sc-417.EXP000465.Bone_marrow_macrophages_ikk--..bed
Rela.EXP032091.Peritoneal_macrophages_of_BALBcJ.100_ngml_Kdo2-LipidA_1_hr.be
anti-STAT1_santa_cruz_sc-417.EXP000469.Bone_marrow_macrophages_ikk--.IFN_for
Stat5b.EXP030970.Dendritic_Cell.IL21.bed
Rela.EXP032261.Macrophage.DMSO_2h_Kdo2_Lipid_A_KLA_1h.bed
Mafk.EXP010616.MEL.None.bed
Irf4.EXP030762.Th0_polarized_cells..bed
Cebpa.EXP032085.Peritoneal_macrophages_of_BALBcJ.no_treatment.bed
Irf4.EXP032885.CD8plus_T_cells..bed
Rela.EXP030645.Macrophage.Kdo2_Lipid_A_KLA_1h.bed
Junb.EXP032881.CD8plus_T_cells..bed
Nr6a1.EXP030574.Dicer_ff_murine_MSC_cell_line..bed
Foxp3.EXP032970.iTreg_cells..bed
Jun.EXP031647.CD4plus_T_Cells.IL21_IRF4KO.bed
Stat3.EXP030967.Dendritic_Cell.IL21.bed
Rela.EXP030646.Macrophage.Kdo2_Lipid_A_KLA_1h.bed
Stat5b.EXP030971.Dendritic_Cell.IL-21_and_GM-CSF.bed
Jun.EXP030714.3T3-L1_cells_ATCC_CL-173..bed
Junb.EXP031535.bone_marrow-derived_macrophages_7th_day_of_differentiation.LPS_
Irf4.EXP031637.CD4plus_T_Cells..bed
Mafk.EXP010248.CH12.None.bed
Cebpa.EXP032254.Macrophage.Kdo2_Lipid_A_KLA_1h.bed
anti-STAT1_santa_cruz_sc-417.EXP000467.Bone_marrow_macrophages_ikk--.IFN_for
Mafk.EXP010956.ES-E14.None.bed
Rela.EXP032262.Macrophage.IBET_2h_Kdo2_Lipid_A_KLA_1h.bed
anti-STAT1_santa_cruz_sc-417.EXP000463.Bone_marrow_macrophages.IFN_for_6_ho
Cebpa.EXP032086.Peritoneal_macrophages_of_BALBcJ.100_ngml_Kdo2-LipidA_1_hr.
Jund.EXP010348.CH12.None.bed
anti-NFATc1.EXP032552.NKC_pancreatic_cancer_cells..bed
Jun.EXP010079.CH12.None.bed
Jund.EXP031903.STHdhQ7..bed
Cebpa.EXP032084.Peritoneal_macrophages_of_C57BL6J.100_ngml_Kdo2-LipidA_1_h
anti-STAT1_santa_cruz_sc-417.EXP000459.Bone_marrow_macrophages..bed
Cebpb.EXP032902.BV2.wt_human_Htt_overexpression.bed
Maff.EXP031307.bone_marrow-derived_dendritic_cells.LPS_0_min.bed
Cebpb.EXP032592.MC3T3-E1_differentiated_for_15_days.ethanol_vehicle.bed
Cebpb.EXP032903.BV2.mutant_human_Htt_overexpression.bed
Junb.EXP031534.bone_marrow-derived_macrophages_7th_day_of_differentiation..bed
Jund.EXP031904.STHdhQ111..bed
Irf4.EXP032094.resting_mature_peripheral_primary_B_cells.stimulated_for_3_days.bed

Cebpb.EXP030681.mouse_brown_preadipocytes_WT_Vec_GFP_CEBPbeta_ChIP..bed
Maff.EXP031310.bone_marrow-derived_dendritic_cells.LPS_60_min.bed
anti-NFATc1.EXP032553.NKC_pancreatic_cancer_cells..bed
Irf4.EXP032093.resting_mature_peripheral_primary_B_cells.stimulated_for_1_day.bed
Jun.EXP030426.primary_bone_marrow-derived_macrophages.LPS-stimulated.bed
Jund.EXP010561.MEL.None.bed
Cebpb.EXP030684.mouse_brown_preadipocytes_MLL4_KO_CEBPbeta_Cre_CEBPbet
Fosl2.EXP031901.STHdhQ7..bed
Meis1.EXP032890.Embryonic_fibroblast..bed
Maf.EXP032674.Activated_CD4plus_T_cells_skewed_towards_a_Th17_subset_..bed
Fosl2.EXP031902.STHdhQ111..bed
Maf.EXP032675.Activated_CD4plus_T_cells_skewed_towards_a_Th17_subset_.mir155
Meis1.EXP032891.Embryonic_fibroblast..bed
Irf4.EXP030761.Th2_polarized_cells..bed
Cebpb.EXP010684.C2C12.EqS_2_0pct_60hr.bed
Jun.EXP031471.C2C12..bed
Fosl1.EXP011098.C2C12.None.bed
Irf4.EXP032291.CD8plus_T_cells.anti-CD3_anti-CD28_and_recombinant_hIL-2.bed
Meis1.EXP032889.Embryonic_fibroblast..bed
Junb.EXP033031.3T3-L1..bed
Jun.EXP033030.3T3-L1..bed
GR.EXP032046.mouse_mammary_cells_express_GFP-GR_and_Cherry-ER_under_a_t

ox.bed
_tet_regulated_promoter.untreated.bed

kamethasone_treated_LPS-stimulated.bed

_tet_regulated_promoter.Dexamethasone_for_30_minutes.bed

kamethasone_treated_unstimulated.bed
_tet_regulated_promoter.Estradiol_for_30_minutes.bed
roblasts.NULL.bed

tet_regulated_promoter.Estradiol_for_30_minutes.bed

_tet_regulated_promoter.Dexamethasone_plus_Estradiol_for_30_minutes.bed

tet_regulated_promoter.Dexamethasone_for_30_minutes.bed
tet_regulated_promoter.Dexamethasone_plus_Estradiol_for_30_minutes.bed

plus-mice..bed

ı_and_lymph_nodes..bed

P..bed
ILL.bed

ɔed
ɔur.bed

ɛd
_6_hour.bed

_10_ngml_for_4hrs.bed

_6_hour.bed

ɔur.bed
bed

r.bed

d

ta_ChIP..bed

5_KO.bed

tet_regulated_promoter.untreated.bed

Table EV3

LIVER-ID genes

LIVER-ID genes defining the GSEA Core Enrichment from Fig.3D, i.e. LIVER-ID genes showing lower repress

GO terms

GO terms defining additional pathways and liver functions less repressed by ERS in NFIL3 KO compared to
BubbleGUM analyses were performed using the ‘‘MousePath_GO_gmt.gmt’’ set of genes from the Gene S
GO terms identified as repressed by ERS in both WT and NFIL3 KO mice were retrieved (FDR<0.25). Then a
Genes defining the different GO terms are also provided.

ion upon ERS in NFIL3 KO mice.

WT mice.
Set Knowledgebase (GSKB) (Lai et al., 2016)
a comparison between gene expression levels in treated WT and NFIL KO mice was used to define GO term

ıs enriched for genes showing lower repression in NFIL3 KO compared to WT livers.

Table EV4
This table provides the list of MUSCLE-ID and UBQ genes used in Appendix Fig.S26

Table EV5
List of primers used in this study for real-time PCR analyses.

Transcriptomic data used in this study

Tissue	Details	Data accession number	Publication
Multiple mouse tissues	Liver, skeletal muscle and control tissues (brown adipose tissue, cerebellum, cerebral cortex, heart, kid	BioGPS - MOE430 atlas (http://biogps.org/#goto=welcome) - GSE10246	Wu C *et al*. BioGPS: an extensible and customizable portal for querying and organizing gene annotation resources*Genome Biol* 2009; Lattin JE et al. Expressi
Livers from mice treated with tunicamycin	IP injection of 1 µg/g tunicamycin and liver collection after 8h or 34h in WT or Atf6 KO mice	GSE48939	Arensdorf A *et al*. Temporal clustering of gene expression links the metabolic transcription factor HNF4α to the ER stress-dependent gene regulatory network
Mouse livers during different differentiation stages	14 time points across the C57/B6 mouse liver development, which include E11.5 (embryonic day 11.5),	GSE13149	Li T *et al*. Multi-stage analysis of gene expression and transcription regulation in C57/B6 mouse liver development*Genomics* 2009
Hepatobiliary single-cell transcriptomes across different timepoints of hepatobiliary lineage developmer	447 hepatobiliary single-cell transcriptomes across 7 timepoints of hepatobiliary lineage development, s	GSE90047	Yang L *et al*. A single-cell transcriptomic analysis reveals precise pathways and regulatory mechanisms underlying hepatoblast differentiation. *Hepatology* 201
Livers from septic mice	IP injection with 8 × 10^8 CFU of live *E. coli* (DH5α) bacteria and liver collection after 16h, bacterial injectio	GSE121847	Paumelli *R et al*. Hepatic PPARα is critical in the metabolic adaptation to sepsi *J Hepatol* 2019
Mouse livers at different stages of repair/regeneration after partial hepatectomy (PHx)	Control livers (0h) or livers obtained 4,10,48h and 1 week after PHx	GSE95135	Rib L *et al*. Cycles of gene expression and genome response during mammalian tissue regeneration*Epigenetics Chromatin* 2018
Livers from HNF4A KO mice subjected to PH	Livers from WT or hepatocyte-specific HNF4A KO mice 5 days after PHx	Data provided by the authors	Huck I *et al*. Hepatocyte Nuclear Factor 4 Alpha Activation Is Essential for Termination of Liver Regeneration in Mic *Hepatology* 2019
Mouse livers in the fasted or fed state	Livers from ZT10 unfed and ZT14 fed mice were used	GSE119713	Kalvisa A et al. Insulin signaling and reduced glucocorticoid receptor activity attenuate postprandial gene expression in liver*PLoS Biol* 2018
Mouse livers in the fasted or fed state	Livers from ZT10 unfed and ZT14 fed mice were used (RNA-seq on total RNA from WT mice	GSE98041	Beneglamo Ger *al*. The RNA-Binding Protein NONO Coordinates Hepatic Adaptation to Feedin*Cell Metab* 2018
Mouse primary hepatocytes treated with thapsigargin	1 µM thapsigargin for 4h	GSE122508	Present study
Livers from NFIL3 KO mice treated with tunicamycin	IP injection of 1 µg/g tunicamycin and liver collection after 8h	GSE122508	Present study
Skeletal muscles from mice treated with tunicamycin	IM injection of 30 µg tunicamycin and muscle collection after 24h	GSE122508	Present study
Livers from mice exposed to an overdose of acetaminophen	Single administration of high dose (300 mg/kg i.p.), livers collected 6h after drug exposure	GSE17649	Liu HHet *al*. An Integrative genomic analysis identifies Bhmt2 as a diet-dependent genetic factor protecting against acetaminophen-induced liver toxicity*Genom*
Livers from mice exposed to the hepatotoxic drug CCL4	s.c. injection of increasing doses of CCL4 (0.1 ml/kg of a 2-8% solution) for 8 weeks	GSE141821	Lefebvre P *et al*. Interspecies NASH disease activity whole-genome profiling identifies a fibrogenic role of PPARα-regulated dermatopontin*JCI Insight* 2017
Livers from mice under MCD-HF	Methionine and choline-deficient (MCD) + high fat (HF) diet for 8 weeks	GSE35961	Kita Y *et al*. Metformin prevents and reverses inflammation in a non-diabetic mouse model of nonalcoholic steatohepatiti*PLoS One* 2012

Mouse liver ChIP-seq of transcriptional regulators used in this study

MGI Symbol	Common name	Full name	Data accession number	Publication
ARNTL	BMAL1	aryl hydrocarbon receptor nuclear translocator-like	GSE39977	Koike N*et al*. Transcriptional architecture and chromatin landscape of the core circadian clock in mammals*Science* 2012
BRD4	BRD4	bromodomain containing 4	GSE104129	Kim Y *et al*. Rev-erbα dynamically modulates chromatin looping to control circadian gene transcription*Science* 2018
CBX5	HP1	chromobox 5	GSE26729	Li Z *et al*. The Nucleosome Map of the Mammalian Liver*Nat Struct Mol Biol* 2011
CEBPA	CEBPA	CCAAT/enhancer binding protein (C/EBP), alpha	E-MTAB-941	Faure AJ *et al*. Cohesin regulates tissue-specific expression by stabilizing highly occupied cis-regulatory modules. *Genome Res* 2012
CEBPB	CEBPB	CCAAT/enhancer binding protein (C/EBP), beta	GSE45674	Everett LJ*et al*. Integrative genomic analysis of CREB defines a critical role for transcription factor networks in mediating the fed/fasted switch in liver.*BMC Ge*
CLOCK	CLOCK	circadian locomotor output cycles kaput	GSE26729	Koike N*et al*. Transcriptional architecture and chromatin landscape of the core circadian clock in mammals*Science* 2012
CREB1	CREB	cAMP responsive element binding protein 1	GSE45674	Everett LJ*et al*. Integrative genomic analysis of CREB defines a critical role for transcription factor networks in mediating the fed/fasted switch in liver.*BMC Ge*
CREBBP	CBP	CREB binding protein	E-MTAB-941	Faure AJ *et al*. Cohesin regulates tissue-specific expression by stabilizing highly occupied cis-regulatory modules. *Genome Res* 2012
CRY1	CRY1	cryptochrome 1	GSE26729	Koike N*et al*. Transcriptional architecture and chromatin landscape of the core circadian clock in mammals*Science* 2012
CRY2	CRY2	cryptochrome 2	GSE26729	Koike N*et al*. Transcriptional architecture and chromatin landscape of the core circadian clock in mammals*Science* 2012
CTCF	CTCF	CCCTC-binding factor	E-MTAB-941	Faure AJ *et al*. Cohesin regulates tissue-specific expression by stabilizing highly occupied cis-regulatory modules. *Genome Res* 2012
E2F4	E2F4	E2F transcription factor 4	GSE17067	Macisaac KD*et al*. A quantitative model of transcriptional regulation reveals the influence of binding location on expression*PLoS Comput Biol* 2010
EP300	P300	E1A binding protein p300	E-MTAB-941	Faure AJ *et al*. Cohesin regulates tissue-specific expression by stabilizing highly occupied cis-regulatory modules. *Genome Res* 2012
ESRRA	ERRA	estrogen related receptor, alpha	GSE43638	Chaveroux C *et al*. Molecular and genetic crosstalks between mTOR and ERRα are key determinants of rapamycin-induced nonalcoholic fatty live*Cell Metab* 2
FOXA1	FOXA1	forkhead box A1	E-MTAB-941	Faure AJ *et al*. Cohesin regulates tissue-specific expression by stabilizing highly occupied cis-regulatory modules. *Genome Res* 2012
FOXA2	FOXA2	forkhead box A2	E-MTAB-941	Faure AJ *et al*. Cohesin regulates tissue-specific expression by stabilizing highly occupied cis-regulatory modules. *Genome Res* 2012
GABPA	GABPA	GA repeat binding protein, alpha	E-MTAB-941	Faure AJ *et al*. Cohesin regulates tissue-specific expression by stabilizing highly occupied cis-regulatory modules. *Genome Res* 2012
GATA4	GATA4	GATA binding protein 4	GSE49132	Zheng R*et al*. Function of GATA Factors in the Adult Mouse Liver*PLoS ONE* 2013
HDAC3	HDAC3	histone deacetylase 3	GSE26345	Feng D*et al*. A circadian rhythm orchestrated by histone deacetylase 3 controls hepatic lipid metabolism.*Science* 2011
HNF1A	HNF1A	HNF1 homeobox A	E-MTAB-941	Faure AJ *et al*. Cohesin regulates tissue-specific expression by stabilizing highly occupied cis-regulatory modules. *Genome Res* 2012
HNF4A	HNF4A	hepatic nuclear factor 4, alpha	E-MTAB-941	Faure AJ *et al*. Cohesin regulates tissue-specific expression by stabilizing highly occupied cis-regulatory modules. *Genome Res* 2012
MTOR	MTOR	mechanistic target of rapamycin	GSE43638	Chaveroux C *et al*. Molecular and genetic crosstalks between mTOR and ERRα are key determinants of rapamycin-induced nonalcoholic fatty live*Cell Metab* 2
NCOR1	NCOR	nuclear receptor co-repressor 1	GSE26345	Feng D*et al*. A circadian rhythm orchestrated by histone deacetylase 3 controls hepatic lipid metabolism.*Science* 2011
NCOR2	SMRT	nuclear receptor co-repressor 2	GSE51045	Sun Z *et al*. Deacetylase-independent function of HDAC3 in transcription and metabolism requires nuclear receptor corepressor*Mol Cell* 2013
NFIL3	E4BP4	nuclear factor, interleukin 3, regulated	GSE59486	Fang B *et al*. Circadian enhancers coordinate multiple phases of rhythmic gene transcription in vivo.*Cell* 2014
NPAS2	NPAS2	neuronal PAS domain protein 2	GSE26729	Koike N*et al*. Transcriptional architecture and chromatin landscape of the core circadian clock in mammals*Science* 2012
NR1D1	REVERBA	nuclear receptor subfamily 1, group D, member 1 (Nuclear Receptor Rev-ErbA-Alpha)	GSE26345	Feng D*et al*. A circadian rhythm orchestrated by histone deacetylase 3 controls hepatic lipid metabolism.*Science* 2011
NR1D2	REVERBB	nuclear receptor subfamily 1, group D, member 2 (Nuclear Receptor Rev-ErbA-Beta)	GSE36375	Bugge A *et al*. Rev-erbα and Rev-erbβ coordinately protect the circadian clock and normal metabolic function*Genes Dev* 2012
NR1H3	LXR	nuclear receptor subfamily 1, group H, member 3 (liver X receptor)	GSE35262	Boergesen M *et al*. Genome-Wide Profiling of Liver X Receptor, Retinoid X Receptor, and Peroxisome Proliferator-Activated Receptor A in Mouse Liver Reveal
NR1H4	FXR	nuclear receptor subfamily 1, group H, member 4 (farnesoid X receptor)	GSE87866	Lien F *et al*. Metformin interferes with bile acid homeostasis through AMPK-FXR crosstalk*J Clin Invest* 2014
NR3C1	GR	nuclear receptor subfamily 3, group C, member 1 (glucocorticoid receptor)	GSE45674	Everett LJ*et al*. Integrative genomic analysis of CREB defines a critical role for transcription factor networks in mediating the fed/fasted switch in liver.*BMC Ge*
NR5A2	LRH1	nuclear receptor subfamily 5, group A, member 2 (liver receptor homologue)	https://sbcl.lcg.ucl.edu/public_data//	Chong HKet *al*. Genome-wide analysis of hepatic LRH-1 reveals a promoter binding preference and suggests a role in regulating genes of lipid metabolism in
ONECUT1	HNF6	one cut domain, family member 1	E-MTAB-941	Faure AJ *et al*. Cohesin regulates tissue-specific expression by stabilizing highly occupied cis-regulatory modules. *Genome Res* 2012
PER1	PER1	period circadian clock 1	GSE26729	Koike N*et al*. Transcriptional architecture and chromatin landscape of the core circadian clock in mammals*Science* 2012
PER2	PER2	period circadian clock 2	GSE26729	Koike N*et al*. Transcriptional architecture and chromatin landscape of the core circadian clock in mammals*Science* 2012
PKNOX1	PREP1	Pbx/knotted 1 homeobox	E-MTAB-941	Faure AJ *et al*. Cohesin regulates tissue-specific expression by stabilizing highly occupied cis-regulatory modules. *Genome Res* 2012
POLR2B	POLR2B	polymerase (RNA) II (DNA directed) polypeptide B	GSE48375	Gilardi F*et al*. Genome-Wide Analysis of SREBP1 Activity around the Clock Reveals Its Combined Dependency on Nutrient and Circadian Signal*PLoS Genet* 2
PPARA	PPARA	peroxisome proliferator activated receptor alpha	GSE35262	Boergesen M *et al*. Genome-Wide Profiling of Liver X Receptor, Retinoid X Receptor, and Peroxisome Proliferator-Activated Receptor A in Mouse Liver Reveal
RAD21	RAD21	RAD21 cohesin complex component	E-MTAB-941	Faure AJ *et al*. Cohesin regulates tissue-specific expression by stabilizing highly occupied cis-regulatory modules. *Genome Res* 2012
RARA	RARA	retinoic acid receptor, alpha	GSE46762	He Y *et al*. The role of retinoic acid in hepatic lipid homeostasis defined by genomic binding and transcriptome profiling*BMC Genomics* 2013
RARB	RARB	retinoic acid receptor, beta	GSE53736	He Y *et al*. Biological functional annotation of retinoic acid alpha and beta in mouse liver based on genome-wide binding*Am J Physiol Gastrointest Liver Physiol*
REST	NRSF-REST	RE1-silencing transcription factor	E-MTAB-941	Faure AJ *et al*. Cohesin regulates tissue-specific expression by stabilizing highly occupied cis-regulatory modules. *Genome Res* 2012
RORA	RORA	RAR-related orphan receptor alpha	GSE59486	Fang B *et al*. Circadian enhancers coordinate multiple phases of rhythmic gene transcription in vivo.*Cell* 2014
RXRA	RXRA	retinoid X receptor, alpha	GSE53736	He Y *et al*. Biological functional annotation of retinoic acid alpha and beta in mouse liver based on genome-wide binding*Am J Physiol Gastrointest Liver Physiol*
SREBF1	SREBP1	sterol regulatory element binding transcription factor 1	GSE48375	Gilardi F*et al*. Genome-Wide Analysis of SREBP1 Activity around the Clock Reveals Its Combined Dependency on Nutrient and Circadian Signal*PLoS Genet* 2
SREBF2	SREBP2	sterol regulatory element binding transcription factor 2	GSE28082	Seo YK *et al*. Genome-wide localization of SREBP-2 in hepatic chromatin predicts a role in autophagy*Cell Metab* 2011
STAG1	STAG1	stromal antigen 1	E-MTAB-941	Faure AJ *et al*. Cohesin regulates tissue-specific expression by stabilizing highly occupied cis-regulatory modules. *Genome Res* 2012
STAG2	STAG2	stromal antigen 2	E-MTAB-941	Faure AJ *et al*. Cohesin regulates tissue-specific expression by stabilizing highly occupied cis-regulatory modules. *Genome Res* 2012
USF1	USF1	upstream transcription factor 1	GSE44609	Shimomura K*et al*. Usf1, a suppressor of the circadian Clock mutant, reveals the nature of the DNA-binding of the CLOCK:BMAL1 complex in mice*Elife* 2013

Chromatin-related ChIP-seq data used in this study

Regulatory factor	Details	Data accession	Publication
H3K4me1	Mouse liver and control tissues (brown adipose tissue, cerebellum, cortical plate, heart, kidney, olfactor	ENCODE (http://www.mouseencode.org/) - GSE29184 - as processed in Table EV	Shen Y *et al*. A map of the cis-regulatory sequences in the mouse genome. *Nature* 2012
H3K4me1	Human skeletal muscle and control tissues (adipose nuclei, brain anterior caudate, brain inferior tempor	ROADMAP (http://www.roadmapepigenomics.org/data/) - as processed in Table EV4	Chen K*et al*. Broad H3K4me3 is associated with increased transcription elongation and enhancer activity at tumor-suppressor genes. *Nat Genet* 2015
H3K36me3	Mouse liver	ENCODE (http://www.mouseencode.org/) - GSE31039	Yue F *et al*. A comparative encyclopedia of DNA elements in the mouse genome. Nature 2014
H3K27ac	Mouse primary hepatocytes subjected to inflammation (combination of 10 ng/mL ILβ and 10 ng/mL IL-6	GSE96770 - Lifted to mm10 using Galaxy Liftover tool	Goldstein *et al*. Synergistic gene expression during the acute phase response is characterized by transcription factor assisted loading. *Nat Commun* 2017
H3K27ac	Hepatocytes vs non-hepatocytes isolated from Alb-NuTRAP mice	GSE92590	Roh H*et al*. Simultaneous Transcriptional and Epigenomic Profiling from Specific Cell Types within Heterogeneous Tissues In Viv*Cell Rep* 2017
H3K27ac	Mouse primary hepatocytes subjected to ER stress (1 µM thapsigargin for 4h)	GSE122508	Present study

Additional ChIP-seq data used in this study

Tissue	Details	Data accession	Publication
Multiple mouse tissues and murine cell lines	657 datasets of transcriptional regulators (listed in Table EV2)	GTRD (http://gtrd.biouml.org/)	Yevshin I *et al*. GTRD: a database of transcription factor binding sites identified by ChIP-seq experiments*Nucleic Acids Res* 2017